SERI/TP-212-3684
UC Category: 232
DE90000344

Vacuum Window Glazings for Energy-Efficient Buildings: Summary Report

D. K. Benson
L. K. Smith
C. E. Tracy
T. Potter
C. Christensen
Solar Energy Research Institute

D. E. Soule
Western Illinois University

May 1990

Prepared under Task No. WG710151

Solar Energy Research Institute
A Division of Midwest Research Institute

1617 Cole Boulevard
Golden, Colorado 80401-3393

Prepared for the
U.S. Department of Energy
Contract No. DE-AC02-83CH10093

PREFACE

This report documents a feasibility study of a laser-sealed, vacuum insulating window invented at SERI. The combination of laboratory research and analysis has resolved most of the technical issues and suggests that the vacuum window is technically feasible and could be beneficially used in colder climates. In the U.S. Pacific Northwest, for example, an average annual energy savings of about 700 MJ per square meter of window area (60 kBtu/ft^2) is projected. This energy conservation potential argues in favor of further development of the vacuum window.

David K Benson

David K. Benson
Principal Investigator

Approved for

SOLAR ENERGY RESEARCH INSTITUTE

L. M. Murphy, Director
Solar Heat Division

ACKNOWLEDGMENTS

The authors gratefully acknowledge the assistance of the Association of Western Universities, which provided partial support to one of the authors (DES), and to various private companies that provided sample materials for testing, including SAES Getters Industries, USA Donnelly Mirrors, and Airco Coatings Technology. Many colleagues have provided valuable research assistance and helpful discussions. Among those to whom we express our appreciation are Michael Rubin and Dariash Arasteh for providing copies of WINDOW 1.0 and 2.0 programs; to Carol Riordan, Thomas Stoffel, and Daryl Myers for helpful discussions on modeling solar spectra; to John Webb, Rita Goggin, Yvonne Shinton, and Ingo Susemihl for optical measurements; and to Yan Li and Gary Jorgensen for assistance with computer programming. This research was jointly funded by the Bonneville Power Administration and the U.S. Department of Energy Office of Buildings and Community Systems.

ABSTRACT

The technical feasibility of a laser-welded, evacuated, insulating window was studied (U.S. patent number 4,683,154). The window has two edge-sealed sheets of glass separated by 0.5-mm glass spheres spaced 30 mm apart in a regular array. The calculated thermal conductance of the window glazing is about 0.35 W/m^2K (thermal resistance 16°F ft^2 hr/Btu). A highly insulating frame is required and several designs were analyzed. The vacuum window's combination of high solar transmittance and low thermal conductance makes it superior to many other windows for use in cold climates. In the United States Pacific Northwest, the vacuum window is predicted to save about 6 MJ of heating energy annually per square meter of window (60 kBtu/ft^2/year) when compared to conventional, double-glazed windows.

A large vacuum laser-welding facility was designed, developed, and installed at SERI to conduct glass welding experiments and to fabricate full-sized (1-x-1-m) vacuum windows. Experiments confirmed the feasibility of laser sealing glass in vacuum, but identified two difficulties. Under some circumstances, bubbles of dissolved gases form during welding and weaken the seal. Glass also vaporizes and contaminates the laser beam steering mirror. A novel moving metal foil mirror was conceived and developed to circumvent the contamination problem, but has not yet been used to complete welding experiments and fabricate full-sized vacuum windows.

SUMMARY

OBJECTIVES

This report summarizes research conducted at the Solar Energy Research Institute (SERI) as part of an evaluation of the technical and economical feasibility of a novel vacuum insulating window invented at SERI. An essential aspect of this invention is the proposed use of laser welding as a means to seal the glass window glazing perimeter rapidly inside a vacuum processing chamber. This proposed fabrication process is designed to circumvent the production bottleneck that would otherwise occur if a window glazing were to be evacuated through a small opening after its perimeter were sealed more conventionally in air. The laser welding in vacuum is thought to be necessary for achieving economic feasibility.

In earlier studies at SERI, the laser welded vacuum insulating window design had been analyzed in some detail, and laboratory experiments had confirmed the effectiveness of individual design elements such as low-emittance coatings and small (0.5-mm) spherical glass spacers periodically arrayed between the two glass sheets. Laser welding of the glass perimeter to create a permanent seal had been demonstrated in air, but facilities had not been available to experiment with laser welding of glass inside a vacuum chamber.

DISCUSSION

A large vacuum laser welding research facility was designed, constructed, and installed at SERI's Field Test Laboratory. A 400-W CW CO_2 laser was coupled into a large custom vacuum furnace capable of operating at 600°C at pressures of less than 5×10^{-6} torr (6.7×10^{-4} Pa). The laser beam can be directed anywhere within the vacuum furnace by a two-axis rotating water-cooled mirror under computer control. The facility is capable of laser welding flat samples up to 1 m x 1 m in dimension.

Preliminary experiments identified two technical barriers to successful laser welding of glass in vacuum. Glass vapor from the molten weld moves freely in the vacuum and condenses on all exposed surfaces, including the laser beam steering mirror. Within a few minutes of starting a welding experiment, a layer of glass a few hundred nanometers thick is deposited on the mirror, where it absorbs a large fraction of the laser beam power. Consequently, critical laser welding experiments requiring constant laser beam power were impossible, as was the fabrication of complete, perimeter-welded window samples.

A second problem occurred under some conditions of laser power and welding rate when gases, dissolved in the glass during its manufacture, evolved as bubbles in molten glass during welding. These bubbles were trapped and weakened the glass weld and could possibly lead to vacuum leaks in a completed window.

Despite the difficulties caused by the glass vapor contamination, it was possible to show that bubble-free welds could be made under some welding conditions. However, it was not possible to determine how rapidly the glass could be welded without deleterious bubble formation, and it is the speed of

welding upon which the potential economic viability of the laser welding process depends.

A novel, moving foil laser mirror was invented, designed, and fabricated to mitigate the glass vapor mirror contamination problem. In this new design a thin foil of aluminum is used as the mirror surface and is continuously unrolled and advanced much as motion picture film is advanced through a camera. The glass vapor contamination is carried away by the exposed foil as fresh, uncontaminated foil replaces it. Unfortunately, this possible solution to the major experimental impediment was not completed until the end of the project and no further experiments could be done.

Detailed computer modeling experiments were done to analyze the thermal performance of a number of proposed window frame designs that might be used with a vacuum window glazing. Even the best of state-of-the-art, commercially available, insulating window frames were shown to dramatically decrease the effectiveness of a highly insulating window glazing. The better the glazing, the more drastic the effect of heat loss through the window frame. With a projected thermal conductance of 0.35 W/m^2K (thermal resistance = 16°F ft^2hr/Btu) at its center, the vacuum insulated window glazing was predicted to have an overall thermal conductance almost twice as high as the glazing alone (0.68 W/m^2K, R = 8.19°F ft^2hr/Btu) when installed in the best of fiberglass insulated window frames. Only a speculative new window frame design incorporating a compact vacuum insulation* within the frame itself showed much promise for a window with overall thermal conductance almost as low as that of the vacuum insulating glazing.

A new superior low-emittance coating for vacuum windows was developed in collaboration with private industry. The new coating is a thin, sputter-deposited coating similar to those commercially produced for use in automobile windshields. Its use in vacuum insulating glazing is predicted to increase the thermal resistance by about 20% when compared to other economically practical alternatives.

The benefits of an insulating window depend as much on its transmission of solar energy as on its resistance to heat loss. Established computer codes used to predict the net energy flow through windows crudely account for the optical characteristics of the window and neglect details such as the spectral transmittance of low-emittance coatings and how the solar spectrum itself changes with latitude, climate, season, and time of day. A more detailed code was developed within this project so that a more accurate account of these spectral characteristics could be made. Comparison of the new and old codes showed that errors in predicted solar transmittance of a few percent up to 11% were typical and errors in predicted visible transmittance were even greater (up to 76% for some north-facing windows).

---

*Compact vacuum insulation is a thin-profile, evacuated metal envelope similar in design to the vacuum window. It is a SERI invention currently under development.

The potential energy conservation benefits of using highly insulating windows in the Pacific Northwest* were estimated. A solar buildings performance modeling technique was used to compare the projected vacuum insulating window with other commercial and developmental windows in typical north- and south-facing orientations in two representative cities (Portland and Boise). The vacuum window was predicted to provide annual heating energy savings of about 5.9 MJ/m^2 (60 kBtu per square foot) of window area when compared to a standard double-glazed insulating window and about 3 MJ/m^2 (30 kBtu per square foot) when compared to a state-of-the-art commercial double-glazed window with low-emittance coating.

A population- and climate-weighted distribution of residential windows was used to estimate the regional impact of using vacuum insulating windows in residential buildings. Using Bonneville Power Administration (BPA) projections for new house construction between 1990 and 2010, we estimate that the substitution of vacuum windows for conventional insulating windows in new construction would reduce the regional heating energy usage annually by 800 TJ (0.0008 quadrillion Btu) for each year of new construction. If all regional residential windows were eventually replaced with vacuum insulating windows, the regional energy savings is estimated to be 80 PJ/yr (0.08 quadrillion Btu/yr).

CONCLUSIONS

The project was successful. Several technical issues regarding the design, fabrication, and benefits of a laser-welded vacuum insulating window were resolved, but critical questions regarding the speed of vacuum laser welding and performance and durability of full-size vacuum windows remain unanswered.

The potential energy conservation benefits of a vacuum insulating window are high, and the remaining issues should be resolved.

*Specifically, the Bonneville Power Administration service area.

TABLE OF CONTENTS

TABLE OF CONTENTS (Concluded)

LIST OF FIGURES

LIST OF FIGURES (Continued)

LIST OF FIGURES (Concluded)

LIST OF TABLES

1.0 INTRODUCTION

1.1 Objectives

The objectives of this project were the development of a proof-of-concept, preprototype vacuum insulating window, its performance analysis, and its engineering evaluation.

Specific objectives of this project included the design, construction, and installation of a vacuum laser welding research facility. With this facility, the feasibility of using laser welding in vacuum could be tested. The facility was to be large enough so that full-scale, laser-welded vacuum insulating windows could be fabricated for engineering-scale evaluation.

A highly insulating window frame is required to take full advantage of a highly insulating window, and analyses were required to determine how best to achieve the quality of window frame needed. A secondary objective of the task was the design of a potentially suitable frame.

In addition, performance prediction tools were to be developed for predicting the potential benefits of using a vacuum insulating window. These tools were to be used to estimate the possible energy conservation potential in the Pacific Northwest.

1.2 Background

The vacuum window design concept is superficially similar to a conventional double-pane sealed insulating glass window. The primary difference is that the space between the two glass panes is evacuated to a very low pressure. The evacuated space provides an effective barrier to heat flow through the window in much the same way as a similar vacuum prevents heat loss from a thermos bottle. Other essential components of the design are an array of small glass spherical spacers that hold the two panes apart against atmospheric pressure and one or more transparent, low-emissivity (low-e) coatings on the inner glass surfaces to reduce radiative heat transfer (Figure 1-1).

Several different concepts for the design of vacuum insulating windows have been researched and even more have been patented (e.g., Collins and Robinson 1990). However, none of these concepts has been successfully developed. In some cases the designs contain fatal flaws which would prevent achieving the requisite design life or acceptable aesthetics. In most cases, the designs are technically feasible but would be impractical or too expensive to manufacture.

In all other vacuum insulating window designs and fabrication processes, the vacuum is established as a separate step after the window envelope has been sealed (except for the evacuation port). The evacuation step then is a slow bottleneck in the manufacturing process, which adds greatly to the costs. The SERI laser-welded vacuum insulating window design envisions the use of laser welding inside an evacuated process chamber to eliminate the time-consuming separate evacuation step. The required vacuum would be present at the time the window is sealed and no further evacuation would be required.

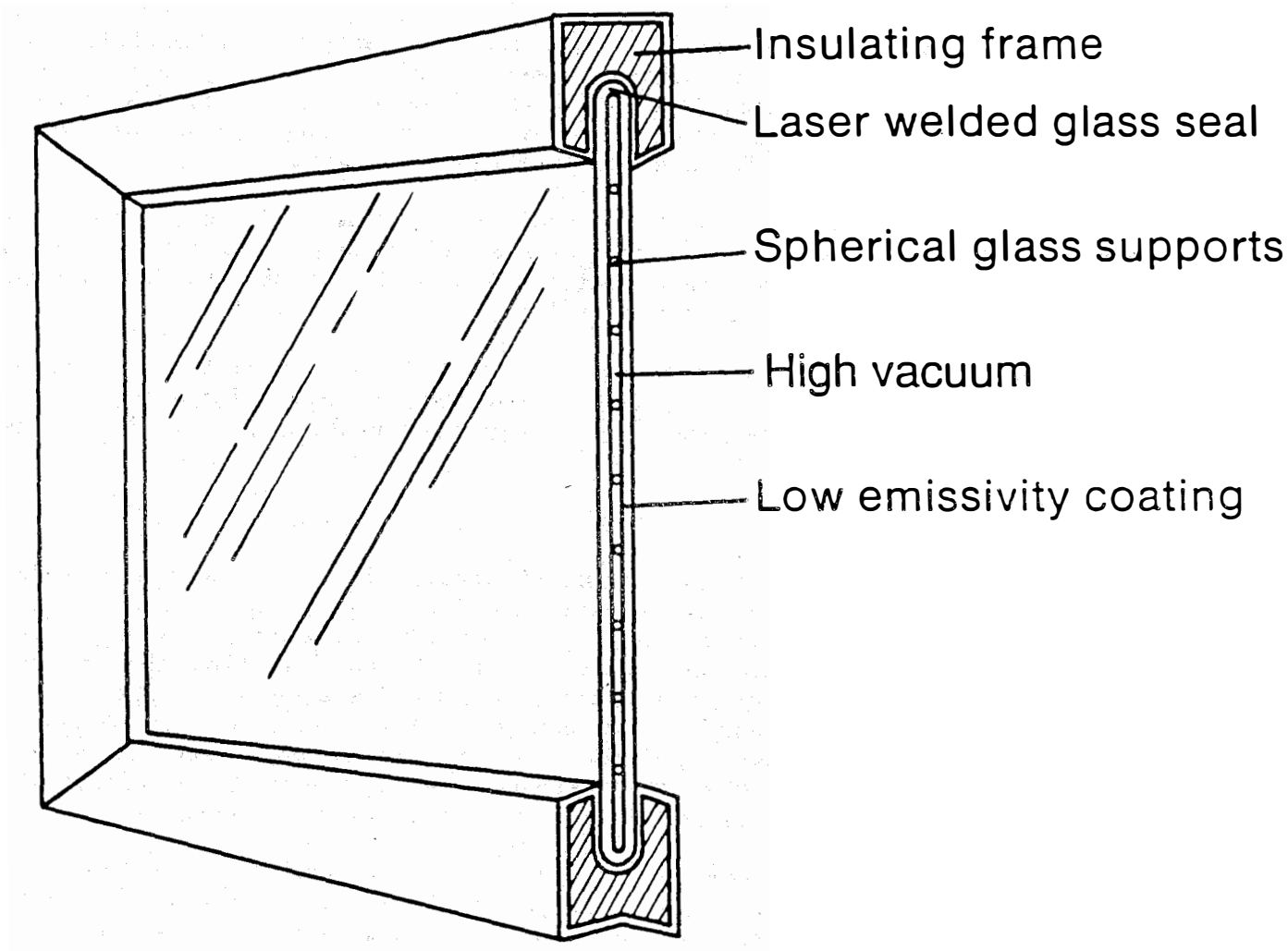

Figure 1-1. Schematic diagram of the evacuated window glazing design

High-throughput, multistage vacuum processing lines are already widely used in the window industry to produce high-performance, low-emittance (so-called low-e) coatings on window glass. Nearly half of all of the windows made in the United States now have low-e coatings. Laser welding is also widely used in the window industry to fabricate the metal spacers used around the perimeter of double-glazed windows. In earlier work, we have shown that we could successfully seal the perimeter of small test windows (10 inches square) by laser welding in air, but no one has reported laser welding of glass in vacuum.

The principal challenge of the research task was to test the feasiblity of laser sealing of the glass window in a vacuum process chamber. It was decided that the apparatus should be large enough that complete, full-sized vacuum windows could be fabricated for engineering evaluation if the welding proved to be feasible. Design and construction of this vacuum laser welding facility required a major effort and occupied most of the time during the project.

Previous research on this vacuum window concept was conducted at SERI with the support of the U.S. Department of Energy (DOE) Office of Buildings and Community Systems. This earlier work included initial engineering design analyses and laboratory studies that helped to resolve some of the issues of technical feasibility. Experiments were done to show that glass sheets could be edge-sealed with a carbon dioxide laser (in air), to show that the stresses developed at the "point" contacts between spherical glass spacers and the flat sheet glass window panes were unlikely to cause fracture, and to show that conventional low-e coatings such as tin-doped indium oxide could withstand the high-temperature vacuum processing and retain their low emissivity ($e \approx 0.10$). Analyses were also done with the assistance of SAES Getters USA, Inc. (manufacturer of reactive metal getters) to determine the kind and amount of getter required in the SERI vacuum window. An analysis was made of the rate at which helium from the atmosphere may compromise the window vacuum by diffusing through the glass during service. Finite-element computer codes were used to estimate the maximum stresses likely to be experienced by a vacuum window in high winds and severe outdoor/indoor temperature differences. All the results of these initial studies were sufficiently encouraging for us to proceed with preprototype test window fabrication. The earlier results are documented in Benson and Tracy (1986) and Benson et al. (1987a).

The vacuum window design is a SERI invention and has been patented (Benson and Tracy 1987b). DOE has conditionally waived patent rights to Midwest Research Institute Ventures (MRIV), a subsidiary of the SERI prime contractor, to facilitate the involvement of private industry in developing and testing the concept.

This project is jointly funded by BPA and the DOE Office of Buildings and Community Systems. The research was conducted at SERI's facilities in Golden, Colorado.

1.3 Scope

This project is a feasibility study. The vacuum insulating window concept under study has been analyzed in detail and appears to be technically and economically feasible. However, available analytical tools are limited, and simplifying assumptions were used in these analyses to make the extensive parametric design calculations tractable. Therefore, it has been necessary to

refine the analyses and to develop laboratory facilities with which to fabricate preprototype samples of the vacuum window for engineering-scale performance verification tests and measurements.

During this project, four types of analyses were conducted and a complete high-temperature vacuum laser welding facility was designed, built, and installed at SERI. The laser welding facility is large enough to allow fabrication of preprototype vacuum window samples as large as 1 m^2. The analyses include estimates of the potential energy savings provided by vacuum window use in the BPA service area, the development of a very detailed computer model for the optical and thermal performance of vacuum and other high-technology windows in any climate, and an analysis of the nature of window frames required for such a highly insulating window glazing. A new, superior low-e coating was designed for the vacuum window in collaboration with Airco Coatings Technology. Technical barriers to vacuum laser welding of glass were identified. Limited glass welding experiments showed that these barriers could be overcome and high-quality continuous glass welds could be made in vacuum. However, time and resources ran out before complete laser-welded vacuum insulating windows could be fabricated for testing.

The report begins with a brief discussion of existing high-performance windows, other proposed and developmental high-performance windows, and the potential advantages of the SERI vacuum window under study. The results obtained during this project are summarized in two sections, one devoted to the analyses and the other to laboratory studies, including the facility development. The discussion section provides an overview of the final status of the project and the remaining technical issues. Conclusions based on the research to date and recommendations for continuing studies are presented in the final section.

This report summarizes work funded by both joint sponsors.

1.4 Highly Insulating Windows

The potential energy savings, added comfort, and reduced building heating costs made possible by use of a more highly insulating window have stimulated several innovative window design concepts over the last decade. Three of these innovations are described briefly here and are compared with the SERI vacuum window under study.

The most significant innovation in the technology of insulating windows since the introduction of the double-pane sealed insulating window is low-e coatings. Low-e coatings consist of thin films of transparent, electrically conductive material applied to the window glass or to a thin sheet of polymer that is suspended between the glass window panes. The conductive material may be a transparent oxide semiconductor such as tin oxide doped with fluorine, indium oxide doped with tin (frequently denoted as ITO), or a very thin metal film such as gold, copper, or silver (<20 nm thick). The metal films are most commonly sandwiched between layers of oxides to stabilize their fragile configuration, to protect them against corrosion, and to reduce reflection from their surfaces. A typical metal-based low-e coating consists of a three-layer deposit on window glass: zinc oxide/silver/zinc oxide (ZnO/Ag/ZnO), sometimes referred to as a ZAZ coating.

Low-e coatings are effective because they reduce the amount of heat lost by thermal radiation from the warmer glass pane to the colder pane. The rate of heat loss is approximately proportional to the emissivity of the warmer surface (see Eq. 2-24), and typical low-e coatings reduce the emissivity of glass by 55% (tin oxide) to 92% (silver multilayer). A low-e coated polymer film suspended between panes accomplishes the same result by reflecting the thermal infrared radiation back to the warmer pane. Table 1-1 lists some commercially available windows that use low-e coatings. Also listed are two very highly insulating windows that are not widely used but are commercially available. One is the Swiss High Insulation Technology (HIT) window produced by Geilinger, Ltd., Winterthur, Switzerland (I in Table 1-1), and the other is the SUPER-E window produced by Alpen, Inc., in Boulder, Colorado (II in Table 1-1). Both windows use two separate suspended polymer films with low-e coatings. The Alpen window has a third low-e coating on the inner glass pane. The Swiss HIT window uses air between the glass panes and an optimum separation between each pair of window elements of 27 mm (1.06 in.). The resulting window is quite thick, 90 mm (3.54 in.), and must be allowed to vent to the atmosphere; otherwise weather-induced changes in atmospheric pressure cause it to bow or bulge excessively. The venting is done through a desiccant filter that adsorbs incoming water vapor and prevents condensation inside the window. The desiccant must be replaced periodically (3-5 years depending on climate), or water condensation may ruin the low-e coatings on the polymer films.

The Alpen window uses a low-conductivity gas (argon) between the glass panes with a smaller optimum spacing of 12.7 mm (1/2 in.) between pairs of window elements. The window is permanently sealed to prevent argon loss and has a total thickness of 44.5 mm (1.75 in.). It must be vented through a capillary vent to a rubber balloon when it is shipped from Boulder, Colorado (elevation about 6000 ft), to lower elevations. The capillary vent is crimp sealed at the building construction site (Clark 1987).

Another highly insulating window concept under study uses a transparent, very low density insulation between two glass panes. The insulation is a very fine grained silica aerogel formed by supercritical drying of an aqueous silica gel. The window must be sealed to prevent the aerogel from absorbing water and other materials from the atmosphere. If a low-e coating is used on one of the inner glass surfaces and the window is evacuated, a very high insulation value is predicted (III in Table 1-1). Light scattering from the aerogel reduces the solar transmittance and distorts the view through this window.

Table 1-1. A Comparison of Insulating Windows and Window Concepts[a]

Commercial Windows	Typical Window Performance Parameters: Center of Window Winter R-Value[c] (°F ft² h/Btu)	Shading Coefficient[d]	Visible Transmittance %	Solar Transmittance %	Comments
Typical Window Designs[b]					
g	0.89	1.0	90	85	Emissivity of glass, e ~ 0.84
g-A-g	2.00	0.89	82	73	
g-A-g-A-g	2.80	0.82	75	64	
g-A-eg	2.5	0.85	77	65	Tin oxide low-e, e ~ 0.38
g-A-el	3.1	0.72	76	57	Silver-based low-e, e ~ 0.11
g-A-ep-A-g	4.5	0.50	55	34	Sputtered low-e, e ~ 0.08
g-R-ep-R-g	5.1	0.71	71	54	Sputtered low-e, e ~ 0.15
I. g-A-ep-A-ep-A-g	9.4	0.46	56	N/A	Sputtered low-e
II. g-R-ep-R-ep-R-eg	10.0	0.56	62	38	Sputtered low-e, e ~ 0.15
New Concepts (calculated values)					
III. g-(20 mm)aerogel/V-eg	17.86	N/A	N/A	42	Questionable optical quality
IV. g*-V-eg*	>15	0.82	77	66	Sputtered low-e, e ~ 0.1

[a]Adapted from Gilmore (1986), Anon. (1985), and Rubin and Lampert (1983).

[b]g = 1/8 in. soda-lime silica glass, A = air, e = low-e coating, l = low-iron solar glass, p = polymer film, R = argon, V = vacuum, g* = 1/8-in. borosilicate glass.

[c]ASHRAE standard winter test conditions.

[d]Total heat gain relative to a single-pane window

N/A: not available

2.0 RESULTS

2.1 Analyses

The energy savings potential and cost-effectiveness of the vacuum window have been estimated in the following sections in comparison to other energy-efficient windows. In the first analysis (Section 2.1.1), a passive solar building design tool was modified in order to estimate the energy savings of different window types in different styles of residential buildings in two typical Pacific Northwest cities. In the second analysis (Section 2.1.2), the total potential residential energy saving in the Pacific Northwest was estimated assuming that existing residential windows were replaced with vacuum insulating windows. In the third analysis (Section 2.1.3), an estimate was made of the cost-effectiveness of substituting more highly insulating windows such as the vacuum window for less highly insulating windows.

The analysis of window effectiveness is hampered by limitations in the analytical tools and also by the incomplete development of the vacuum window. In Section 2.1.4 different frame design options were analyzed in order to determine the likely overall thermal performance of a fully developed vacuum window (including frame). Section 2.1.5 describes an important extension to the window modeling state-of-the-art. In this new approach, the detailed optical performance of the window glazing is taken into account, thereby avoiding large errors inherent in conventional, more approximate approaches.

Section 2.1.6 describes a finite difference, thermal network model used to estimate the heat flow in the vacuum window glazing. Finally, in Section 2.1.7, the thermal model and the detailed optical model are combined and used to calculate typical performance results for the vacuum window in comparison to a conventional, double-glazed window.

2.1.1 Impact of Energy-Efficient Windows on Building Energy Use

Because of the high cost and subtle performance differences of many new window designs, it is particularly important to accurately evaluate their potential for conserving energy. The relative merits of windows can be assessed by comparing their annual energy performance in different climates and different orientations.

The Bonneville Power Administration serves the Pacific Northwest, including the states of Washington, Oregon, Montana, and Idaho. The energy impact of vacuum glazings within this service area was estimated.

A simple method was developed to predict the heating performance of high-technology windows in buildings. The method extends a passive solar building design analysis tool that uses well-established correlations for buildings with standard windows. The use of nonstandard windows is accounted for by introducing modified building parameters.

The annual space heating energy use was estimated for typical residential buildings in Portland, Oregon, and Boise, Idaho. In each location the energy use was estimated for the same building with a variety of different types of windows including the SERI vacuum window. The use of the vacuum window is

predicted to reduce annual heating energy requirements by 51 to 67 kBtu per square foot of window area (160-211 kWh/m^2) compared to the use of ordinary double-pane insulating windows. The energy savings depends upon climate and window orientation.

A simple method is presented for predicting heating performance of nonstandard glazing types in passive solar heated buildings with direct solar heat gain through the windows. The method extends solar load ratio (SLR) calculations by use of modified building and climate parameters to account for nonstandard glazing characteristics. Results are given for a range of glazing types, climates, and building types (conventional, superinsulated, and passive solar). Predicted net energy savings (relative to double glazing) are 15 to 48 $kBtu/ft^2$ yr for glazings with suspended plastic films and low-e or, in some cases, antireflectance coatings. Further savings of approximately 10 to 20 $kBtu/ft^2$ yr are possible, particularly for south glazings, with the use of low-iron glass and a low-conductance gas fill. For an evacuated glazing, predicted net energy savings are 51 to 67 $kBtu/ft^2$ yr, which is superior to savings with all other glazing types analyzed and approximately three to five times better than with other glazing types that do not require the use of suspended plastic films.

2.1.1.1 Seasonal Performance of Advanced Glazings

Several energy-efficient glazings are available with thermal performances superior to that of typical double glazing. The superior insulating values are achieved with the use of low-e coatings, additional interpane spaces (created by additional glass panes or plastic films that could have low-e or antireflecting coatings), and/or low-conductance fill gases. Several of these measures involve a reduction in solar transmittance and hence a tradeoff between improved R-value and reduced solar heat gains. On the other hand, the solar transmittance of windows can be increased by use of low-iron glass and/or antireflectance coatings.

Glazing characteristics such as the overall heat-transfer coefficient and shading coefficient are often available from the manufacturer or can be calculated (Arasteh et al. 1986). Based on such values, performance at winter or summer design conditions can be determined. Seasonal performance can be estimated from glazing characteristics in a manner analogous to calculations for solar collectors (Harrison and Barakat 1983), but this approach requires an assumption of heating season length and does not account for the degree of thermal storage in the building. Hourly simulations can be used to include these aspects of building performance (Rubin and Selkowitz 1981), and correlation methods based on hourly simulations have been developed. However, these simulations have been limited to a few standard glazing types such as single, double, or triple glazing with or without night insulation (Balcomb et al. 1984). In this report, a simple method has been used to extend SLR calculations to nonstandard glazing types.

2.1.1.2 Analytical Approach

Glazings can be characterized in terms of overall heat-transfer coefficient (U) and shading coefficient (SC). For a given area (A), heat loss is proportional to UA. The SC, as defined by the American Society of Heating,

Refrigerating and Air-Conditioning Engineers (ASHRAE), is the ratio of the solar heat gain through the glazing (including the fraction of solar radiation absorbed in the glazing that is subsequently transferred into the room) to the solar heat gain through single glazing. The SC can be thought of as an effective transmittance relative to single glazing.

The method described in this paper is based on the following premises for direct gain buildings:

- o A change in the UA of the glazing is indistinguishable from a similarly sized change in the overall building UA.
- o A change in the SC of the glazing is indistinguishable from a similarly sized change in the window area or the transmitted solar gains.

Hence, nonstandard glazing types can be analyzed with the monthly SLR method or with the annual load collector ratio (LCR) method by using modified building and climate parameters to account for differences from standard glazing properties. This section presents the modifications necessary to enable use of this approach with the fast solar load ratio (FSLR) method developed by Wray (1983).

This approach depends on the assumption that glazing performance can be adequately based on U and SC. The validity of using constant Us and SCs to estimate seasonal glazing performance has been confirmed by comparison with detailed hourly calculations (Arasteh et al. 1986). To account for variation in solar transmittance at off-normal incidence angles, SCs could be based on average incident-angle transmittances or on a more detailed optical analysis (see Section 2.1.5). Some effects are not accounted for in this approach [or in some hourly simulations such as DOE-2 (anon., 1989) and SERIRES (Palmiter, 1988)]: (1) effects of the infrared coupling between the inner surface of the glazing and other building interior surfaces and (2) effects of mean radiant temperature on occupant comfort.

2.1.1.3 The Fast Solar Load Ratio (FSLR) Method

The following relationships are used in the FSLR method:

$$Q_{aux} = Q_L(1 - SHF_Y) \tag{2-1}$$

$$Q_L = (BLC + G*A_s)DD_Y \tag{2-2}$$

$$SHF_Y = (1 - e^{-SLR_m})\ (1 - a\ e^{-SLR_m}) \tag{2-3}$$

$$SLR_m^* = [F*(VT_s/DD)_m*\alpha]/(LCR + G)\ , \tag{2-4}$$

where

Q_{aux} = auxiliary heating (Btu/yr)

Q_L = building heating load (Btu/yr)

SHF_Y = annual solar heating fraction (i.e., the fraction of the building's annual heating energy supplied by solar gain through fenestration)

BLC = building load coefficient (Btu/°F day), not including $U*A_s$

G = effective glazing conductance (Btu/°F day ft^2)

A_s = south glazing area (ft^2)

DD_Y = annual heating degree days (°F day), based on the balance point temperature T_b

a = location-dependent correlation factor

SLR_m^* = scaled solar load ratio for the month with minimum SHF

F = system-dependent scale factor

$(VT_s/DD)_m$ = ratio of monthly solar radiation transmitted through vertical south glazing to monthly degree days (Btu/ft^2 °F day), for month with minimum SHF

α = effective solar absorptance

LCR = load collector ratio (BLC/A_s).

The parameters a, F, G, and α were determined from hourly simulations and tabulated (Wray 1983).

2.1.1.4 Modified Parameters

To extend the FSLR method for additional glazing types, modified input parameters are used to account for the new glazing properties U' and SC' (where U and SC are properties of the reference glazing type; i.e., double glazing). Four modified parameters are to be used in Eqs. 2-2 through 2-4:

$$G' = G - 24(U - U') \tag{2-5}$$

$$(VT_s/DD_m)'' = (VT_s/DD_m)' \ (SC'/SC) \tag{2-6}$$

$$DD_Y' = DD_Y \text{ based on } T_b' \tag{2-7}$$

$$a' = \text{the correlation factor "a" based on } T_b' \ , \tag{2-8}$$

where

$$(VT_s/DD_m)' = (VT_s/DD_m) \text{ based on } T_b'. \tag{2-9}$$

Values for DD_Y', a', and $(VT_s/DD_m)'$ can be determined from tabulated FSLR data by interpolation based on the modified balance point temperature:

$$T_b' = T_{set} - \frac{Q_{int} + VT_n \ A_n SC'}{BLC + G'A_s - 24(U - U')A_n} \ , \tag{2-10}$$

where

Q_{int} = internal heat gains from appliances, people, etc. (Btu/day)

T_{set} = thermostat heating set point (°F)

VT_n = monthly solar radiation transmitted through vertical north glazing (Btu/ft^2 month)

A_n = north glazing area (ft^2).

2.1.1.5 Glazing, Climate, and Building Data

Glazing characteristics are shown in Table 2-1. U-values and SCs shown in the first and second data columns are for standard soda-lime glass double glazing with an air gap. The U-values shown in the third data column are for the same window with a krypton gas fill. The SCs shown in the fourth data column are for low-iron glass. In all cases, the gaps between panes are assumed to be 0.5 in.

Climate characteristics for Portland and Boise are extracted from tabulated FSLR data (Wray 1983).

Building characteristics include T_{set} = 70°F, Q_{int} = 50,000 Btu/day, and A_n = 50 ft^2. The conventional BLC value of 10,800 Btu/°F day is representative of a residential building of approximately 1500 ft^2. The passive solar BLC is 8400 Btu/°F day and the superinsulated BLC is 6000 Btu/°F day. The passive

Table 2-1. Glazing Characteristics

Glazing Type	U	SC	U^k	SC^l
1.‡ g-g	0.50	0.88	0.46	0.94
2. g-eg	0.34	0.77	0.27	0.82
3. g-ep-g	0.24	0.67	0.20	0.71
4. g-ep-ep-g	0.15	0.60	0.11	0.63
5. g-a-g	0.34	0.85	0.30	0.91
6. g-a-a-g	0.26	0.82	0.23	0.88
7. g-v-eg*	0.10	0.82	--	--

U-value units are Btu/h ft^2 °F; to convert to W/m^2 K, multiply by 5.68.

g = glass (1/8 in. thick)

e = low-e coating on glass (eg) or plastic film (ep) with low-e coating on inside surface (emittance = 0.15)

a = plastic film with antireflectance coatings on both surfaces

v = vacuum

l = low-iron glass (1/8 in. thick)

k = krypton gas fill in place of air

* estimated characteristics for vacuum glazing (with borosilicate glass)

‡ numbers 1 through 7 refer to labeled points on the horizontal axes of Figures 2-1, 2-2, and 2-3.

solar south glazing area is 200 ft^2. The conventional and superinsulated south glazing areas are 50 ft^2. The passive solar value of F corresponds to a recommended level of storage mass (6 ft^2 of 4-in.-thick concrete or its equivalent per ft^2 of south glazing). The conventional and superinsulated values of F correspond to the mass of drywall and lightweight building materials relative to 50 ft^2 of south glazing.

2.1.1.6 Results and Discussion

Glazing performance is shown in terms of

- o Net useful flux (per ft^2 of glazing) calculated as the difference in auxiliary energy use with and without the glazing (indicates the absolute energy value of glazing)
- o Net energy savings (per ft^2 of glazing) calculated as the difference in net useful flux for the particular glazing vs. double glazing (indicates the incremental energy value vs. conventional double glazing).

Figure 2-1 shows net useful flux per ft^2 of glazing in Portland and Boise. For north glazing net useful flux is virtually identical regardless of building type. For south glazing, the trends in net useful flux are similar for all building types (i.e., the curves are approximately parallel) and the levels of net useful flux depend on building type.

Figure 2-2 shows net energy savings (relative to double glazing). For south glazings in Portland (Figure 2-2a), net energy savings are lower in the passive solar building (by less than 10%) compared to the conventional building. Net energy savings in the superinsulated building compared to the conventional building are slightly higher for glazings with low-e films and slightly lower for glazings with antireflectance films. For north glazings in Portland (Figure 2-2b), net energy savings are insensitive to building type, except that savings are slightly lower for the passive solar building. For south glazings in Boise (Figure 2-2c), net energy savings show a complex dependence on building type and glazing type. For north glazings in Boise (Figure 2-2d), net energy savings are approximately 15% lower in the passive solar building than in the other building types.

The use of different kinds of glass and fill gases affects the window performance. Figure 2-3 shows the effects of low-iron glass and low-conductance gas fill, singularly and together, in the conventional building in Portland, the conventional building in Boise, and the passive solar building in Boise. In Portland, the results for the solar building (not shown) are virtually identical to the conventional building results. In all cases, the savings for the combination approximately equal the sum of the savings for low-iron glass and the savings for gas fill separately. For north glazings, most of the savings result from the gas fill. For south glazings in the conventional building in Portland and the passive solar building in Boise, the savings owing to low-iron glass and the savings owing to gas fill are approximately equal. For south glazings in the conventional building in Boise, the savings are greater than in other building types and climates, and savings resulting from low-iron glass are greater than savings resulting from gas fill. The increase in savings is especially large for the second glazing type, i.e., with low-e coating on the glass.

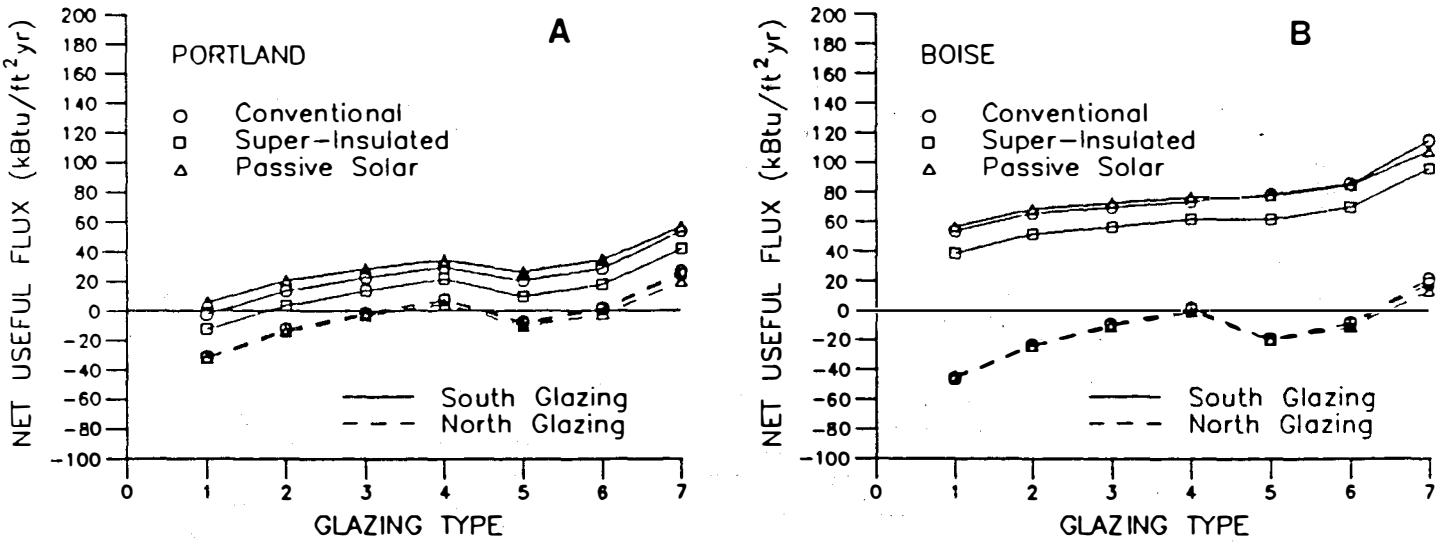

Figure 2-1. Net useful flux for glazing types described in Table 2-1 for three building types (to convert from kBtu/ft^2 yr to kWh/m^2 yr, multiply by 2.72)

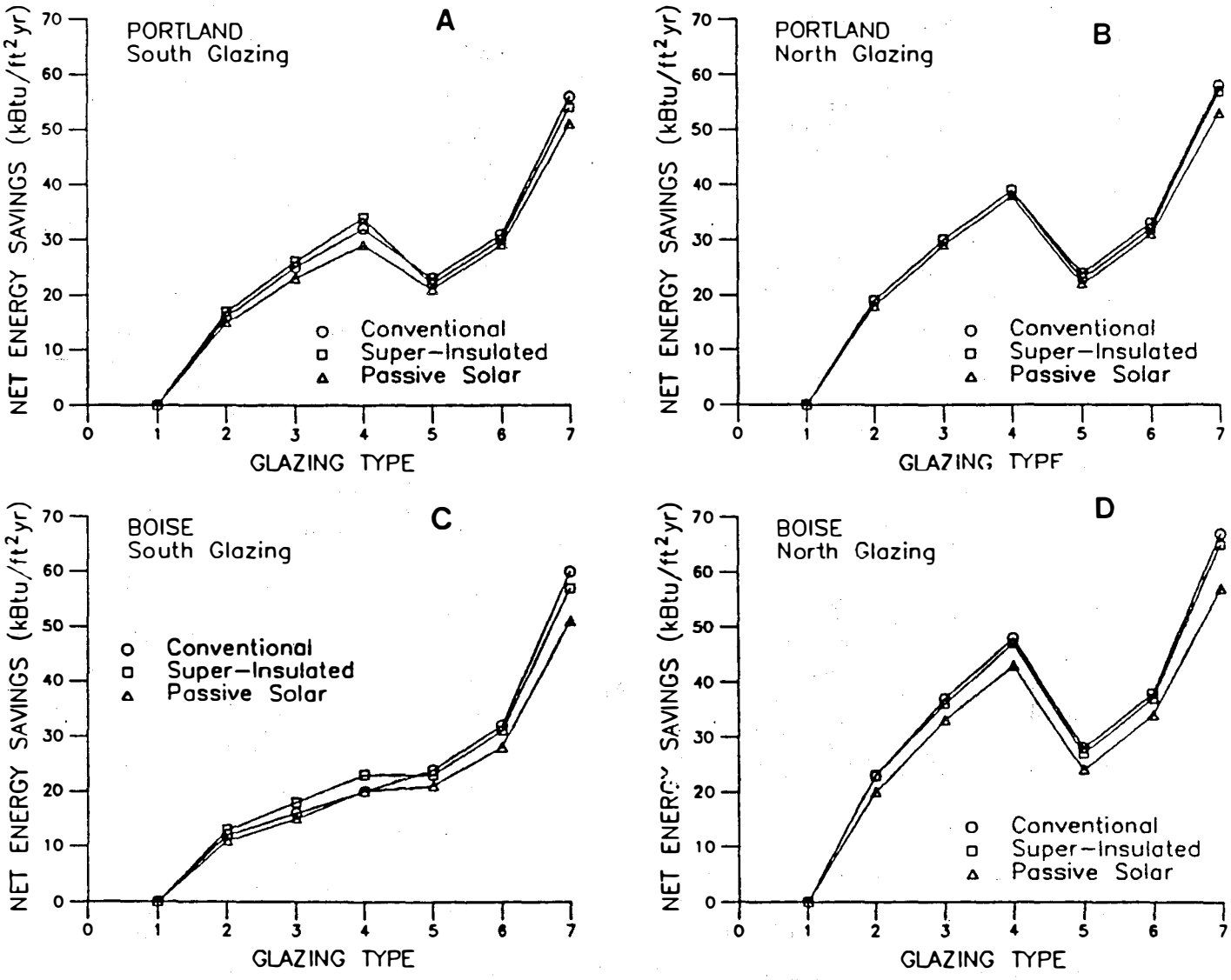

Figure 2-2. Net energy savings (relative to double glazing) for glazing types described in Table 2-1 for three building types

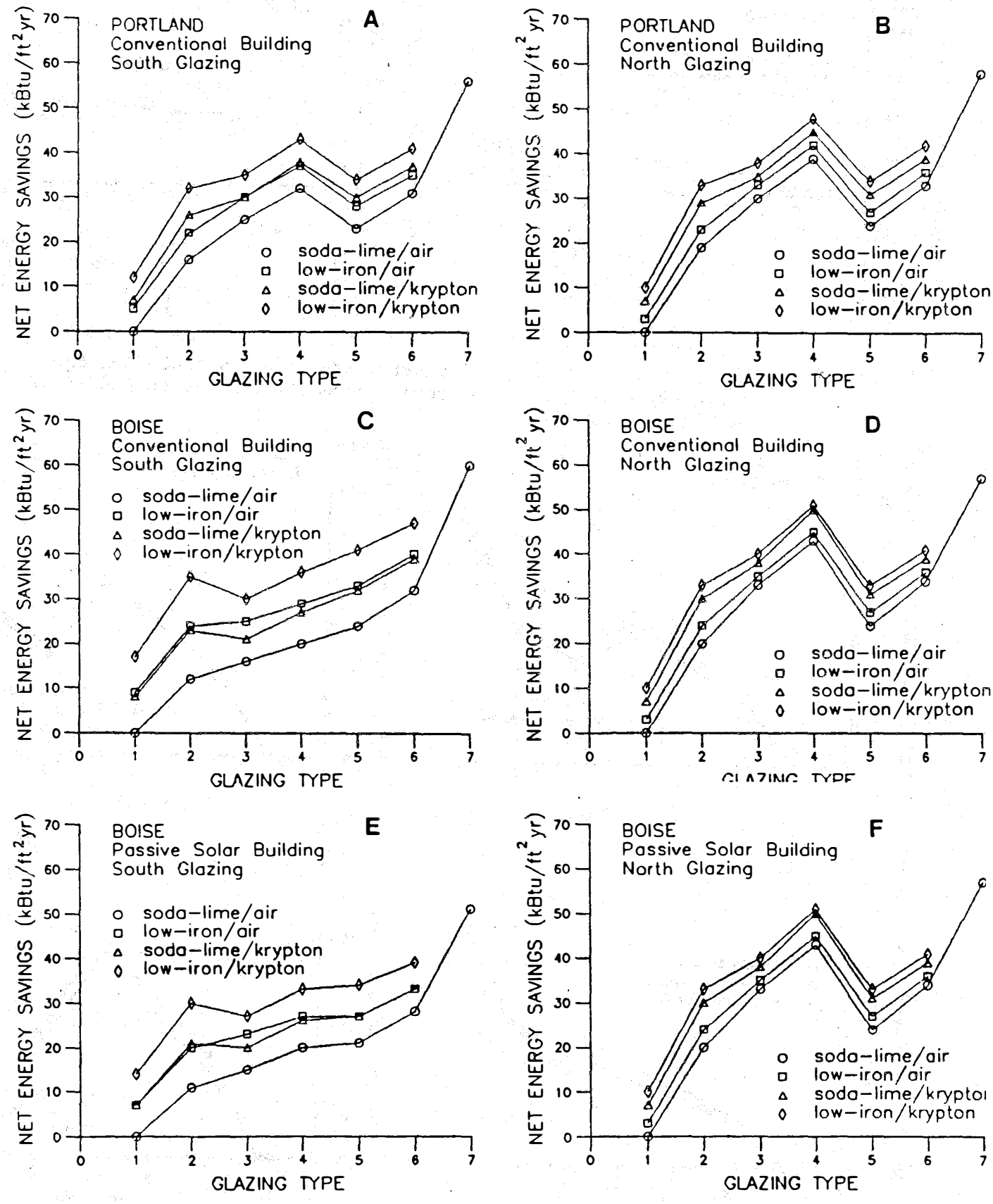

Figure 2-3. Net energy savings (relative to double glazing) for glazing types described in Table 2-1 for four combinations of glass type and fill gases

2.1.1.7 Conclusions

Nonstandard glazing types in direct-gain buildings can be analyzed with SLR methods by using modified building parameters to account for differences from standard glazing properties.

For glazings with suspended plastic films and low-e or, in some cases, anti-reflectance coatings, net energy savings (relative to double glazing) are 15 to 48 kBtu/ft^2/yr, depending on building type and glazing orientation. Further savings of approximately 10 to 20 kBtu/ft^2/yr are possible, particularly for south glazings, with the use of low-iron glass and a low-conductance gas fill. Predicted savings for an evacuated glazing are 51 to 67 kBtu/ft^2/yr, superior to all other glazing types analyzed and approximately three to five times better than other glazing types that do not incorporate suspended plastic films. Table 2-2 summarizes comparisons for conventional buildings.

Table 2-2. Summary of Predicted Net Annual Energy Savings vs. Standard Double Glazing in a Conventional Building (kBtu/ft^{2}yr)

	Portland		Boise	
Glazing Type	South Glazing	North Glazing	South Glazing	North Glazing
g-g	--	--	--	--
g-eg	16	19	12	23
g-ep-g	25	30	16	37
g-ep-ep-g	32	39	20	48
g-a-g	23	24	24	28
g-a-a-g	31	33	32	38
g-v-eg*	56	58	60	67

g = glass (1/8 in. thick)

e = low-e coating on glass (ep) or plastic film (ep) with low-e coating on inside surface (emittance = 0.15)

a = plastic film with antireflectance coatings on both surfaces

v = vacuum

l = low-iron glass (1/8 in. thick)

* estimated characteristics for vacuum glazing (with borosilicate glass)

note: 1 kBtu/ft^{2}yr = 11.35 MJ/m^{2}yr

Net energy savings (relative to double glazing) for south glazing in Boise are lower than for north glazing in Boise or for either orientation in Portland.

Net energy savings for south glazing in Boise are more sensitive to building type, and the pattern of energy savings among glazing types is different.

2.1.2 Energy Savings Projections for the Pacific Northwest

2.1.2.1 Residential Savings

The primary market for vacuum glazing will be for residential use. The square footage of existing residential windows in the BPA area is an estimated 800 million square feet (1987 figures). (The total number of households in the area in 1987 was 3.3 million; these residences include approximately 78% single-family homes, 14% multi-family homes, and 8% manufactured homes [BPA 1988].) The national average single-family home is 1,870 ft^2 (174 m^2), the average multi-family home is 920 ft^2 (85 m^2) (Biggers U.S. Census Bureau 1987), and the manufactured home is approximately 500 (46 m^2). We assumed that window area roughly equals 15% of the floor area.

The energy savings that would result if all existing windows were replaced with vacuum glazing systems was estimated by the following equation.

$$Q = (1/R_o - 1/R_n) * A_w * DD * 24 / 10^{15}) \qquad (2\text{-}11)$$

where

R_o = R-value of original windows (h-ft^2-F/Btu)

R_n = R-value of new windows (h-ft^2-F/Btu)

A_w = Area of windows (square feet)

DD = Heating degree days per year, base 65°F (F-days/yr)

Q = Savings during the heating season (QBtu/yr)

24 = Conversion factor (hours/day)

10^{15} = Conversion factor (QBtu/Btu)

The average R-value of the existing windows was estimated as R-1.2 h-ft^2-F/Btu (R-0.21 m^2-°C/W; U-4.7 W/m^2-°C) (averaging U-values). This assumes that the relative number of high-performance windows is negligible, that half of the existing windows have insulated glazing, and that the other half have only single-pane glazing. The average R-value of the new vacuum glazing window assemblies was projected to be R-9.3 hr-ft^2-°F/Btu.

The number of heating degree days (°F-dzy) per year in the region's more populated cities ranges from approximately 4424 in Seattle, Washington, to 8760 in Idaho Falls, Idaho. A population-weighted average of the major cities in the Pacific Northwest gives approximately 5500 degree days per year. Using this as a representative figure for the heating climate, the potential savings from replacing all residential windows with vacuum glazing systems amounts to 0.08 quad/yr (84 PJ/yr).

This estimation of potential energy savings (unlike the more detailed estimates of Table 2-2) does not include the effects of solar gains. It neglects the changes in solar gains (resulting from replacement of double-pane glazing with vacuum glazing) during the heating season and assumes that

residential air conditioning systems are not a significant contributor to the total residential space conditioning energy budget.

If the energy savings is calculated only for the projected new building market between 1990 and 2010 (assuming 1987 projections), the average end-use energy savings over that period will be 0.0008 Quad/yr (0.84 PJ/yr), assuming all homes would otherwise be built with insulated glazing systems and assuming BPA's projected (1988) quantity and percentages of housing stock for the year 2010 (4.8 million units: 70% single-family units, 18% multi-family units, and 12% manufactured homes) with an estimated 15 million ft^2 (1.4 m^2) new windows installed each year. This savings is the equivalent of 0.04 power plants not added to the capacity each year.

For the cooling season, the energy savings is relatively small. The low-emissivity coating on the vacuum glazing will significantly reduce radiative heat gains; however, standard insulating glazings can also incorporate low-e coatings, so this effect cannot be considered in a comparison. The temperature difference between the inside and outside is relatively small during the cooling season compared to that of the heating season, so the number of cooling degree days is small. Furthermore, even in mechanically cooled residences, much cooling is accomplished passively by opening windows. For these reasons, possible energy savings resulting from reduced cooling requirements were not included in this analysis.

Besides energy savings, occupant comfort in these spaces will be enhanced year around, because the higher resistance across the glazing allows for a temperature on the interior surface of the glazing that is nearer to the room temperature.

2.1.2.2 Commercial Savings

The benefits of the vacuum window are clear for the residential market. The window's value to the commercial market is less obvious; however, small commercial buildings of lightweight construction will also benefit.

Effect During Heating and Cooling Seasons. In large commercial buildings, the heating season is shorter because of greater internal heat gains from occupants, lighting, and appliances and equipment. These gains effectively lower the building's balance temperature (the point at which the heating system is switched on) during the daytime and therefore shift the loads--from daytime to nighttime and from heating to cooling. The heating season for commercial buildings is about three months long and generally during unoccupied hours only, compared to the residential heating season of nearly nine months, 24 hours per day. This shorter heating season would appear to reduce the economic value of the vacuum glazing during the nominal heating season.

The internally generated load does not usually offset the heating requirements of the perimeter zones, because the heat exchange between the interior and perimeter zones is minimal. Typically, excess heat from the interior zone is released to the outside, and heating requirements in the perimeter zones are satisfied by additional heating, ventilating, and air conditioning (HVAC) equipment. This complex problem is difficult to quantify and can only be addressed in a building simulation program for a large commercial building, a

program in which parametric runs of conventional and vacuum windows could estimate the relative benefit of the vacuum glazing's insulating qualities in typical buildings in various climates. The effect of the vacuum glazing in large commercial buildings during the cooling season is similar to that in residential buildings.

Effect on Human Comfort. Another issue that must be addressed while considering the value of an energy-saving retrofit is human thermal comfort. Human comfort in the perimeter zones of a large commercial building is greatly influenced by the conductivity of a nearby window. This is true not only in the winter when the interior glazing surface is cold, but in the summer as well. The comfort of an occupant working near a window strongly affects his or her productivity. Although it is difficult to quantify, it has been estimated that employee productivity is 100 times more valuable than the cost of the energy required to maintain a comfortable environment (Selkowitz 1985). The interior surface of a vacuum window would maintain a more constant temperature, thereby providing a more comfortable environment and reducing losses in employee productivity.

Effect on HVAC Equipment Needs. To combat heat loss in the perimeter zones, specialized heating equipment is necessary. Electric baseboard heating is often used because the units are easy to install and require no additional mechanical systems; the unit cost is $1.80 per square foot of floor area (Means 1984). Electric systems are, however, the most costly sources of heat energy. If both the initial cost of this equipment and the heating energy cost are taken into account the initial cost of the vacuum window would be offset and the payback period reduced.

Effect on Architectural Design. Because the vacuum window has an R-value comparable to the walls of a large commercial building, larger areas of glazing could be used on the exterior without effecting the building's thermal performance. This would give architects more flexibility in designing the aesthetic features of a large building.

2.1.2.3 Summary of Savings Projections

An estimated 0.08 quads of energy per year (84 PJ) could be saved in residential buildings during the heating season. Residential cooling and commercial heating/cooling were not considered in this estimate for reasons stated above.

Cost savings to the consumer will be achieved by energy and demand savings. Large commercial users will save money because of the improved ability to control perimeter temperatures and because the size of heating equipment needed to offset window heat losses will be reduced. Another effect is that architectural design of large buildings can include more glazing without incurring significantly greater heating/cooling costs.

2.1.3 Economic Considerations

Once preprototypes have been fabricated and are shown to perform well, the questions of practicality and marketability will remain. These questions concern the issue of market value vs. cost, neither of which has been analyzed adequately. In this section, preliminary analyses of this marketability issue are presented.

The value of a highly insulating window is fourfold:

- o Reduced heat loss
- o Useful solar heat gain
- o Increased comfort near windows
- o Increased architectural design freedom.

Reduced heat loss is important in cold climates and is an important attribute for windows having any orientation--north, south, east, or west. The amount of heat lost is

$$\text{LOSS (Btu/yr)} = 8766\overline{\Delta T}\ AR\ , \qquad (2\text{-}12)$$

where $\overline{\Delta T}$ is the average temperature difference between indoors and outdoors (positive differences only)* in °F, A is the window area (ft^2), R is the area-averaged thermal resistance of the window (°F h ft^2/Btu), and 8766 is the number of hours per year. By substituting a higher resistance window the loss is reduced:

$$\text{SAVINGS (Btu/yr)} = \text{LOSS}(R_o) - \text{LOSS}(R)$$

$$= 8766\ \overline{\Delta T}\ A\ \left(\frac{1}{R_o} - \frac{1}{R}\right)\ . \qquad (2\text{-}13)$$

The value of the energy savings depends on fuel costs. Table 2-3 shows energy savings and cost savings per unit window area. The value of energy saving per unit window area (assuming a $10/million Btu delivered cost of heating energy) is the same number in cents per square foot per year as the number of kBtu/ft^2 saved each year. An R-value of 1°Fhr/ft^2/Btu is typical of a single sheet of glass; R = 2 is typical of a conventional double-glazed sealed insulating glass unit; R = 3 to 4 is typical of a double-glazed sealed insulating glass unit with a low-emissivity coating. An R ≈ 10 is the expected area-averaged insulating value of a prototype vacuum window.

The likely substitutions are R10 for R3 or R2, which would have incremental annual benefits ranging from 22¢/ft^2 yr to 96¢/ft^2 yr depending on the severity of the heating season. This analysis accounts for only decreased thermal loss, whereas useful solar gain and other comfort benefits must also be considered in the total benefits equation.

Useful heat gain is dependent on both climate and window orientation. If $\bar{H}$ is the solar insolation incident on a window averaged over the heating season, then the useful solar gain can be expressed as

$$\text{GAIN (Btu/yr)} = 8766\ F\ \bar{H}\ A\ , \qquad (2\text{-}14)$$

where F is the average fraction of incident solar insolation that is transmitted/conducted through the window, A is the area of the window (ft^2), $\bar{H}$ is expressed in Btu/ft^2 h, and 8766 is the number of hours per year.

---

*The average annual temperature difference between indoors and outdoors (positive difference only) is reported by the U.S. Weather Service as the difference between 65°F and the mean daily ambient temperature, with positive values only included in the compilation. This value is reported as the annual average number of degree days for specific locations.

Table 2-3. Incremental Energy and Cost Savings

Window Area-averaged R-Values °F h ft^2/Btu	Energy saved per ft^2 of window each year--kBtu/ft^2 yr (cents saved per square foot each year--¢/ft^2 yr*) DD-Heating Degree Days (°F day/yr) 4000 DD$^+$	6000 DD$^+$	8000 DD$^+$	10000 DD$^+$
$R_o \rightarrow R^‡$				
1 → 2	48	72	96	120
2 → 3	16	24	32	40
3 → 4	8	12	16	20
4 → 5	4.8	7.2	9.6	12
5 → 10	9.6	14.4	19.2	24
3 → 10	22	33	44	55
2 → 10	38.4	57.6	76.8	96

*The savings per year is estimated for an assumed energy cost of $10/MBtu.

$R^‡$ - insulating value of window being replaced or substituted.

R_o - insulating value of incrementally superior window.

DD$^+$ - annual heating degree days is defined as the annual sum of positive temperature differences between 65°F and the mean daily ambient outdoors temperature over the entire year (with only the positive differences included).

A solar efficiency can be defined for a window as

$$\text{EFFICIENCY} = \frac{\text{GAIN - LOSS}}{\text{INCIDENT}} = \frac{8766\ (F\ \bar{H}A - \overline{\Delta T}\ A/R)}{8766\ \bar{H}A}$$

$$= F - \left(\frac{\overline{\Delta T}}{\bar{H}}\right)\frac{1}{R}\ , \qquad (2\text{-}15)$$

where the ratio $\overline{\Delta T}/\bar{H}$ may be thought of as an indicator of the severity of the climate for that location and window orientation (Harrison and Barakat 1983; Neeper 1985). Figure 2-4 shows this function plotted for several types of windows including the prototypical vacuum window and for an opaque R = 11 wall where F 0. The climate severity scale is annotated with typical locations and orientations representative of the United States. Note that the vacuum window is predicted to provide a net annual useful solar gain over the entire spectrum of conditions including north-facing windows in locations like Caribou, Maine, and that the vacuum window is predicted to be superior to all common types of commercially available windows in all climates except the very mildest where insulating windows are not needed.

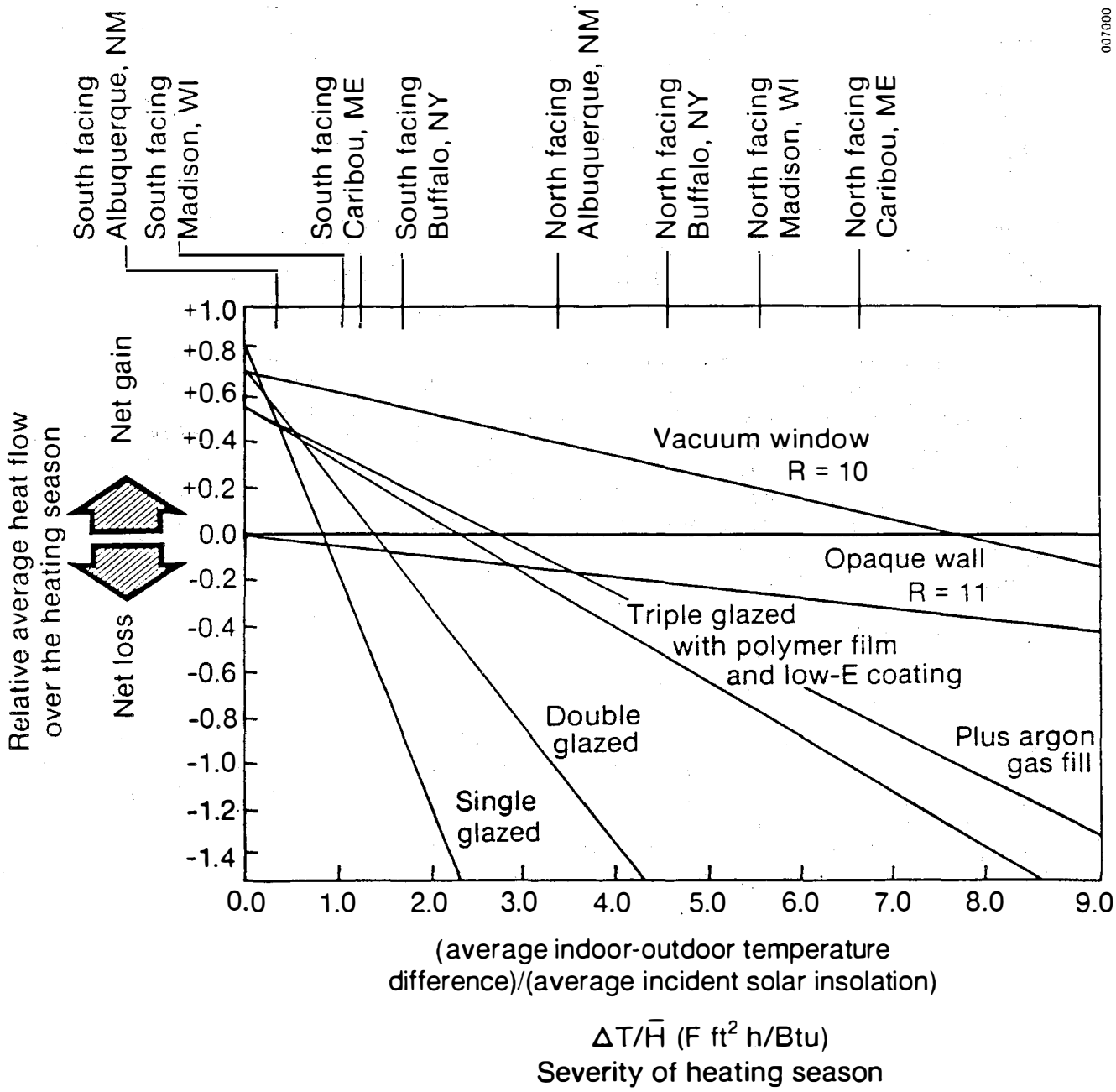

Figure 2-4. Comparison of predicted window efficiencies for a range of climates

Increased comfort is another valuable benefit of a highly insulating window. During cold weather, a poorly insulating window has a cold interior surface. Cold, convective drafts from this surface commonly make the floor area near such a window uncomfortable. People near a cold window also feel a general chilling because of their radiative heat loss to the window. Because a highly insulating window will always have an inside surface temperature closer to the indoor air temperature, it will provide greater comfort by reducing these two effects.

Expensive insulating draperies and electric room-perimeter heaters are often used to offset the effects of cold drafts and radiative losses to windows. A highly insulating window should be credited for making these expenses unnecessary.

Increased design freedom not only is an important aesthetic benefit of insulating windows but may also improve the economics of housing. If architects/developers have highly insulating windows available, they might be able to orient windows to take advantage of daylighting, passive solar heat, and aesthetics. Because they will be able to use larger window areas without fear of creating uncomfortably cold spaces nearby, they might design a building with a larger share of the daylighting and heating requirements met by the windows. In addition, they might be able to make more flexible and economical use of available land.

2.1.4 Window Frames

2.1.4.1 Objective of Frame Analyses

As advances continue in the thermal performance of glazings, such as the development of vacuum glazings, it is important to consider the thermal performance of frames and their various effects on overall window performance. The objectives of this section are to (1) review and modify computer simulation algorithms for overall window performance and (2) investigate the effect of frame design on the performance of window assemblies with vacuum glazing.

2.1.4.2 Background

Glazings. Numerous advances in glazing systems have significantly increased their thermal performance. These advances include glass-coating technology, the use of low-conductivity gases or transparent insulating materials within insulated glass cavities, and evacuated gaps. The thermal performance of glazings is generally measured through the center-of-glass where heat flow can be accurately represented as one-dimensional, traveling from the warm side to the cold side in a direction perpendicular to the glass panes.

Currently available glazing systems have R-values ranging from below R-1 up to R-10 hr-ft^2-^{o}F/Btu (1.76 m^2-^{o}C/W). Single pane glazings have a center-of-glass resistance of approximately R-0.87 h-ft^2-^{o}F/Btu (0.15 m^2-^{o}C/W), primarily because of the air films along the inner and outer surfaces of the glazing. Double-pane glazings have twice the resistance, approximately R-2 h-ft^2-^{o}F/Btu (0.35 m^2-^{o}C/W), primarily from the air films plus the layer of still air sandwiched between the two glazings. Further improvements in glazing design reduce thermal radiation by adding low-e film coatings to one

or more glass surfaces. Low-e glazings in double-pane systems achieve center-of-glass resistances of R-2.5 to R-3.1 h-ft^2-^{o}F/Btu (0.44-0.955 m^2-^{o}C/W). With additional glass panes or polymer films, the center-of-glass R-value reaches R-5 h-f5^2-^{o}F/Btu (0.88 m^2-^{o}C/W), but with a sacrifice in solar transmittance. Other improvements in glazings focus on reducing convective heat losses by replacing the air with other gases. Gases such as argon have lower thermal conductivities, which enables them to better insulate the gap; and they are heavier than air, which reduces their ability to develop convective heat-transfer loops. (A general discussion of currently available glazing systems was given in Section 1.4.)

A transparent, low-density, silica aerogel that has been partially evacuated and sealed within the glazings (Quantum Optics 1988) is predicted to achieve a thermal resistance of R-17.8 hr-ft^2-^{o}F/Btu (3.0 m^2-^{o}C/W) through the center-of-glass. The vacuum glazing under development at SERI is predicted to achieve a thermal resistance of greater than R-16 hr-ft^2-^{o}F/Btu (2.8 m^2-^{o}C/W) through the center-of-glass. It consists of two panes of glass that are held apart by small glass spheres and laser-welded along the perimeter in order to maintain a high vacuum within the glass envelope (see Figure 1-1). Low-e coatings reduce heat transfer from radiation while the high-vacuum/spacer gap virtually eliminates convective heat transfer and keeps conduction to a minimum.

Frames. The window frame commonly accounts for 20% to 30% of the area of the window* and, based on area alone, is a significant contributor to energy loss or gain through the window. Most frames have the thermal resistance of approximately R-2 h-ft^2-^{o}F/Btu (0.35 m^2-^{o}C/W), similar to a standard double-glazing yet far less effective than the adjoining R-13 hr-ft^2-^{o}F/Btu (2.3 m^2-^{o}C/W) wall (standard frame construction with 3.5-in. [89-mm] fiberglass cavity insulation). As glazing performance increases, frames remain the weakest thermal link in the building envelope.

The materials used in the frame, along with its configuration, dimensions, and operational type, affect its thermal performance. Because of complicated configurations and numerous different materials used, it is difficult to rate a frame's thermal resistance. Heat transfer through wood frames can be approximated by one-dimensional flow perpendicular to the plane of the window. (Frame and edge-of-glass heat transfer, discussed below, for such frames were shown to be roughly independent of one another [Arestah, Hartmann, and Rubin 1987]. Low-resistance frames, such as aluminum frames, have two-dimensional flow and tend to further degrade the performance of the glazing because of amplified edge effects [Reilly 1989].)

Residential windows with aluminum frames commonly have values of R-0.5 to R-1 (0.09-0.18 m^2-^{o}C/W); with wood frames their values are R-2.5 hr-ft^2-^{o}F/Btu (0.44 m^2-^{o}C/W) (ASHRAE 1989). More recent innovations in frames use skeletal polyvinylchloride (PVC) or fiberglass for structural support, leaving hollow spaces between the members. Such frames have two advantages. They have

*A typical residential window, as specified by ASHRAE, is 3 ft wide x 4 ft high (0.91 m x 1.22 m). With a 2.7-in. (69-mm) frame, the window has a relative frame area of 25%. Larger windows have a lower percentage frame area.

relatively low thermal conductivities, and they can provide adequate structural support in a thinner profile, which reduces the relative area of the frame and increases the solar transmittance area. The performance of these hollow frames depends on the number, size, and relative positioning of the internal cavities: The more vertical partitions, the lower the effective conductivity of the air enclosures (Carpenter 1987). Such frame structures can be designed with thermal breaks, where a less conductive material breaks the span to impede the flow of heat through the structural members (Arasteh, Reilly, and Rubin 1989). In general, hollow PVC frames are comparable in thermal performance to wood frames.

Hollow frames of this type can be filled with fiberglass or polyurethane foam insulation to further improve their thermal resistance. One study of frames concluded that PVC frames filled with polyurethane foam outperform aluminum, fiberglass (skeletal frame), PVC (skeletal frame), and wood frames (Carpenter 1987). Fiberglass-insulated frames with a calcium carbonate-filled polymer skin also outperform these frames, according to a manufacturer's data (Owens Corning 1988).

A number of vacuum insulations now under development could prove useful in window frame applications, either as insulation filling or as surface covering. Because of the structural requirements of the frame and because the need for operable windows further complicates the structure, the available number of cavities that can be filled with insulation is minimal. Also, there remain many short-circuit heat-flow paths through the structural members. A frame covering, or jacket, of a thin high-R insulation might more effectively reduce conduction through the structural members.

Thermal performance information on frames is very limited and is complicated by the various configurations, thicknesses, and material combinations used in frame construction. It is the focus of current research (Arasteh, Reilly, and Rubin 1989).

Frame/Glazing Interface. The frame/glazing interface includes the edge of glass (the perimeter region between the center of glass and the frame), the spacer (which separates the two glass panes), and the bite (also known as the lip; the portion of the frame that overlaps the glazing). (See the window cross section in Figure 2-5.) As mentioned, the flow of heat is one-dimensional through the center-of-glass and is nearly one-dimensional through some frame types. At the frame/glazing interface, the heat flow deviates from one-dimensional flow. The resistance of the gap between the panes, the conductivity of the spacer, and the extent of the bite interact thermally so that a two-dimensional pattern of heat flow develops in this region. At the corners of the frame the heat flow further deviates into a three-dimensional flow.

Spacer Effects. A continuous spacer is used to separate the panes of glass in typical insulated glazing units. Spacers are commonly made of aluminum in the form of a square channel, as shown in Figure 2-5. The high thermal conductivity of aluminum combined with its thickness perpendicular to heat flow allows significant heat flow through the spacer. Such a spacer creates a thermal short circuit where heat flow that is impeded by the more resistant glazings or frames finds a path through the spacer. Consequently, it is necessary to consider the two-dimensional heat-transfer effect at the edge of the glass and through the spacer. Figure 2-6 shows the direction and

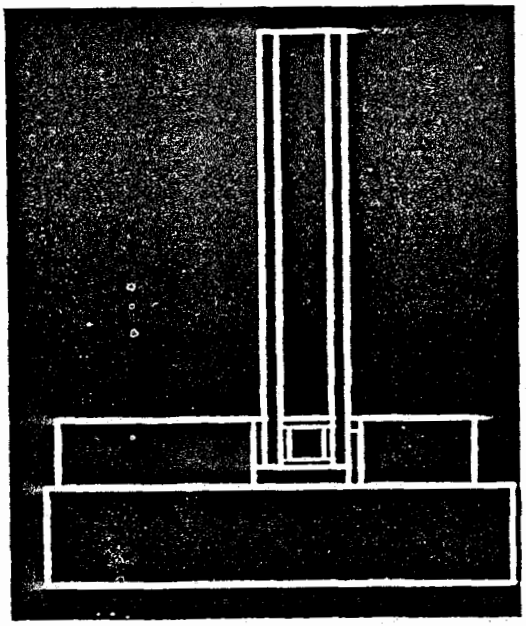

Figure 2-5. Frame/glazing interface

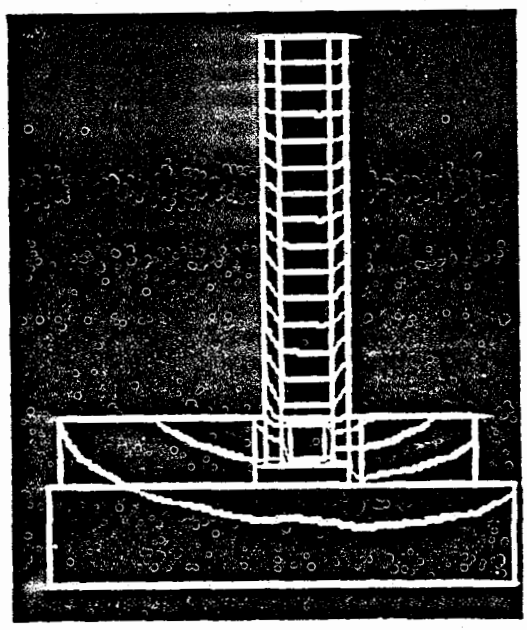

Figure 2-6. Heat flow diverted through a highly conductive spacer (Note: Each contour line represents a heat flux of 0.04 Btu/h-in [0.5 W/m].)

magnitude of heat flow through an aluminum spacer in a window with double-pane glazing and a wood frame. Each line is an adiabat that represents heat flow per unit length of frame (in the third dimension). Heat flow between any two adjacent lines is 0.04 Btu/h-in (0.5 W/m).

Finite difference analyses for standard insulated glass units have shown that two-dimensional heat transfer occurs within a 2.5-in. band around the perimeter of the visible portion of the glazing called the edge-of-glass (ASHRAE 1989).

An extensive study (Carpenter 1987) using a computer simulation of window frames evaluated the effect of spacer types on the overall performance of various window assemblies. The improved spacers were made of low-thermal-conductivity materials and/or constructed with very thin profiles to restrict conduction. The study concluded that an improved spacer such as butyl rubber, fiberglass, or thin stainless steel could reduce the overall window heat loss by 3% to 6% when used with conventional double-pane glazings. The improvement in the thermal performance of windows with high-efficiency glazings is even greater, as much as 12%. The greater improvement in windows with advanced glazings occurs because the greater temperature difference between the inner and outer glazing surfaces magnifies the short-circuit effect of the spacer. (The greater temperature difference is caused by the higher thermal resistance across the gap between panes.)

Bite Effects. The bite is the portion of the frame that overlaps the glazing and holds it in place as shown in Figure 2-5. A larger bite decreases the glazing area exposed to solar radiation. The Carpenter study also evaluated the effect of bite size on frames. He concluded that a larger bite increases the thermal resistance of windows with poor spacers but decreases resistance when an improved spacer is used. The larger bite effectively elongates the heat-transfer path from the warm side of the glazing to the cold side, which dampens the short-circuit effect with a poor spacer.

In summary, the factors that influence overall window thermal performance include the glazing configuration and coatings, the type of gap fill, the materials and configuration of the frame, the type and thickness of the spacer, and the size of the bite. All of these factors must be considered in order to predict the overall performance of a window assembly.

2.1.4.2 Results of Frame Analyses

The developers of the FRAME program report that window manufacturer compared FRAME results with measured results and obtained a high level of accuracy (McGowan 1989). FRAME is based on the Swedish computer program BJ2ST (Jonsson 1985), which was experimentally validated to predict measured R-values within a 10% level of accuracy. Window manufacturers test the thermal performance of their products; however, the results of these tests are usually kept confidential. We obtained proprietary test results for one window assembly, modeled it with the FRAME program, and predicted the test measurements within a 3% margin.

FRAME is a two-dimensional, steady-state, finite-difference computer model for analyzing heat flow in window frames (Carpenter 1987). The modeling method is detailed in Appendix A. Figures 2-7 and 2-8 show the graphic results of the FRAME program. Each contour line or adiabat identifies the direction of heat

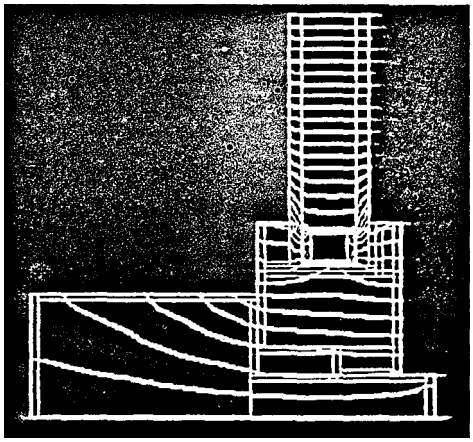

Figure 2-7. Double-pane glazing with aluminum channel spacer and wood frame

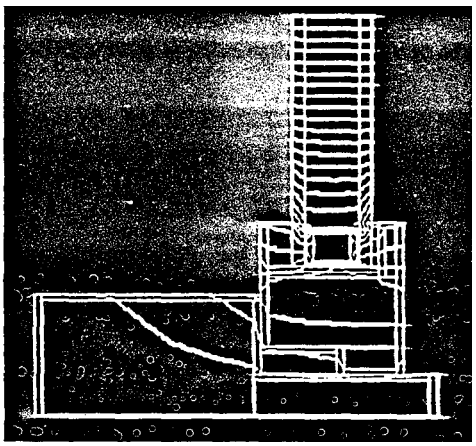

Figure 2-8. Double-pane glazing with aluminum channel spacer and fiberglass-insulated frame

flow through the cross-sectional portion of the window. The increment between the lines represents heat flow of approximately 0.04 Btu/h-in. depth (0.5 W/m depth) (depth means the average of the interior and exterior perimeter distance around the frame). Closely spaced lines indicate a large heat flux; widely spaced lines indicate little heat flux.

Figure 2-7 is the model of the double-pane glazing with an aluminum channel spacer and a wood frame. The figure shows how heat tends to flow along the higher-thermal-conductivity aluminum spacer. A high heat flow occurs at the frame/glazing interface where the thermal short-circuit effect is evident: The heat from the exposed interior glazing surface is directed from the frame to the spacer, and follows the spacer around to the cold exterior side. Farther away from the spacer the one-dimensional nature of the heat flow through the center-of-glass is evident, as the effect of the spacer gradually decreases.

Figure 2-8 shows the identical frame configuration modeled as a fiberglass-insulated frame. As expected, less heat flows through the fiberglass-insulated frame than through the wood frame, although the skin of each frame component conducts a significant amount of heat through the frame. The heat flow through the spacer is virtually identical in the two frames.

Figure 2-9 shows a third type of frame, a wood frame with a thin exterior cladding of compact vacuum insulation (CVI) (Benson and Potter 1989). The frame clearly performs better than the solid wood frame and appears comparable to the fiberglass-insulated frame. The lateral heat flow is impeded by the layer of vacuum insulation on the exterior surface of the frame, so it is diverted through the spacer. Heat crosses the barrier via the metal envelope, flowing along the warm side of the vacuum insulation to reach the cold exterior surface.

The other frames were also modeled with vacuum glazing. Figure 2-11 shows a wood frame coupled with vacuum glazing; Figure 2-12 shows the fiberglass-insulated frame with vacuum glazing; Figure 2-13 shows the wood frame sheathed with vacuum insulation and coupled with vacuum glazing; and Figure 2-14 shows the fiberglass-insulated frame with vacuum insulation cladding.

Comparing these figures with the figures of double-pane glazing, it is evident that the different spacer and different glazing have some effect on the heat flow through both the frames. Note when comparing Figures 2-11 and 2-12 with Figures 2-7 and 2-8 that the high resistance of the vacuum glazing causes more heat to travel through the wood and fiberglass-insulated frames. This effect is not observed with the more resistant vacuum insulation-clad frames. In the windows with aluminum spacers and double-pane glazing, some heat flow through the frames is diverted toward the spacer. This effect is minimal with vacuum glazing.

Figures 2-15 though 2-18 show the same frames modeled with an edge-modified vacuum glazing. The elongated heat-flow path along the edge clearly reduces the amount of heat flow through the edge, as the heat flow through the glass panes begins to level off (become one-dimensional) at a point closer to the edge.

The quantitative results of each modeled window assembly are given in Table 2-4 in terms of the overall window R-value. Results from the FRAME

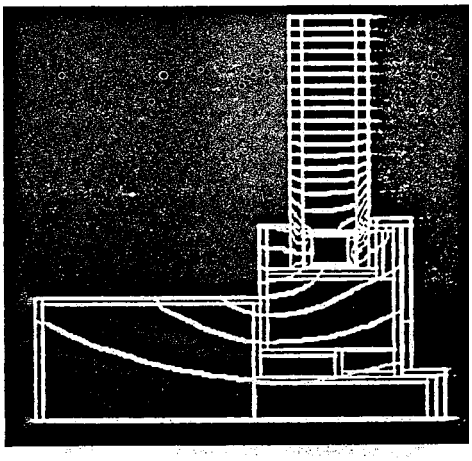

Figure 2-9. Double-pane glazing with aluminum channel spacer and wood frame with CVI cladding

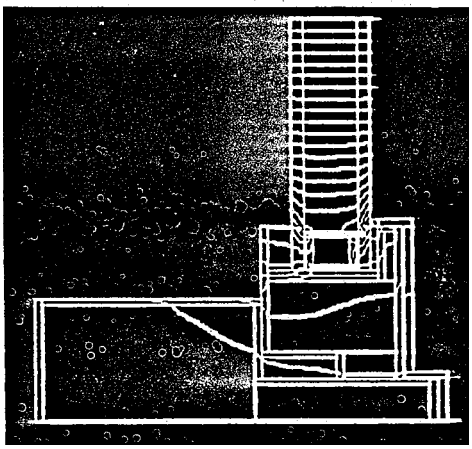

Figure 2-10. Double-pane glazing with glass spacer and fiberglass-insulated frame with CVI cladding

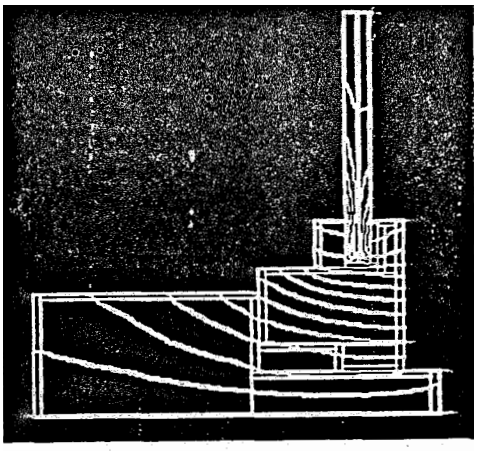

Figure 2-11. Vacuum glazing with glass spacer and wood frame

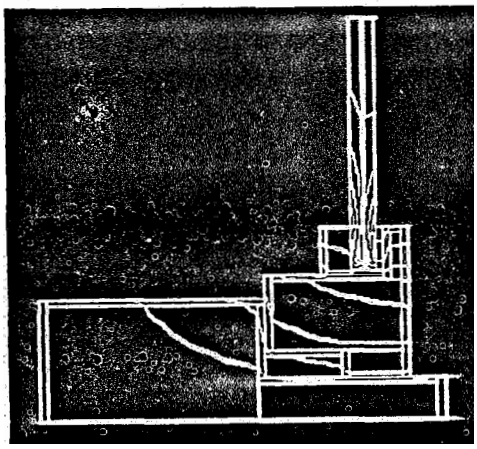

Figure 2-12. Vacuum glazing with glass spacer and fiberglass-insulated frame

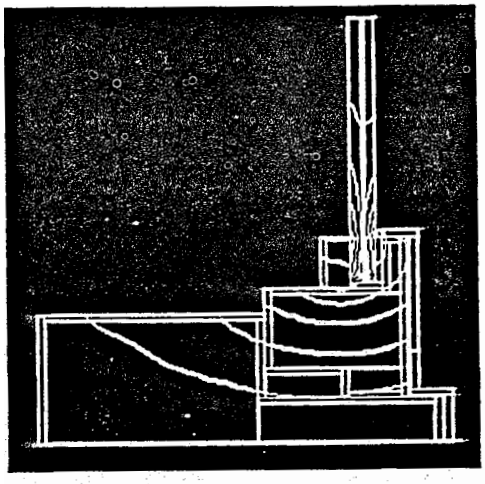

Figure 2-13. Vacuum glazing with glass spacer and wood frame with CVI cladding

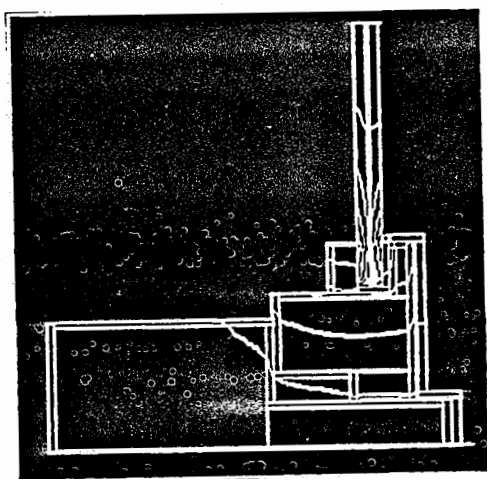

Figure 2-14. Vacuum glazing with glass spacer and fiberglass-insulated frame with CVI cladding

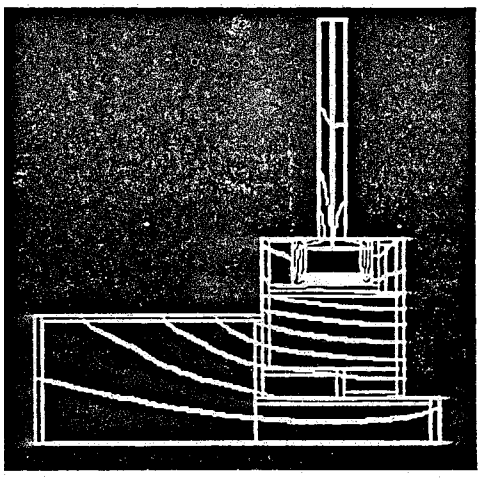

Figure 2-15. Vacuum glazing with modified glass spacer and wood frame

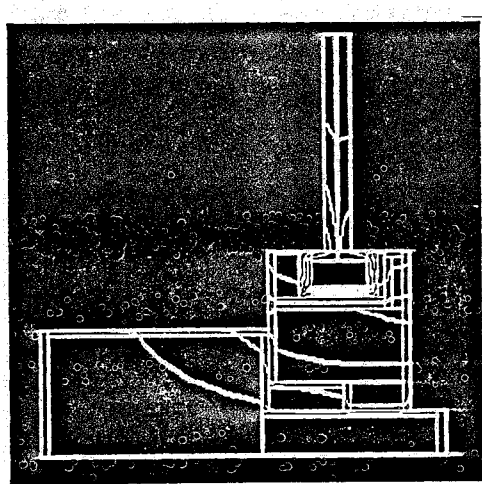

Figure 2-16. Vacuum glazing with modified glass spacer and fiberglass-insulated frame

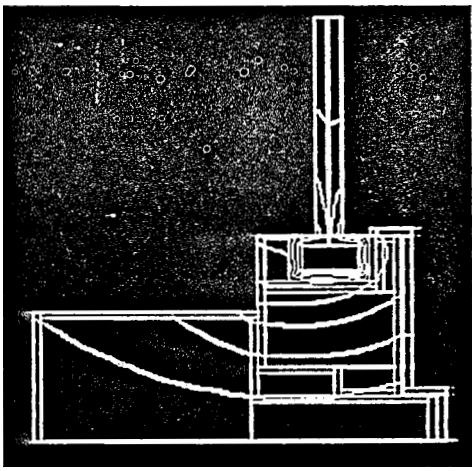

Figure 2-17. Vacuum glazing with modified glass spacer and wood frame with CVI cladding

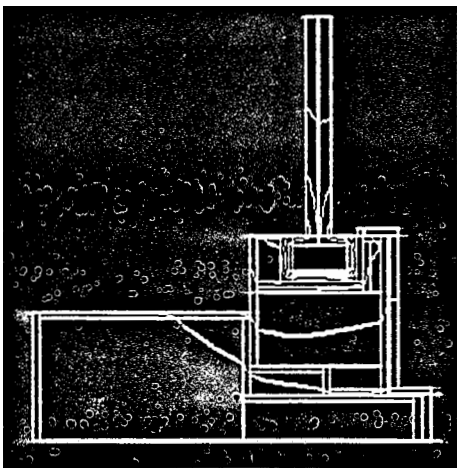

Figure 2-18. Vacuum glazing with modified glass spacer and fiberglass-insulated frame with CVI cladding

Table 2-4a. Component and Overall R-Values (English Units)

Glazing Type Center-of-Glass R-Value ($hr-ft^2-{}^oF/Btu$)	Frame/Spacer Type Frame/Edge-of-Glass R-Value ($hr-ft^2-{}^oF/Btu$)	Overall R-Value
Double-Glazing (R-2.04)	Wood/Aluminum (R-2.03)	2.04
Double-Glazing	Fiberglass/Aluminum (R-2.24)	2.13
Double-Glazing	Wood+CVI*/Aluminum (R-2.33)	2.17
Double-Glazing	Fiberglass+CVI (R-2.42)	2.21
Vacuum Glazing (R-16.00)	Wood/Glass (R-3.66)	6.13
Vacuum Glazing	Fiberglass/Glass (R-4.64)	7.37
Vacuum Glazing	Wood+CVI/Glass (R-5.28)	8.12
Vacuum Glazing	Fiberglass+CVI/Glass (R-5.74)	8.63
Vacuum Glazing (R-16.00)	Wood/Modified-Glass (R-4.27)	6.91
Vacuum Glazing	Fiberglass/Modified-Glass (R-5.35)	8.19
Vacuum Glazing	Wood+CVI/Modified-Glass (R-5.78)	8.67
Vacuum Glazing	Fiberglass+CVI/Modified-Glass (R-6.37)	9.29

Table 2-4b. Component and Overall R-Values (Metric Units)

Glazing Type Center-of-Glass R-value ($m^2-{}^oC/W$)	Frame/Spacer Type Frame/Edge-of-Glass ($m^2-{}^oC/W$)	Overall R-Value
Double-Glazing (0.36)	Wood/Aluminum (0.36)	0.36
Double-Glazing	Fiberglass/Aluminum (0.40)	0.38
Double-Glazing	Wood+CVI/Aluminum (0.40)	0.38
Double-Glazing	Fiberglass+CVI (0.43)	0.39
Vacuum Glazing (2.80)	Wood/Glass (0.64)	1.10
Vacuum Glazing	Fiberglass/Glass (0.82)	1.30
Vacuum Glazing	Wood+CVI/Glass (0.93)	1.40
Vacuum Glazing	Fiberglass+CVI/Glass (1.00)	1.50
Vacuum Glazing (2.80)	Wood/Modified-Glass (0.75)	1.20
Vacuum Glazing	Fiberglass/Modified-Glass (0.94)	1.40
Vacuum Glazing	Wood+CVI/Modified-Glass (1.00)	1.50
Vacuum Glazing	Fiberglass+CVI/Modified-Glass (1.12)	1.60

program are shown. The calculated R-value for the portion of the window that was modeled by FRAME (the edge-of-glass and frame components) can be used in the one-dimensional model described in Appendix A to determine the overall window R-value in conjunction with a given center-of-glass R-value.

The results demonstrate that heat flow through the frame is not independent of the heat flow through the glazing and spacer. They indicate that a greater percentage improvement in overall window performance occurs when an improved

frame is coupled with vacuum glazing. Comparing the advanced frame with the wood frame, a 4% to 8% improvement occurred in the double-pane system. A 20% to 41% improvement resulted in the vacuum glazing system and a 19% to 34% improvement resulted in the edge-modified vacuum glazing unit. The greater percentage increase in the advanced glazing systems is caused by the increase in the inside glazing temperature with better spacer designs.

The welded glass edge of vacuum glazing is a less conductive spacer than the aluminum channel. Three factors influence this: the thermal conductivity of the material, the heat-flow path length, and the cross-sectional area perpendicular to heat flow. For the aluminum spacer each of these factors contributes to heat transfer more than in the glass spacer as shown in Table 2-5.

Table 2-5. Comparison of Welded Glass and Aluminum Channel Spacers

	Aluminum Spacer	Glass Spacer
t	0.07 in. (1.7 mm)	0.12 in. (3 mm)
l	0.5 in. (12.7 mm)	0.02 in. (0.5 mm)
k	1100 Btu-in/h-ft^2-^{o}F (160 W/m-^{o}C)	7.3 Btu-in/h-ft^2-^{o}F (1.05 W/m-^{o}C)
Q/p-ΔT	23 Btu/h-ft-^{o}F (43 W/m-^{o}C)	3.7 Btu/h-ft-^{o}F (6.3 W/m-^{o}C)

t = thickness of the spacer (perpendicular to the direction of heat flow), k = thermal conductivity, l = length of the heat flow path, and Q/p-ΔT = heat flow per degree temperature difference per perimeter distance around the frame.

Table 2-6. Effect of Changed Bite Size

	Resistance h-ft^2-^{o}F/Btu (m^2-^{o}C/W)
Wood Frame with Vacuum Glazing	8.34 (1.47)
10% bite increase	8.65 (1.52)
20% bite increase	8.83 (1.55)
30% bite increase	8.64 (1.52)

The bite size influences the thermal performance of the window. Table 2-6 shows the results of changing the bite size of the window. A 20% increase in bite size is the optimum for the vacuum glazing with the unmodified edge.

2.1.5 Predicting Window Optical Performance

Available methods for estimating the performance of windows are limited but provide adequate estimates for conventional windows. High-technology windows, on the other hand, may not be accurately modeled with these methods. Of particular concern is the spectral selectivity of high-technology windows and the difficulty (or impossibility) of modeling their optical performance with only average values of solar transmittance (or shading coefficient). As the sun angle changes throughout the day and from season to season, the amount of solar energy penetrating a window changes dramatically for several reasons:

- The reflectance of the window changes with the angle of incident solar radiation.
- The spectrum of the incident solar radiation changes with the sun's azimuth angle and with the season and climate.
- The mix of direct beam and diffuse radiation changes with the sun's azimuth angle and the season and climate.
- The spectrum of the direct and diffuse components of the incident solar radiation differ significantly.
- The adjacent ground-plane reflection can provide a large fraction of the total incident radiation, and the spectral reflectance of ground cover varies significantly.
- Finally, the compass orientation of the window profoundly affects both the magnitude and the spectral content of the solar radiation falling on it throughout the year.

During this project, a computer algorithm was developed for calculating the performance of windows, explicitly accounting for all of these spectral and temporal changes throughout the year (Soule 1988). The new algorithm uses the most recent solar spectral model, which includes direct normal, diffuse, and ground cover-reflected components of the incident solar spectrum. Preliminary results clearly show the importance of accounting for such effects and provide some insight into the probable magnitude of errors introduced by available window performance models that do not account for all these effects.

The following sections provide the physical basis for the calculational algorithm, compare predictions for elements of the window performance with and without explicit detailed accounting for spectral effects, and compare the predicted performances of different kinds of windows using the detailed algorithm.

The performance criteria used to judge the quality of a window depend on many factors, among them the following:

- Primary function served by the window (view, daylighting, solar heating, ventilation)
- Type of building in which it is installed
- Climate
- Compass orientation of the window.

For example, a window installed on the south side of a residential building in a cold climate is likely to be judged by its ability to admit solar radiation while preventing heat loss. On the other hand, a window installed on the south side of a commercial building in a moderate climate is more likely to be judged by its ability to admit daylight while preventing solar heat gain, with little value placed on its ability to prevent heat loss.

This project is concerned with insulating windows that will find primary application in residential buildings, particularly in cold climates. Thus, solar heat gain and resistance to heat loss are of primary importance.

The net power per unit area passing through a window at any instant of time may be expressed as

$$\dot{Q} = T_s \qquad (2\text{-}16)$$

where

T_s = solar transmittance of the window
I_o = total incident solar irradiance (W/m^2)
U_T = thermal conductance through the window (W/m^2 K)
ΔT_w = temperature difference between indoors and outdoors (K)
Q = net heat flux through the window (W/m^2).

If this net power is integrated over an entire heating season, the annual net energy benefit of the window can be calculated.

The parameters of the equation, T_s, I_o, U_T, and ΔT_w, are commonly approximated. Typically, the solar transmittance is approximated by a single number; the incident solar irradiance is approximated by a fixed standard solar spectrum, corrected only for the geometry of the window and average solar beam direction; the thermal conductance is approximated by a single number; and the temperature difference is obtained from typical hour-by-hour meteorological data for a city near the building's location.

From our perspective, the most questionable approximations in this calculation procedure are the two that estimate the solar heat gain through the window. Both the solar transmittance of the window, T_s, and the spectral content of the incident solar irradiance, I_o, change dramatically as the sun's azimuth angle changes. These spectral changes are all the more critical for high-performance windows that invariably include components, such as low-e coatings, which are spectrally selective transmitters. As the sun's azimuth changes and the solar spectral content changes, these spectrally selective components transmit more or less solar radiation. The window modeling program under development explicitly accounts for this changing solar spectrum and the window's changing solar transmittance (Soule 1989).

The following sections develop the basis for the more accurate, detailed treatment of window performance and illustrate the differences between detailed and simple modeling approaches with several examples.

2.1.5.1 Modeling the Incident Solar Irradiance

The Solar Spectrum. A detailed spectral analysis is required to accurately estimate energy transfer through windows at different orientations and locations. A recent clear-sky solar spectral model presented by Bird,Hulstrom, and Lewis (1983) takes into account variation in air mass (AM),* atmospheric turbidity, precipitable water vapor, and ozone content; it also separates the global into the direct normal and diffuse components and adds a spectrally dependent ground reflection. In this model, the total global solar irradiation is given by

$$I_o = I_D \cos\theta + I_{DS} + \qquad (2\text{-}17)$$

where

I_D = direct normal component with θ = incident solar angle
I_{DS} = diffuse sky component
I_{GR} = diffuse reflected ground component.

The spectral and angular dependences are given by

$$I_o(\lambda,\varepsilon) = I_D(\lambda)\cos\theta + I_S(\lambda)\{[[I_D(\lambda)\cos\theta/I_E(\lambda)\,D\cos Z)]$$
$$+ 0.5\,(1+\cos\varepsilon)\,[1 - I_D(\lambda)/[I_E(\lambda)\,D)]]\}$$
$$+ 0.5\,I_{TH}(\lambda)\,R_{GR}\,(1-\cos\varepsilon)\,, \qquad (2\text{-}18)$$

where

θ = incident solar angle
ε = tilt angle between the surface of interest and the ground
D = earth-sun distance factor
Z = apparent solar zenith angle
I_E = extraterrestrial solar irradiance
I_D = direct normal solar irradiance

I_{TH} = global irradiance on a horizontal surface
I_S = total scattered irradiance
R_{GR} = ground reflectance.

The updated solar spectra based on this model for AM-1.5 incident on a surface tilted 37° up from the horizontal and azimuthally rotated to face the sun are given in Figure 2-19, including the global, direct normal, and diffuse components. Th spectra are shown for atmospheric parameters $\tau = 0.27$, $\alpha = 1.14$, $O_3 = 0.356$ (atm.-cm), W = 1.42 cm, SPR = 840 mB, and Nday = 93. This spectrum

*Air mass is a term used to describe the amount of atmosphere through which the sun's radiation must penetrate to reach the surface of interest. It is the ratio of optical thickness of the atmosphere through which the solar beam radiation passes compared to the optical thickness at sea level when the sun is at the zenith.

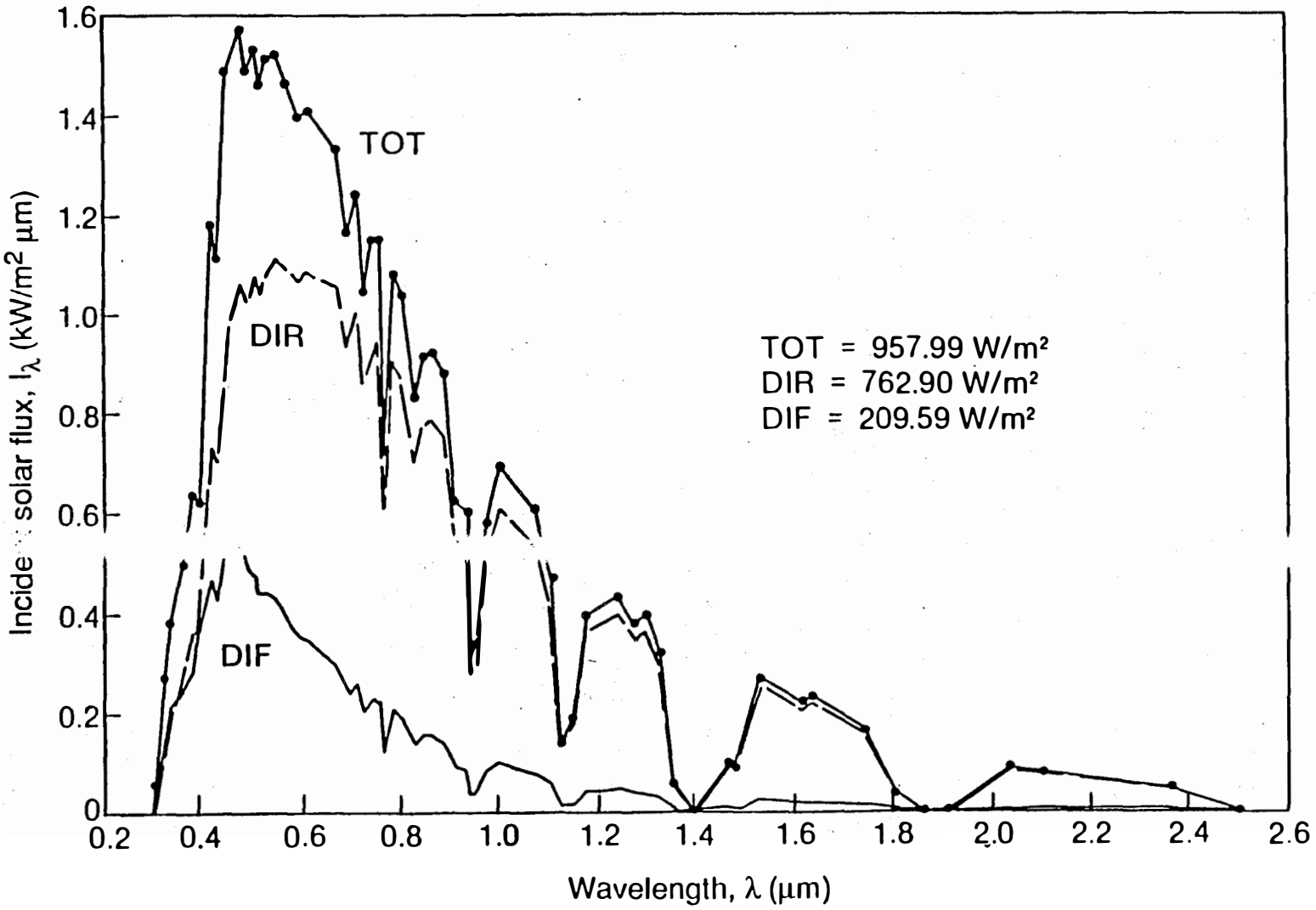

Figure 2-19. Updated solar spectra on 37° tilted surface

TP-3684

is useful for a fixed average solar weighting and is similar to spectra conventionally used for solar calculations.

Solar Irradiance on a Vertical Surface. The computer model SPECTRAL adapted from the previous parametric model of Bird and Riordan (1986) is introduced here to compare the local instantaneous spectrum incident on vertical windows facing south, east, west, and north at a given time and location. This model incorporates Eq. 2-18, including the atmospheric parameters relevant to the location, time, and orientation.

To shorten the computation time, the original 122-wavelength point solar spectrum from 0.30 to 2.54 μm was reduced by the ordinate weighting scheme to a spectrum of 61 points, which are shown in Figure 2-19. This was accomplished with small loss of accuracy. The integrated fluxes (W/m^2) for the revised 61-point spectra agree with the original spectra to within 0.47% for the global and 0.37% for the direct normal, and to within 0.83% for the diffuse spectra. The 61-point computed spectrum is used for the instantaneous solar irradiance function in the present analysis and for the spectral analysis of all the optical properties of individual elements of a window.

The daily global horizontal solar irradiance has been measured for a number of locations and is well documented in the form of monthly averages in the solar and meteorological (SOLMET) tables (Knapp, Stoffel, and Whitaker 1980). These tables also include the monthly average clearness ratio $\bar{K}_T$. These local SOLMET data are converted to the local diurnal global irradiance on a horizontal surface by using the algorithm of Collares-Pereira and Rabl (1979):

$$\bar{I}_t = \bar{K}_T \cdot \bar{H}_E \text{ (daily)} \cdot R_H \cdot (a_3 + b_3) \cos \omega^i \ , \qquad (2\text{-}19)$$

where

$$\bar{H}_E \text{ (daily)} = \frac{24}{\pi} I_E \left(\frac{\bar{R}}{R}\right)^2 \left[\omega_s \sin \phi \sin \delta + \cos \phi \cos \delta \sin \omega_s\right]$$

$$R_H = \frac{\pi}{24} \frac{\cos \omega^i - \cos \omega_s}{\sin \omega_s - \omega_s \cos \omega_s}$$

ω^1 = instantaneous hour angle (15°/h from solar noon)

$a_3 = 0.4090 + 0.5016 \sin (\omega_s - 60°)$

$b_3 = 0.6609 - 0.4767 \sin (\omega_s - 60°)$

ω_s = sunrise hour angle = $\cos^{-1} (-\tan \phi + \tan \delta)$

ϕ = latitude (deg)

δ = declination angle (deg)

I_E = extraterrestrial solar flux = 1377 W/m^2

A conversion is next made to the global radiation on the tilted surface in question. The Hay and Davies tilt algorithm (1978) is employed by Bird and Riordan (1986) and is included as the second and third terms of Eq. 2-18. The spectral tilt model SPECTRAL2 with the diurnal Eq. 2-19 provides the link for the instantaneous spectra incident on the vertical windows oriented south, north, east, and west as computed in the window simulation model SPECOPT6.

An example of these spectra incident on vertical windows of different orientations at peak solar times on the summer solstice, June 21, at Denver, Colorado (39.75°N), is shown in Figure 2-20. The relative contributions of the diffuse vs. the direct-beam components progressively change from the south-facing window (diffuse/total = 0.229) to the north (ratio = 0.709), with a corresponding change in the total spectral profile. For the double-glazed window with a ZnO/Ag/ZnO low-e coating shown here, the resultant changes in the transmitted solar, visible, and ultraviolet components are apparent.

Taking Account of Ground Plane Reflection. The spectral content of ground reflection has heretofore not been taken into account in window models. The spectral differences between typical ground covers can be significant, as shown in Figure 2-21 for green vegetation, bare soil, clear water, dry sand, and fresh snow (Lillesand and Kieffer 1979; Powell 1986). Inspection of quoted hemispherical reflection spectra for a range of ground covers shows that they can be adequately represented for the present purpose at 12 key wavelengths: 0.3, 0.4, 0.5, 0.6, 0.8, 1.0, 1.3, 1.4, 1.7, 1.9, 2.2, and 2.5 μm as shown in Figure 2-21.

Figure 2-22 shows typical examples of incident and transmitted spectra on a south-facing window on July 21 at 1200 solar time and on January 21 at 1200 hours. The contribution of the ground-reflected component, I_{GR}, to the total incident irradiance, I_o, ranges from 2% for clear water up to 32% for fresh snow. In fact, for a north-facing window in January with a large diffuse radiation component, hemispherical reflection from fresh snow can contribute up to 80% of the total solar irradiance on the window. In climates in which snow cover is common, the solar gain potential of north-facing windows could be grossly underestimated by other window models if this ground reflectance effect were not included.

The resultant effects for a conventional double-glazed window are given in Table 2-7. These results show that the spectral reflectance of different ground covers can make a significant difference in the actual flux transmitted through a window and justify their inclusion in a detailed model.

2.1.5.2 Modeling the Optical Characteristics of the Window

Spectral Weighting of Optical Properties. A spectrally weighted value of a parameter $X(\lambda)$ is defined as the integral of the parameter times a weighting function over all values of wavelength. For example, the solar-weighted value of X would be

$$X_{SOLAR} = \int_0^{\infty} X(\lambda) \frac{I(\lambda)}{I_o} d\lambda = \int_{\lambda_{min}}^{\lambda_{max}} X(\lambda) \frac{I(\lambda)}{I_o} d\lambda \ , \qquad (2\text{-}20)$$

Double glazed
Soda lime glass (1/8")
ZnO/Ag/ZnO (surface 3)
Denver, Co (39.75°N) June 21

BA-G0220602

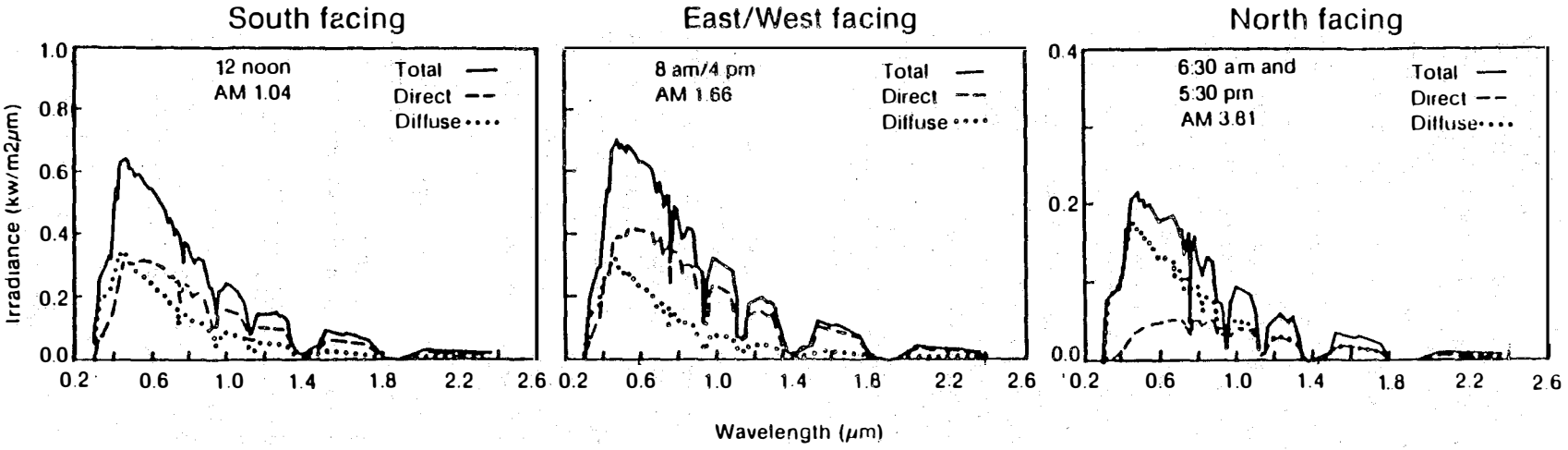

	Insolation		
	366 W/m²	430 W/m²	126 W/m²
Transmitted			
Solar =	40.0%	47.5%	42.5%
Visible =	61.5%	74.3%	65.4%
Ultraviolet =	37.9%	48.4%	40.3%
Reflected Solar =	44.2%	36.4%	41.2%
Absorbed Solar =	15.8%	16.1%	15.9%

Figure 2-20. Incident solar spectra and resulting optical performance of a double-glazed window with low-e coating

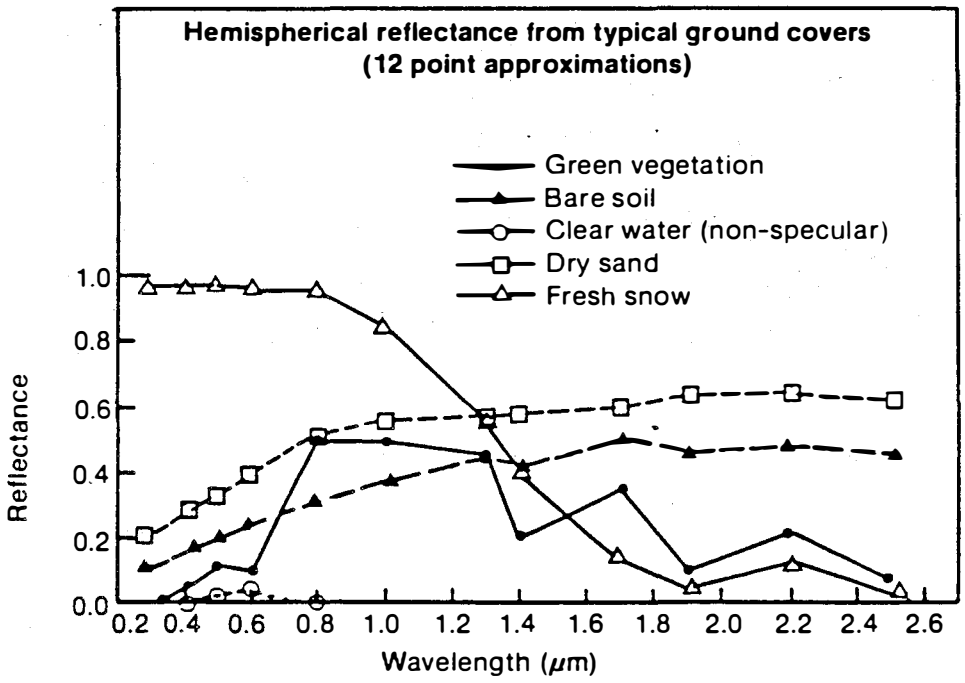

Figure 2-21. Hemispherical reflectance from typical ground covers

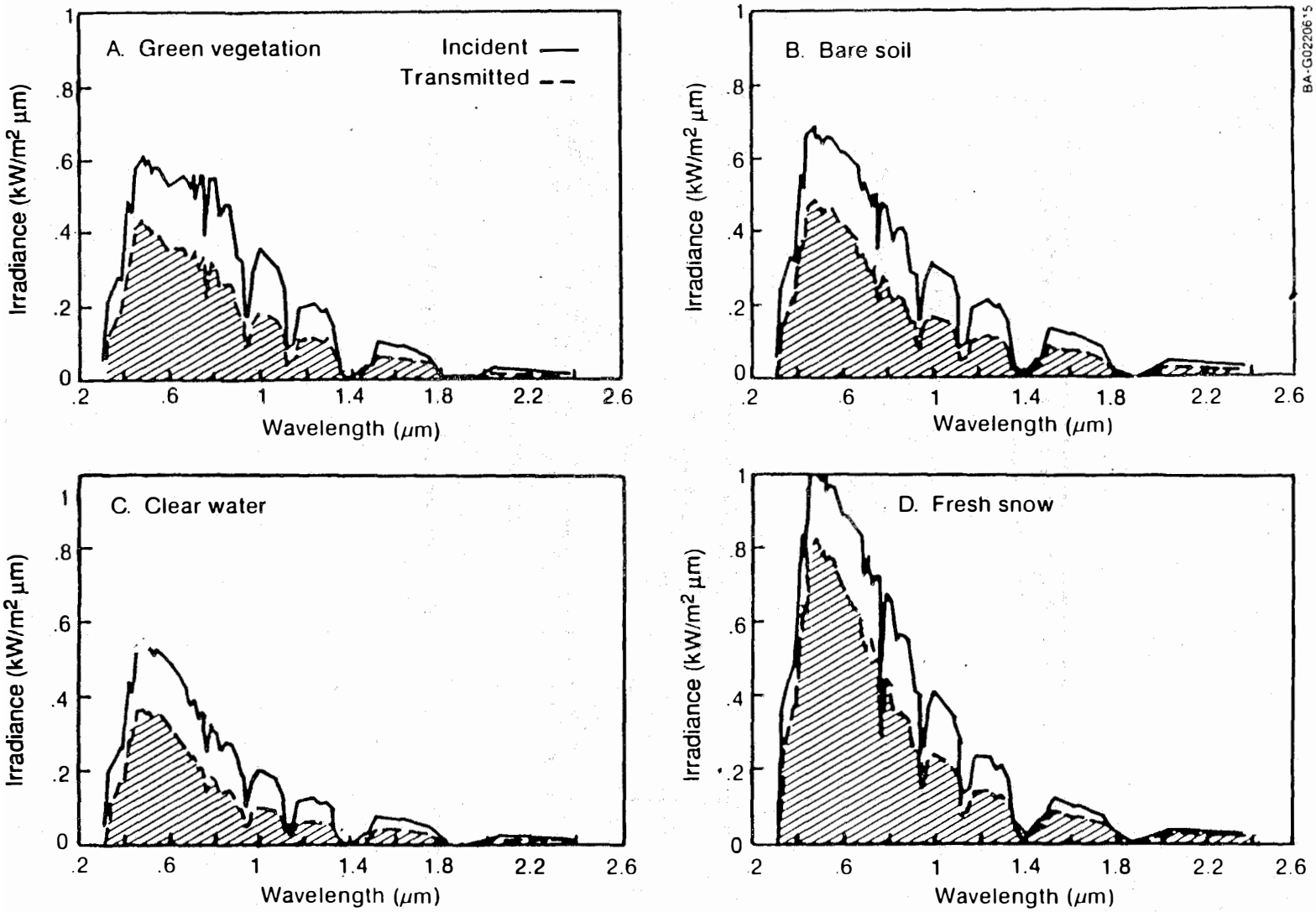

Figure 2-22. Hemispherical ground reflection (south-facing double-pane soda-lime glass window), Denver, Colorado (39.75°N)

Table 2-7. Effect of Hemispherical Ground Reflection on a South-Facing Double-Pane Window

Ground Plane	Time	GR (%)	I_T (W/m^2)	V_T (W/m^2)	T_S (%)	T_V (%)
Green vegetation	July 21 (1200)	27	260	42	61.3	69.4
Bare soil	July 21 (1200)	29	271	48	62.1	69.6
Clear water	July 21 (1200)	2	190	36	60.3	67.0
Fresh snow	Jan. 21 (1200)	34	418	79	70.6	78.7

Location: Denver, Colorado

GR = Percent of incident irradiance from ground plane reflection
I_T = Total radiant power per unit area transmitted through window
V_T = Total visible radiant power per unit area transmitted through window
T_S = Solar-weighted transmittance
T_V = Visible-weighted transmittance.

Table 2-8. Comparison of Optical and Thermal Properties with Low-Conductivity Gas-Fill and Low-e Coatings for Three Double-Pane Windows in Figure 2-24

	Air Gap		Krypton Gap		Evacuated Gap	
	No low-e	Low-e	No low-e	Low-e	No low-e	Low-e
T_V	0.81	0.75	0.81	0.75	0.87	0.77
T_S	0.74	0.57	0.74	0.57	0.83	0.62
R_T	2.0	3.2	2.2	4.1	1.6	7.3
$(T_S \cdot R_T)_R^*$	2.1	2.6	2.3	3.3	1.9	6.4

*See Eq. 2-28.

where

$I(\lambda)$ is the incident solar irradiance spectrum and

$$I_o = \int_{\lambda_{min}}^{\lambda_{max}} I(\lambda)\, d\lambda \qquad (2\text{-}21)$$

is the total integrated solar flux. The limiting wavelengths, λ_{min} are some judiciously selected minimum wavelength below which there is very little solar energy and λ_{max} is a similarly selected upper limit.

The optical portion of the electromagnetic spectrum may be conceptually divided into mutually exclusive fractions representing the ultraviolet, visible, and infrared portions as shown in Figure 2-23 along with the typical AM-1.5 solar spectrum, S, and a 288-K black-body thermal radiation spectrum, P. The visible portion is defined by the sensitivity of the light-adapted human eye (Anon. 1981) and extends from about 0.41 μm to 0.72 μm.

Role of Spectra Selective Low-e Window In advanced windows in which the conductive and convective heat losses are suppressed, the radiative component becomes of primary importance. A comparison of the performance of windows with and without low-e coatings is shown in Figure 2-24 and Table 2-8. Here the energy transfer in double-pane windows has been calculated for three kinds of gap filling--air, krypton, and vacuum (Benson et al. 1987a)--and then compared with and without an ITO low-e coating* (e = 0.1). For the air and krypton cases, soda-lime silica glass with 0.5-in. spacing is used. For the vacuum window, borosilicate glass lites with 0.016-in. gap are used. The figure shows the visible and solar transmittances, T_V and T_S, and the R-factor, R_T. The effect of a low-e coating increases from the air to krypton to vacuum-filled windows, where the relative increase in R_T with low-e goes from 1.6x to 4.5x, showing the marked benefit of suppressing radiative heat transfer when convection is already suppressed. In the vacuum window the integral interpane spacers and fused window edge cause some thermal shorting. Without the vacuum or low-e coating, the thermal resistance would be only $R_T = 1.6$. With the vacuum and the single low-e coating for radiative heat-transfer suppression, the thermal resistance is increased to $R_T = 7.3$. Pyrex also improves the T_V and values to 0.77 and 0.62, respectively, over those of soda-lime glass with and 0.57. The energy-transfer ratio $(T_S \cdot R_T)_R$ shows the combined effect, where, for example, the vacuum window with low-e coating is 6.4 times more effective than a single soda-lime silica glass light in net solar heat gain.

The range is wide for spectral transmittance and reflectance contours of available selective low-e coatings for window applications (Lampert 1981). Coatings are of different types including doped semiconductors and dielectric/metal/dielectric multilayers. Three examples illustrated in Figure 2-25 show a range of spectral characteristics: ITO film on soda-lime glass; ITO film on 0.043-in. (1.3-mm) Pyrex glass, and ZAZ‡ multilayer on soda-lime glass. The

*ITO, indium oxide (tin doped) is a transparent conductor deposited onto glass or polymer films to produce a lower emissivity surface (0.1 emissivity vs. 0.84 emissivity of bare glass).

‡ZAZ, zinc oxide/silver/zinc oxide

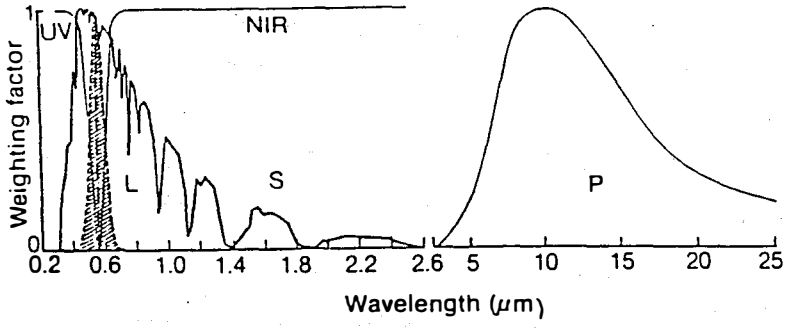

Figure 2-23. Spectral weighting functions: solar (S), luminosity (L), ultraviolet (UV), near infrared (NIR), and far infrared Planck distribution (P)

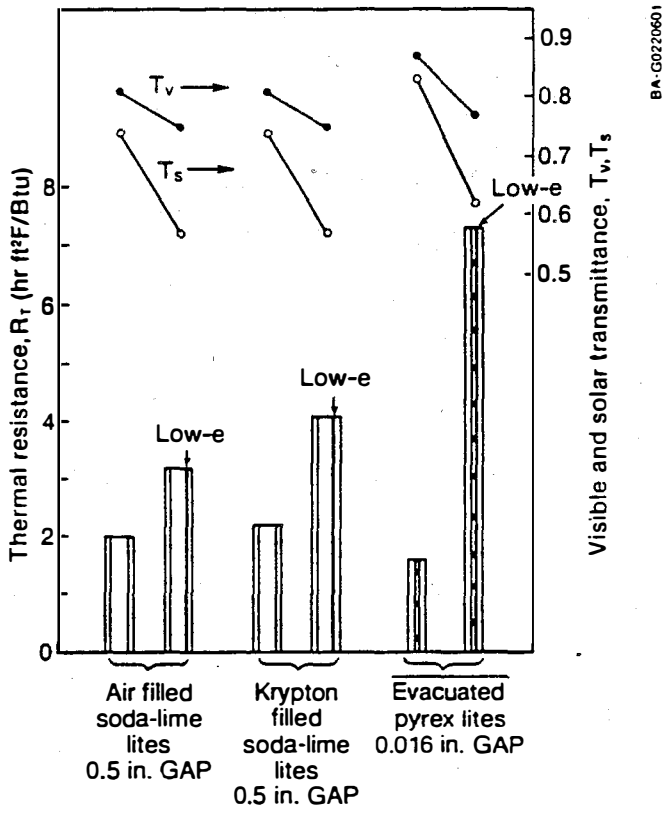

Figure 2-24. Optical and thermal properties of double-pane windows with different fill gases

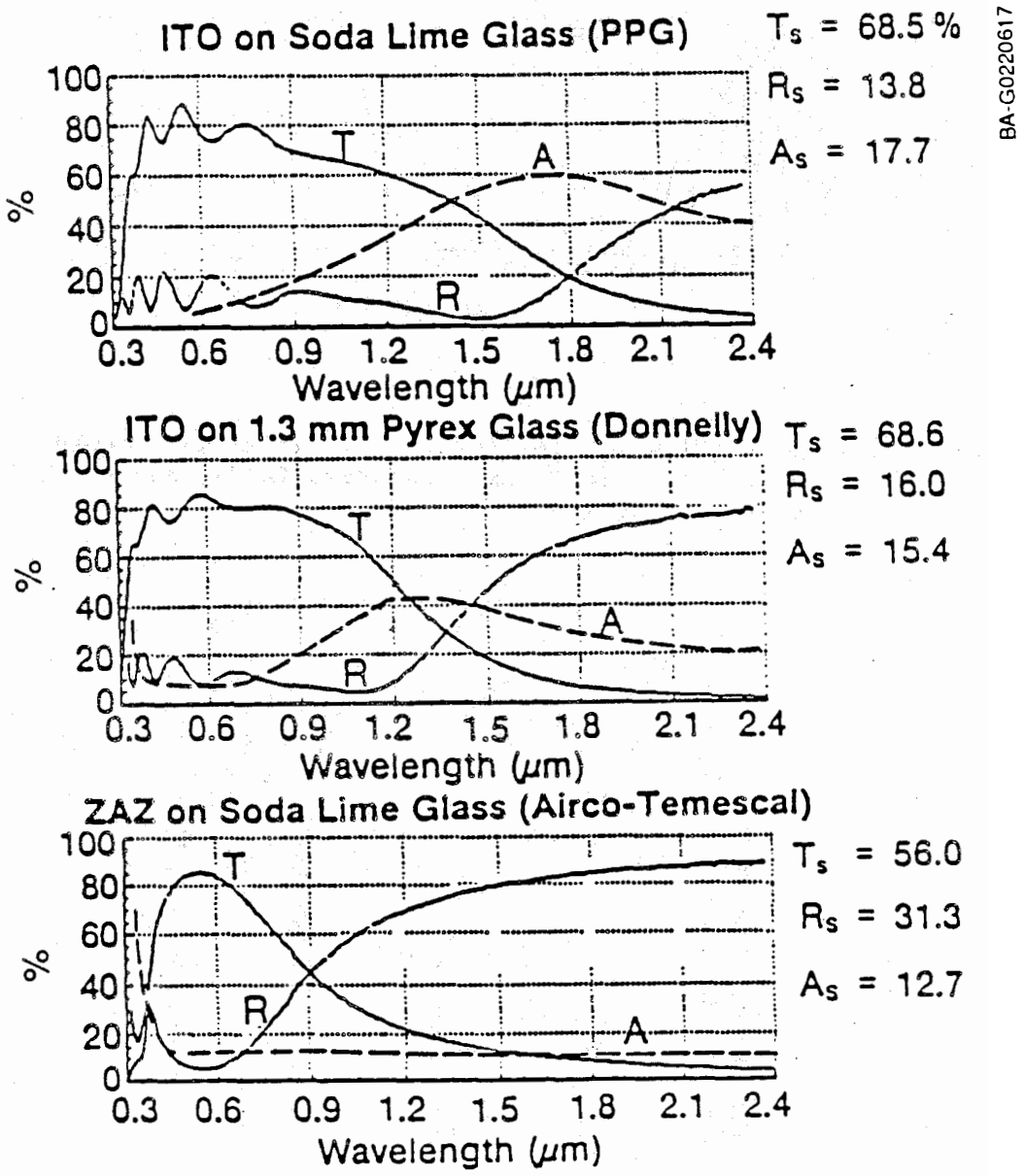

Figure 2-25. Spectral transmittance (T), reflectance (R) and abosrptance (A) of three low-e coated window glasses (Solar-weighted values shown as T_s, R_s and A_s)

spectral contours may be classified by five measured spectral parameters; peak wavelength λ_o, the peak transmittance T_o and reflectance R_o, the bandwidth BW, and the infrared reflectance R (at 10-μm wavelength, the peak of the Planck thermal radiation distribution at 288 K). The choice of 288 K (15°C) for the relevant thermal radiation is based on an average of ASHRAE (ASHRAE 1985a) inside and outside winter and summer temperatures. The quantity (1 - R [10μm]) is a useful indicator for the relative emittance of the coating surface. A comparison of these parameters for the three low-e coatings is given in Table 2-9. Although their peak wavelengths λ_o are tuned to maximize the visible transmittance and their peak transmittances are in the 0.80-0.86 range, their bandwidths and reflectances vary widely. The wide range of bandwidths affects the solar transmittance, which varies from 68.5% to 55.9%. The visible reflectances R_o vary by a factor of 2.3 and the effective emittances (1 - R [10 μm]) vary by 3.5x, a highly significant difference in coatings for advanced windows, as explained below.

The strong spectral dependence of the spectrally selective low-e films shown in Figure 2-25 profoundly affects the spectrally integrated solar transmittance. An instructive comparison is made in Table 2-10, where the monochromatic transmittance is taken at the peak solar wavelength λ_o = 0.515 μm and the T_s is solar weighted by an AM-1.5 solar spectrum. Also shown is the transmittance at the peak visible wavelength λ_o = 0.56 μm compared to a visible weighted T_v, where the weighting functions are shown in Figure 2-23. Clear glass data for soda-lime silica and borosilicate glass are shown in Figure 2-25 for comparison. As noted in Table 2-10, using single wavelength values rather than solar-weighted values would cause errors in solar transmittances running from 1.8% for Pyrex up to 51.8% for the low-e coating, ZAZ. For the visible transmittances the differences are relatively small. This comparison emphasizes the need for detailed spectral analyses of windows that include spectrally selective low-e films, whereas such detail has been unnecessary for the relatively uniform spectral behavior of uncoated clear glass windows.

The Infrared Optical Properties and Radiative Heat Transfer in Windows. The radiative heat transfer in windows is governed by the emittance of each glass surface. The emittance is estimated from the measured far infrared (IR) reflectance. The IR reflectances and transmittances are shown in Figure 2-26 for several clear glasses (soda-lime silica, borosilicate, and low-iron soda-lime silica) from 2.5 μm to 25 μm for near normal incidence (15° off-normal incidence). For comparison, also shown are measured data for the low-e coatings.

Table 2-9. Low-e Coating Spectral Contour Parameters

	λ_o (μm)	T_o	R_o	BW (μm)	1-R (10 μm)	
ITO (PPG)	0.56	0.80	0.12	1.19	0.14	0.150
ITO (Donnelly)	0.56	0.80	0.10	0.94	0.11	0.113
ZAZ (Airco)	0.55	0.86	0.053	0.54	0.04	0.054

e_T^* = measured emittance

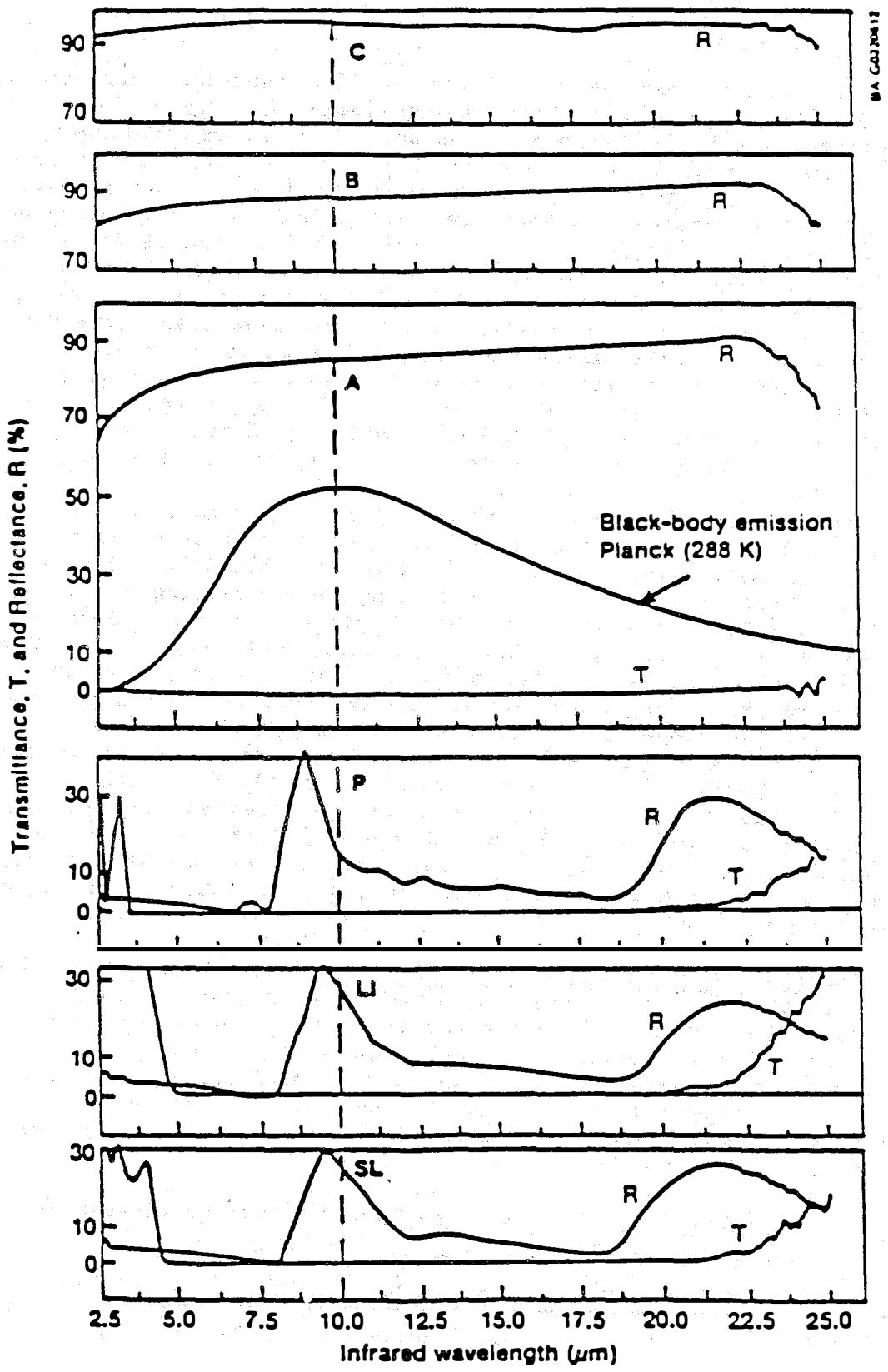

Figure 2-26. Infrared spectral transmittance and reflectance of three low-e coated window glasses for Pyrex (P), low-iron (LI), and soda lime (SL), and for ITO-PPG (A), ITO-Donnelly (B), and ZAZ-Airco (C). A near room-temperature, thermal radiation spectrum (Planck 288 K) is also shown for reference.

Although the glass reflectances range from 0% to 35%, the low-e coating reflectances are between 0.86 and 0.96 at 10 μm. The back surface reflectances for the coated glass were also measured, but they show reflectances very similar to those of the uncoated glass itself and so are not shown in the figure. These measured data are included, however, in the calculation of radiative heat transfer in windows.

In window applications the total hemispherical emittance $e_T(T)$ is important. Its angular dependence on the measured directional spectral reflectance $R(\lambda, \theta)$ (see next section below) is given in the following integral (Siegel and Howell 1972),

$$e_T(T) = \frac{2}{\sigma T^4} \int_0^{\pi/2} \int_0^{\infty} [1 - R(\lambda, \theta)]\, P(\lambda, T) \sin\theta \cos\theta \, d\lambda \, d\theta \,, \quad (2\text{-}22)$$

where σ = Stefan-Boltzmann constant = 5.670×10^{-8} W/m^2 K^4. The Planck distribution function $P(\lambda, T)$ is given by

$$P(\lambda, T) = C_1/\lambda^5 \, (e^{C_2/\lambda T} - 1) \,, \quad (2\text{-}23)$$

where $C_1 = 3.740 \times 10^{-16}$ W/m^2 and $C_2 = 0.01439$ m K.

Table 2-10. Solar and Visible Weighted vs. Monochromatic Transmittances for Glasses and Low-e Coatings

Single Sheet (thickness)	$T\lambda_1$[a]	T_S	Error %	$T\lambda_2$[b]	T_V	Error %
Pyrex (0.123 in.)	0.925	0.909	2	0.929	0.928	0.1
Soda lime (0.124 in.)	0.901	0.855	6	0.901	0.896	0.6
ITO + Pyrex (0.043 in.)	0.823	0.686	20	0.827	0.772	7
ZAZ + soda lime (0.125 in.)	0.849	0.559	52	0.855	0.855	<0.1

[a] λ_1 = 0.515 μm [b] λ_2 = 0.560 μm

For a window with parallel lights that are effectively opaque to thermal IR radiation, the relevant IR emissive flux density exchange between facing surfaces is (Siegel and Howell 1972)

$$J_E = \frac{\sigma (T_2^4 - T_1^4)}{\frac{1}{e_{T_1}} + \frac{1}{e_{T_2}} - 1} \quad \text{(expressed in W/m}^2\text{)} \,, \quad (2\text{-}24)$$

where T_1 and T_2 and e_{T_1} and e_{T_2} are the surface absolute temperatures and total hemispherical emittances, respectively. For the case of a double-pane window with and without a low-e coating of $e_T = 0.1$, where the emittance of soda-lime glass is 0.837 (Rubin 1985) and for winter ASHRAE conditions of $T_1 = 255$ K and $T_2 = 294$ K, the results are

Clear glass double pane $J_E = 132\ W/m^2$
Clear glass + low-e coated glass $J_E = 7.3\ W/m^2$.

Directional Dependence of the Optical Properties of Windows. The directional spectral transmittance, reflectance, and absorptance of clear glasses and selective low-e coatings are important for an understanding of the diurnal and seasonal behavior of windows. Directional spectral transmittance $T(\lambda, \theta)$ is essential for calculating hour-by-hour solar gain from the direct normal incidence solar component. For diffuse solar components, the total hemispherical transmittance T_H is given by (Siegel and Howell 1972)

$$T_H = 2 \int_0^{\pi/2} \int_{0.30\ \mu m}^{2.54\ \mu m} T(\lambda, \theta) \sin\theta \cos\theta \, d\lambda \, d\theta \ . \qquad (2\text{-}25)$$

The directional spectral reflectance $R(\lambda, \theta)$ is used to find the total hemispherical emittance e_T, as shown in Eq. 2-22. The directional spectral absorptance $A(\lambda, \theta)$ is calculated from the measured $T(\lambda, \theta)$ and $R(\lambda, \theta)$ by the relation $A(\lambda, \theta) = 1 - T(\lambda, \theta) - R(\lambda, \theta)$. The absorptance affects the glass temperature and hence IR emission.

The dependence of transmittance and absorptance on incident angle θ can be represented by a polynomial in cos (θ) (Stephenson 1965) which to the fifth order is given by

$$T(\lambda, \theta) = \sum_{i=0}^{5} C(\lambda)_i \cos\theta_i \quad \text{and} \quad A(\lambda, \theta) = \sum_{i=0}^{5} K(\lambda)_i \cos\theta_i \ . \qquad (2\text{-}26)$$

Least-squares fits to the measured orientational data are shown in Figure 2-27 for a ZAZ low-e coating on soda-lime silica glass at 0.550 μm with unpolarized radiation. For comparison, the measured directional visible-weighted data for clear soda-lime silica glass (SL) are also shown in Figure 2-27 (Rubin 1985). As noted, the reflectance tends toward 1.0 at 90° and the transmittance tends toward zero. The absorptance grows with θ because of an increasing path length but ultimately drops off toward 90° because of the dominating reflective loss term. This rollover in slope occurs between 75° and 90° and poses a problem for a good polynomial fit. The T and R data, however, can be fitted well with a fifth-order polynomial. A comparison of absorptances for the two materials shows that for ZAZ, A = 0.088 at 10° rises to 0.130 at 75°, and for SL, A = 0.021 at 10° rises to 0.027 at 80°. The resulting coefficients for the fifth-order polynomial fit to the absorptance in the two materials are given in Table 2-11.

Table 2-11. Curve Fitting Parameters (Eq. 2-26)

	K_0	K_1	K_2	K_3	K_4	K_5
ZAZ	-0.00244	1.453	-5.838	10.542	-8.994	2.930
SL	-0.000428	0.305	-1.188	2.096	-1.742	0.550

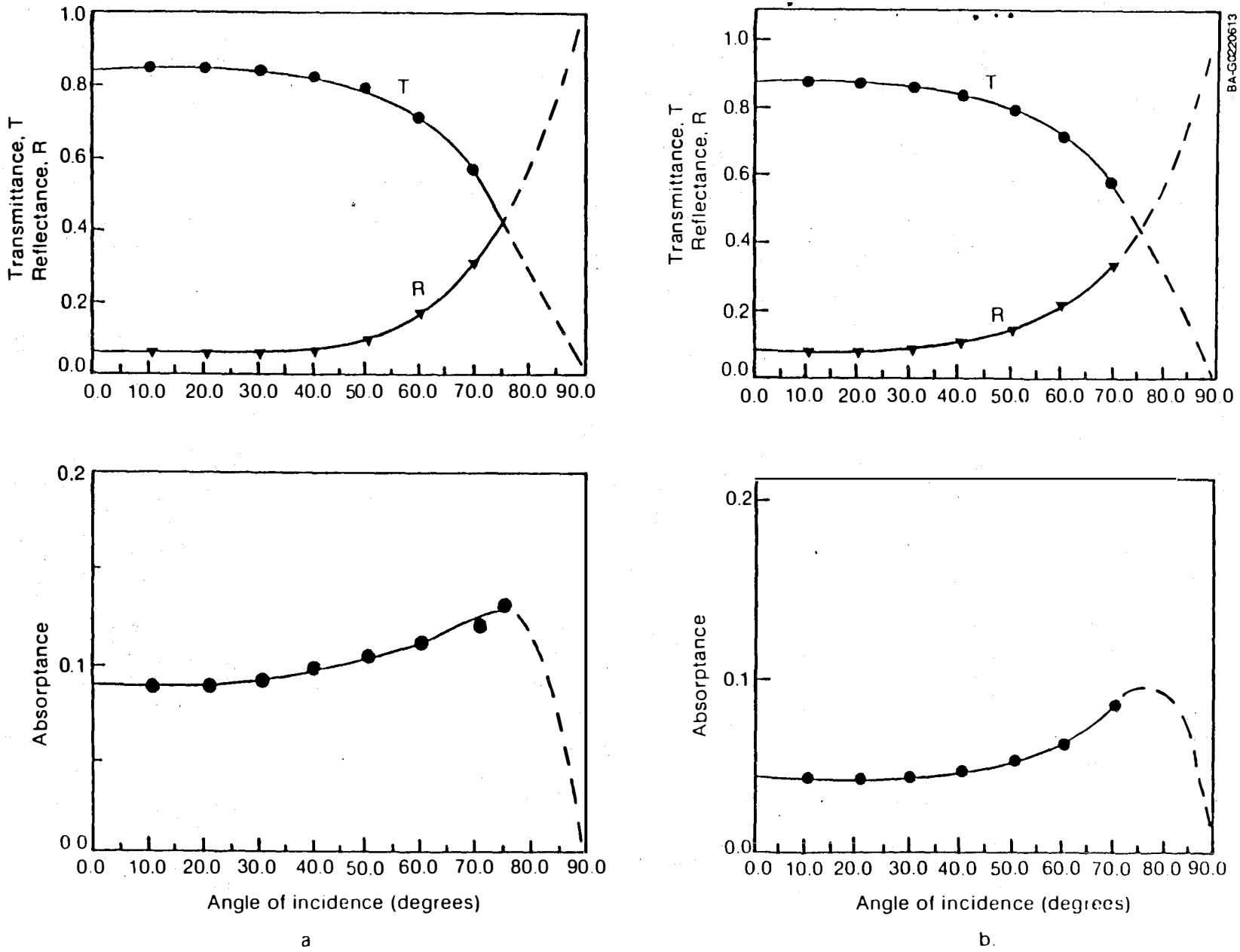

Figure 2-27. Orientation dependence of transmittance, reflectance, and absorptance for (a) ZAZ low-e coating on soda-lime silica glass and (b) uncoated soda-lime silica glass

Combining Solar Spectra and Optical Properties for Advanced Windows. Performance parameters for three different advanced window systems are summarized in Figure 2-28. These representative window types illustrate the primary approaches toward more efficient energy transfer in windows. A leading example of a multipane window is the quad-pane window shown at A with conventional soda-lime silica glass panes (Rubin 1985) and air-filled gaps. With its convective heat loss suppressed by the multiple panes, an R-value of 4.3 h ft^2 °F/Btu can be reached. The solar transmittance T_S, however, is limited to 48% and the visible transmittance T_V to 66%.

The second type of window is the tri-pane shown as B in Figure 2-28. This window has added features of low-iron krypton gas fill and an ITO-selective low-e coating (e = 0.15) on the middle light (on surface number 3, counted from the outside). Depending on the application, this coating could also be located on surface 4 or 5. This tri-pane window has T_S increased to 56% and T_V to 70%, and an increase in R_T to 5.6. This window effectively combines the advantages of a higher transmittance low-iron glass, the reduced convective loss of a heavy-molecular-weight gas fill (krypton), and a lower radiative loss of the low-e coating.

A third type of window is a double-pane evacuated window shown as C in Figure 2-28. In this design, the convective and gas-phase conductive losses are eliminated by evacuation of the inner space between the panes. Spacing under atmospheric pressure is maintained by small transparent glass spheres (0.5 mm in. diameter) that are uniformly spaced 30 mm apart with a very low light blocking factor of 0.014%. An associated ITO low-e coating (e = 0.11) on surface number 3 significantly reduces the radiative loss, which is the major loss component. Thermal resistance was calculated to be of R_T = 7.3 °F ft^2 h/Btu for the vacuum window (see Section 2.1.6). The T_V and T_S values for window C were calculated from SPECOPT and measured on a window section consisting of an outer borosilicate glass pane plus an inner ITO-coated 0.051-in. borosilicate glass pane. The calculated T_S differs by 5.4% from the measured value:

T_S (measured)	T_S (calculated)	T_V (calculated)
0.661	0.625	0.774

The Diminishing Benefits of Multiple Panes. Figure 2-29 shows the variation of spectral transmittance and reflectance for a total window with multiple lights. Two types of glass are shown: soda-lime silica (LOF, 0.124 in.) and borosilicate (Corning 7044, 0.123 in.). With increasing numbers of panes, the transmittance for each type of glass shows an increasing spectral dependence, the effect being more pronounced in the soda-lime silica glass. A comparison of monochromatic (λ_o = 0.515 μm) and solar-weighted transmittances with number of panes is given in Table 2-12. For borosilicate glass, the deviation increases from 1.8% to 8.7% from one to five panes and for soda lime from 6.3% to 33.7%, a large difference that would introduce a large error into a simple window model. Over the solar wavelength range, the transmittance of

Quad-pane
(soda-lime - air filled)

$R_T \simeq 4.3$
$T_S = 48$
$T_V = 66$
$(T_S \cdot R_T)_R = 2.9$

Tri-pane
(low-iron - Kr filled)

$R_T \simeq 5.6$
$\varepsilon = 0.15$
$T_S = 56$
$T_V = 70$
$(T_S \cdot R_T)_R = 4.3$

Double-pane
(Pyrex-evacuated)

$R_T \simeq 7.3$ hr ft² °F/Btu
$\varepsilon = 0.11$
$T_S = 62$ %
$T_V = 77$ %
$(T_S \cdot R_T)_R = 6.3$

BA-G0220603

Figure 2-28. Representative advanced window systems

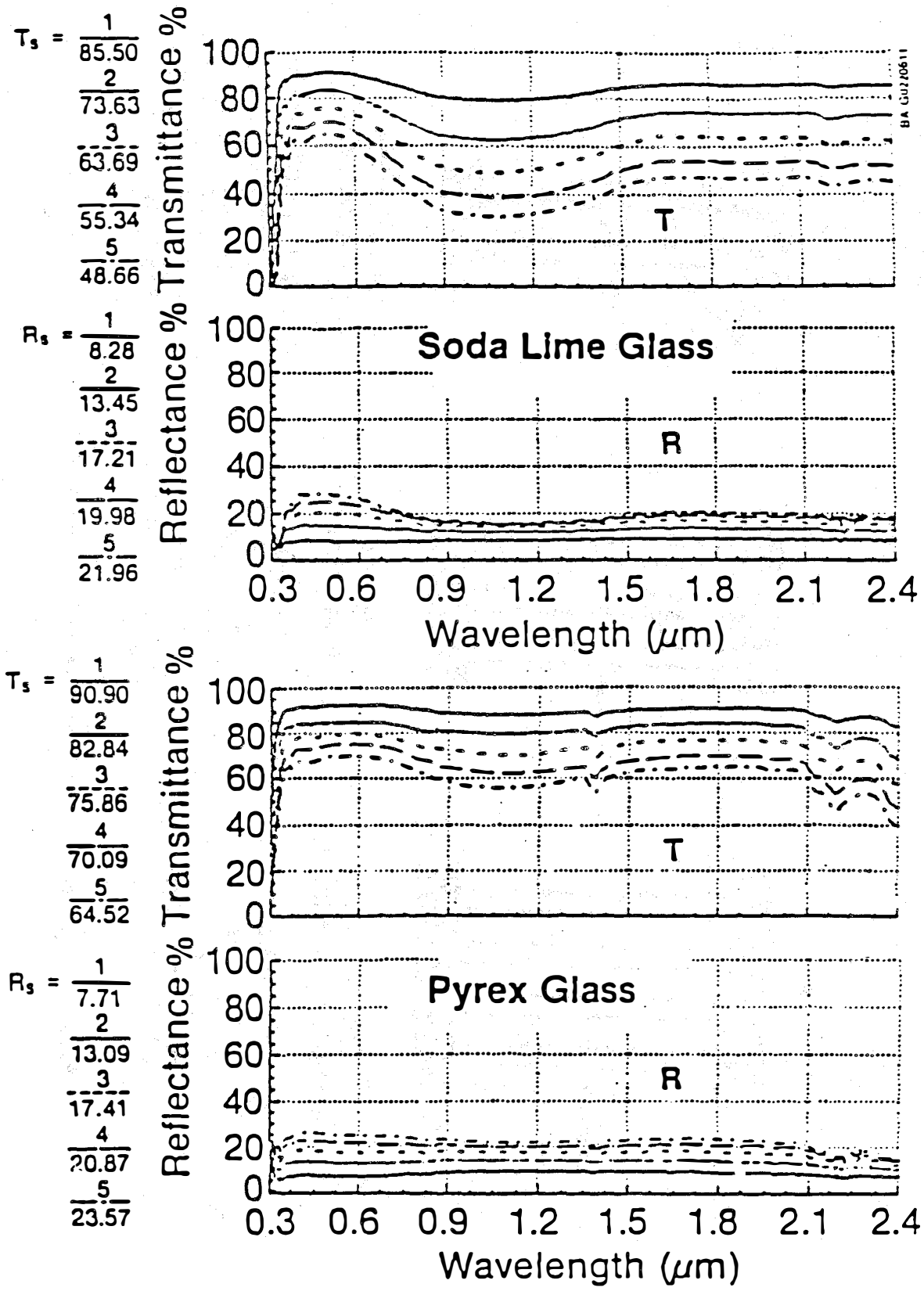

Figure 2-29. Multipane transmittance and reflectance for soda-lime and Pyrex glasses

borosilicate glass also shifts in overall magnitude, but less than soda-lime silica glass (29% vs. 43%).

The overall spectral dependent optical properties of a window with N panes were calculated in the SPECOPT6 program by the method of Rubin (1985). The resulting weighted values for T_S, R_S, and A_S are given in Table 2-13 for a multiple-pane window with borosilicate glass.

The same multiple-pane window was also measured at normal incidence for $T(\lambda)$, $R_F(\lambda)$, and $R_b(\lambda)$. The solar-weighted absorptance A_S was found from the relation $A_S = 1 - T_S - R_S$. The resultant measured values are also given in Table 2-13, where for borosilicate glass, they compare within 0.7% for transmittance and within 3.3% for reflectance. The difference in absorptance proceeding from one to five panes is very significant, where A_S from 0.014 to 0.119 for borosilicate glass. The corresponding shift for soda-lime silica glass is from 0.062 to 0.293. The effect of absorptance on the individual pane temperature and the panes' corresponding thermal emittances significantly affect the window radiative heat transfer.

Table 2-12. Solar-Weighted vs. Monochromatic Transmittances for Multipane Windows

No. of Panes	Soda Lime Silica Glass			Borosilicate Glass		
	T_{λ_1}[a]	Error T_s[b] (%)	Error (%)	T_{λ_1}[a]	Error T_s[b] (%)	Error (%)
1	0.909	0.855	6	0.925	0.909	2
2	0.831	0.736	13	0.852	0.828	3
3	0.761	0.637	20	0.795	0.759	5
4	0.704	0.553	27	0.742	0.701	6
5	0.651	0.487	34	0.702	0.645	9

[a]Transmittance at a single wavelength, $\lambda_1 = 0.515$ µm
[b]Solar-weighted transmittance (AM=1.5)

The transmittances T_S and T_V for three types of glass, soda-lime silica, borosilicate, and low-iron, as normalized to a thickness of 0.123 in., are compared in Figure 2-30. Soda-lime silica glass is distinctive not only for its low T_S, but also for its wide divergence between T_V and T_S. For low-iron glass, on the other hand, T_V and T_S are close together even out to a five-pane window. Borosilicate glass is distinctive in that its T_V is significantly higher—the best of the group with $T_V = 0.928$ and $T_S = 0.909$ for one pane progressing down to 0.718 and 0.639, respectively, for five panes.

The lower part of Figure 2-30 shows the corresponding effect on thermal loss, represented by the thermal resistance. A baseline for soda-lime silica glass with air-filled gaps is shown ranging from $R_T = 0.88$ up to 5.42. The effect of a low-e coating is shown by the dashed line, where the increase in R_T is as

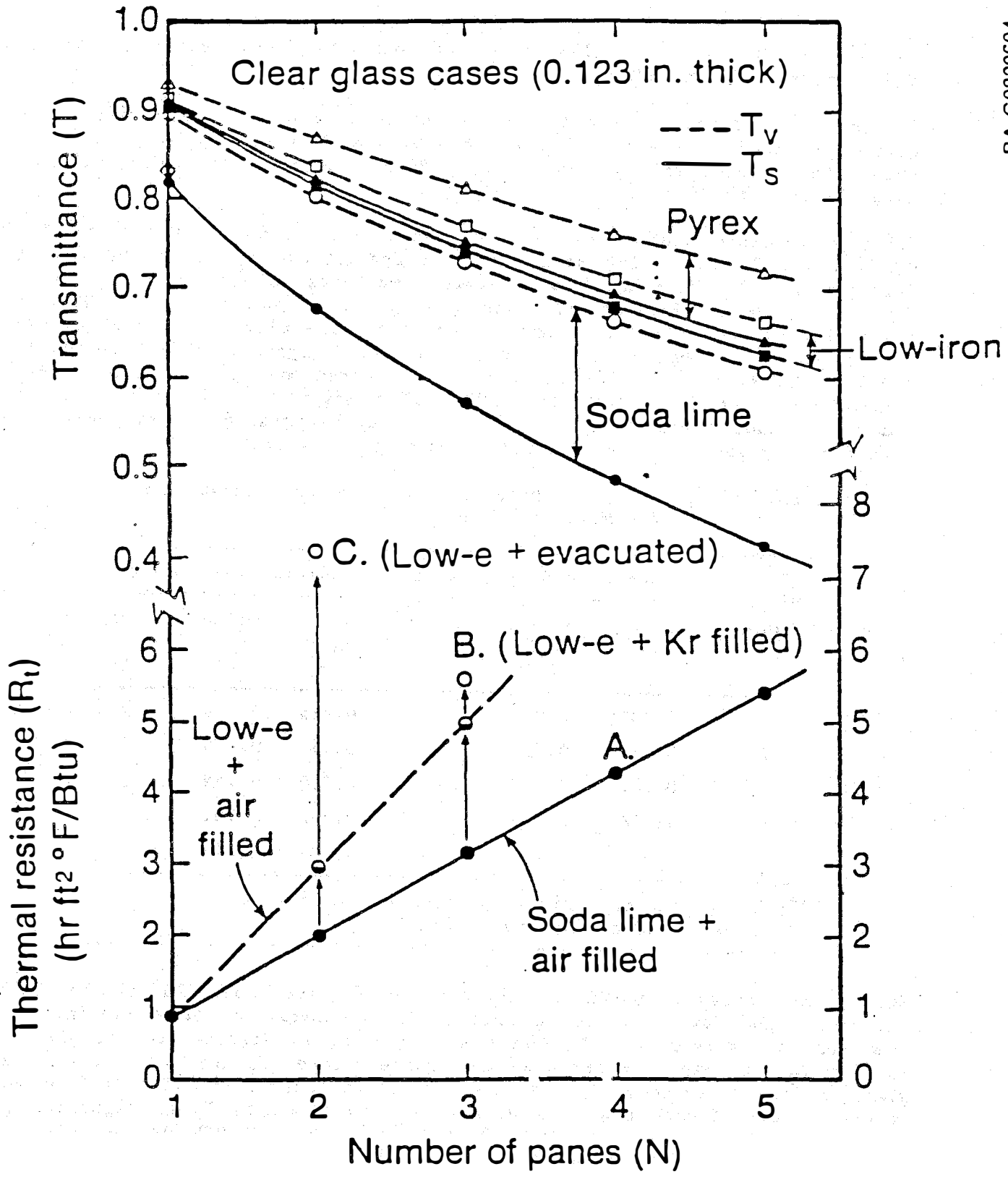

Figure 2-30. Multipane window transmittance and thermal resistance

Table 2-13. Comparison of Calculated and Measured Properties for Multipane Borosilicate Glass Windows

No. of Panes	T_S[a] (meas.)	T_S[a] (calc.)	R_S[a] (meas.)	R_S[a] (calc.)	A_S[b] (meas.)	A_S[c] (calc.)
1	0.909	0.909[d]	0.077	0.068	0.014	0.023
2	0.828	0.828	0.131	0.124	0.041	0.048
3	0.759	0.758	0.174	0.171	0.067	0.071
4	0.701	0.696	0.209	0.210	0.090	0.094
5	0.645	0.641	0.236	0.244	0.119	0.115

[a] T_S and R_S weighted by AM-1.5
[b] Calculated from measured values of T_S and R_S
[c] Calculated from calculated values of T_S and R_S
[d] Normalized at one pane

much as 60%, demonstrating the clear advantage of low-e coatings for advanced window systems. The tri-paned window case B with krypton-filled gaps shows a further rise of 12% over the air-filled case. For the two-pane case, the evacuated window C gives a 148% rise in R_T over the air-filled case.

Defining a Solar Window Figure of Merit. It is clear from the optical and thermal calculations shown in Figure 2-30, where T_S falls and R_T rises with N, that a compromise is required for a solar heating window. A useful approach is to define a new figure of merit ($T_S \cdot R_T$). This is proportional to the net instantaneous solar gain, where the solar gain and thermal loss of the window are combined as

$$T_S \cdot R_T \propto \frac{\text{solar gain}}{\text{thermal loss}} , \qquad (2\text{-}27)$$

which is to be maximized for a given window situation. This figure of merit can be related to a reference window, such as a single pane of soda-lime silica glass, to form the ratio

$$(T_S \cdot R_T)_R = \frac{(T_S \cdot R_T)\ (\text{window})}{(T_S \cdot R_T)\ (\text{single reference pane})} . \qquad (2\text{-}28)$$

This dimensionless energy-transfer ratio is similar to the ASHRAE-defined shading coefficient, except that it includes both solar gain and thermal resistance.

Figure 2-31 shows a plot of the energy-transfer ratio $(T_S \cdot R_T)_R$ for multipane windows (N = 1 → 5) including the quad-pane at A. The tri-pane window (B) with low-e coating and krypton gas-fill is also shown; note the dramatic rise in the energy-transfer ratio to 4.33. A further sharp rise to 6.25 is seen for the evacuated window C. This overall effect is very significant and again stresses the importance of spectrally selective low-e coatings in advanced window systems.

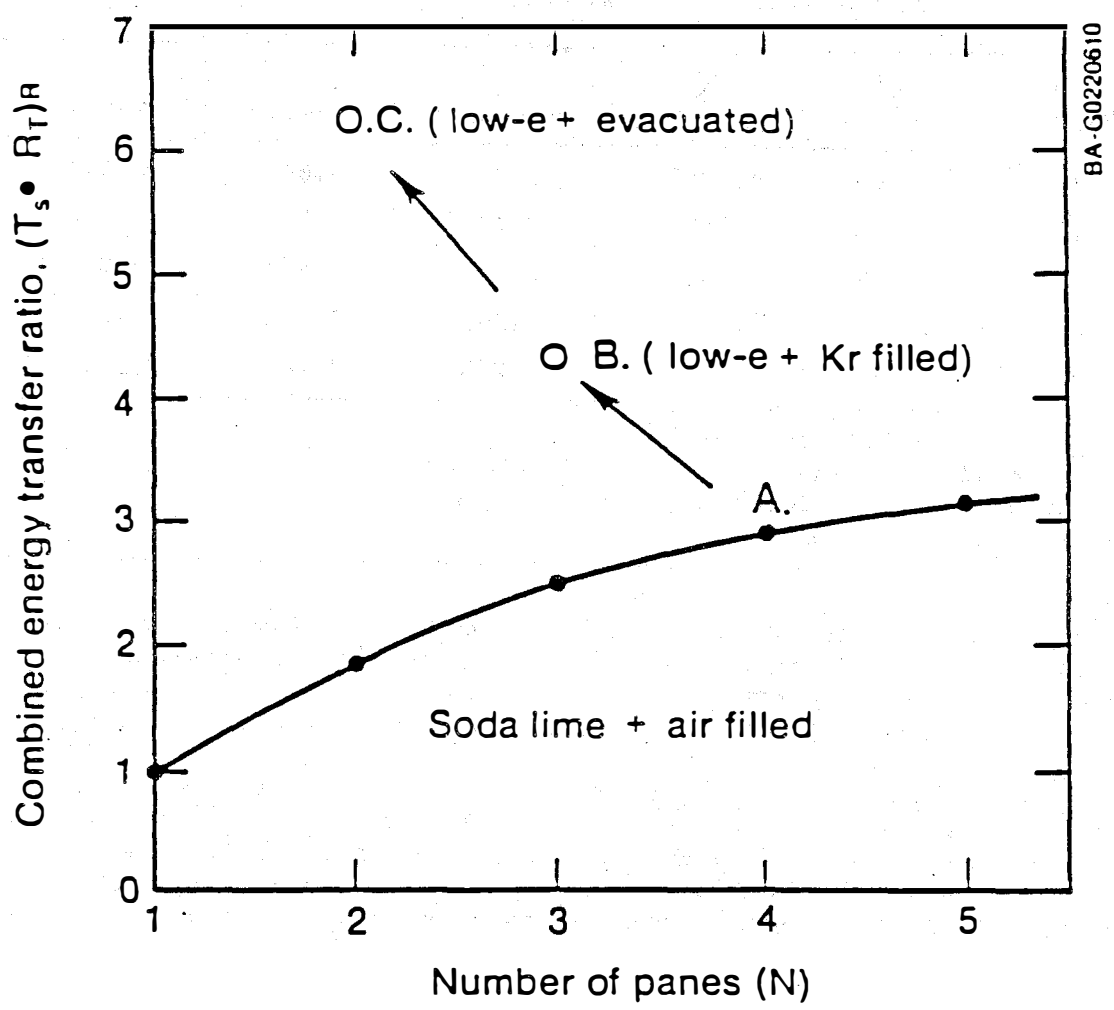

Figure 2-31. Combined energy-transfer ratio for solar gain and thermal loss

A Comparison of Modeling Methods. The spectrally detailed modeling technique has been compared to the more conventional modeling technique to judge the significance of the various refinements incorporated in the more detailed model. Three window types were used in this comparison: a standard double-pane window of soda-lime silica glass, a vacuum window of borosilicate glass with ITO low-e coating (e = 0.11 on surface number 3), and a soda-lime silica double-pane window with a particularly good ZAZ low-e coating (e = 0.05).

Table 2-14. Percent Difference between a Static AM-1.5 and a Detailed, Dynamic Spectral Model for Three Window Types

Window Orientation (time)	Standard Double-Pane		Vacuum Window		Double-Pane with Low-e	
	ΔT_S	ΔN_V[a]	ΔT_S	ΔN_V[a]	ΔT_S	ΔN_V[a]
Instantaneous Values for Denver, Colo., at the Indicated Times						
A. January 21, with bare soil ground reflectance						
S (1200)	0.3	6.8	0.8	5.9	1.5	7.0
E/W (900/1500)	1.1	18.2	2.8	17.0	5.6	18.4
N (1200)	0.6	16.0	-3.4	-15.2	5.8	16.2
B. July 21, with green vegetation ground reflectance						
S (1200)	1.5	21.3	-0.1	20.3	3.7	21.5
E/W (800/1600)	0.7	11.8	-0.2	10.9	1.5	12.0
N (1200)	3.9	75.8	0.2	74.7	11.0	76.2

[a] N_V is the fraction of the total transmitted solar flux that is visible (see Figure 2-23). It is an indication of the daylighting ability of the window under the indicated circumstances.

Results of these comparisons are shown in Table 2-14 as percent differences calculated as

$$\% \text{ Difference} = 100 \times \frac{\text{Detailed Model Result} - \text{Simple Model Result}}{\text{Detailed Model Result}} \quad (2\text{-}29)$$

The magnitude of the percent differences varies from insignificant to a very significant 76.2%. Careful examination of Table 2-14 reveals that the most significant differences occur for north-facing windows and that the differences are sensitive to the ground reflectance. In general, the magnitude of the differences clearly justifies the use of the more detailed spectral modeling technique.

2.1.6 Computer Model for Vacuum Window Thermal Performance

A model for the heat flow in a vacuum window has been developed at SERI. It has been used to guide the engineering design effort and has been integrated with the optical performance model for windows to provide overall optical and thermal performance predictions. The model is an electrical resistance analog of the thermal resistances through the window. Because the thermal radiation between the hot and cold glass panes is a large component of the overall heat transfer and is a nonlinear phenomenon, it is not possible to obtain analytical solutions to the heat losses through the vacuum window. Instead, the electrical analog model must be solved by computer iteration to a steady-state condition for each set of indoor and outdoor temperatures and wind conditions.

The physical basis for the model is described and results are presented in a parametric form to show how such a model can guide the window design process. Most of this design modeling work was done earlier and is included here for completeness.

A thermal resistance network model was developed to represent the heat flows in the evacuated window. An iterative computer program (Appendix A) was written to calculate the steady-state heat flows and temperatures in this model as a function of imposed indoor/outdoor temperatures and wind velocities. It was explicitly dependent on the particular values of window design parameters, for example spacer diameter and separation and internal surface coating emissivity. By repeatedly computing the overall thermal resistance through the model as design parameters are systematically varied, we are able to determine the interaction between design parameters. Thus, we can see where tradeoffs may be made between one constrained design parameter (such as the separation between spacers, which must be limited because of possible contact stress fracture) and the remaining parameters in order to maintain a high thermal resistance.

The thermal network that was modeled is shown schematically in Figure 2-32. Conductance of heat across the glazing was assumed to occur by radiative exchange between the inner and outer panes and by conduction through the support spheres and the edge seal. Gas-phase conductive and convective transfer between the inner and outer glazing was neglected because a highly evacuated enclosure was assumed.

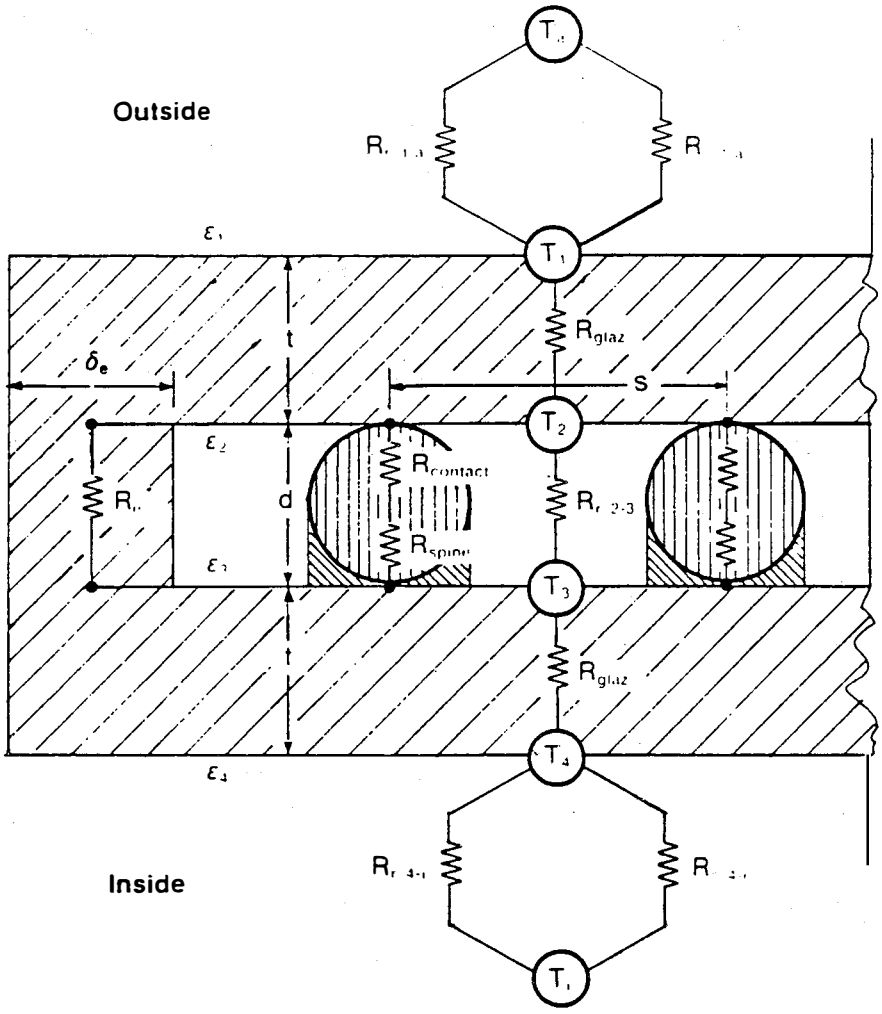

Figure 2-32. Diagram showing how thermal resistance of a vacuum was modeled with an electrical circuit

Coupling to the ambient and interior room was by parallel radiative and convective resistances. The radiative terms following (Duffie and Beckman 1980) were

$$R_{r,4\text{-}i} = \frac{1}{A\varepsilon\sigma\,(T_i + T_4)\,(T_i^2 + T_4^2)} \tag{2-30}$$

and

$$R_{r,1\text{-}a} = \frac{1}{A\,\varepsilon_1\sigma\,(T_1 + T_{sky})\,(T_1^2 + T_{sky}^2)}\,, \tag{2-31}$$

where

σ = Stefan-Boltzmann constant = 5.67032×10^{-8} ($W/m^2\,K^4$)

ε_n = Emittance of n^{th} surface (surfaces are numbered from the outside)

T_n = Temperature of n^{th} surface (K)

T_a = Ambient temperature (K)

T_i = Interior temperature (K)

A = Area of glazing (m^2)

For purposes of this analysis, the sky temperature, T_{sky}, was assumed equal to the ambient temperature, T_a, because the view for a vertical window is half sky and half ground.

The convective film resistances used were those given in Lauer (1953):

$$R_{c,4\text{-}i} = \frac{1}{1.776A\,(T_i - T_4)^{1/4}}\ (K/W) \tag{2-32}$$

and

$$R_{c,1\text{-}a} = \frac{1}{6.518A\,(v)^{3/4}}\ (K/W)\,, \tag{2-33}$$

where v = wind velocity (m/s).

Radiative exchange between the glazings was calculated as in Duffie and Beckman (1980):

$$R_{r,2\text{-}3} = \frac{\frac{1}{\varepsilon 2} + \frac{1}{\varepsilon 3} - 1}{A\sigma\,(T_2 + T_3)\,(T_2^{\,2} + T_3^{\,2})}\ (K/W)\,. \tag{2-34}$$

The thermal resistance through the glass plates is

$$R_{glaz} = \frac{t}{Ak}\ (K/W) \tag{2-35}$$

where t = thickness of the glazing (m)
k = thermal conductivity of glass = 1.05 ($W/m^2\,K$).

The thermal resistance of a single support spacer was considered to be the resistance of the sphere in series, with a constriction resistance occurring at the contact area between the sphere and the glazing. The sphere resistance was approximated as a spine, or right circular cylinder, of radius a and height d/2 (= a) plus a hemispherical cap. The cylindrical spine resistance is

$$R_{cylinder} = \int_o^a \frac{dx}{k\pi a^2} = \frac{1}{k\pi a} . \qquad (2\text{-}36)$$

Note that this is accurate for the lower half of the support spacers shown in Figure 2-33, where the spheres are assumed to be intimately bonded to the outer glazing, the bond weld forming a cylindrical shape. The upper hemisphere is included as

$$R_{spine} = \int_o^a \frac{dx}{k\pi a^2} + \int_o^{x_c} \frac{dx}{k\pi r^2(x)} \qquad (2\text{-}37)$$

$$= \left(\frac{1}{k\pi a}\right) \left[1 + \arctan\left(\frac{x}{a}c\right)\right] ,$$

using, from Figure 2-33:

$$x_c = (a^2 - r_c)^{1/2}$$

and

$$r^2(x) = a^2 - x^2 \text{ and } \frac{x_c}{a} = \left(1 - \frac{r_c}{a}\right)^{1/2} .$$

Abramowitz and Stegun (1964) give a suitable approximation for the arctan function:

$$\arctan(Z) = \frac{Z}{1 + 0.28\, Z^2} + \text{error}(Z)$$

$$\text{where } |\text{error}(Z)| \leq 0.005 \text{ for } 0 \leq Z \leq 1.$$

This approximation over the range of arguments used in the model is in error by less than 1%.

Thus the total spine resistance is

$$R_{spine} \quad \frac{1}{k\pi a}\left[1 + \frac{Z}{1 + 0.28\, Z^2}\right] \qquad (2\text{-}38)$$

where

$$Z = \left(1 - \frac{r_c}{a}\right)^{1/2} = \left(1 - \frac{r_c}{r}\right)^{1/2} .$$

For an isothermal circular contact area of radius r_c, the contact resistance between a sphere and a plate is (Chen and Tien 1973)

$$R_{contact} = \frac{0.53}{kr_c} \text{ (K/W)}. \qquad (2\text{-}39)$$

Then, the total thermal resistance of a single support sphere is

$$R_s = R_{spine} + R_{contact} . \qquad (2\text{-}40)$$

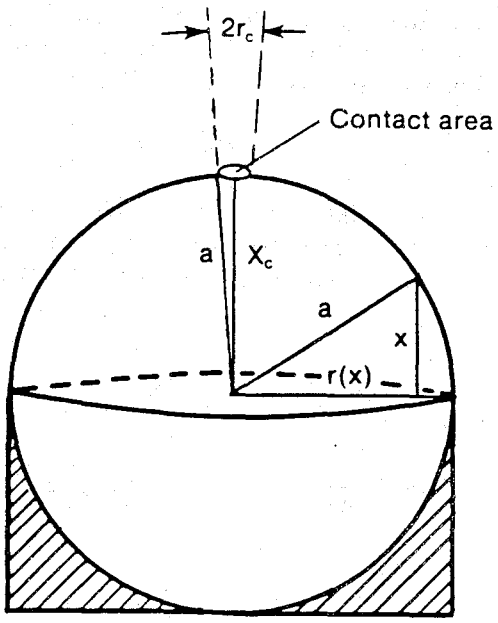

Figure 2-33. Diagram showing assumed geometry of a spherical spacer in bonded contact with one flat glass sheet (bottom) and in point contact with the second flat glass sheet (top)

The contact radius can be derived from the expression given by Johnson (1982) for the contact between two spherical bodies (letting $\frac{1}{r} \to o$ for one of the spheres) as

$$r_c = \left[\frac{3}{4} F \left(\frac{1 - \mu^2}{E}\right) d\right]^{1/3} , \qquad (2\text{-}41)$$

where

μ = Poisson's ratio for glass = 0.21

E = Young's modules for glass = 6.37×10^{10} N/m^2

F = Compressive force applied normal to the glazing area.

The number of spheres N in a uniform hexagonal array with spacing, s, contained in an area A is $2A/\sqrt{3}s^2$. For N spheres compressed by atmospheric pressure, P, between two plates, the compressive force experienced by each sphere is

$$F = \frac{PA}{N} = \frac{Ps^2\sqrt{3}}{2} , \qquad (2\text{-}42)$$

and so

$$r_c = \left[\frac{3\sqrt{3}}{8} \frac{P}{E} (1 - \mu^2)\, s^2 d\right]^{1/3} . \qquad (2\text{-}43)$$

The total thermal resistance from N support spheres in parallel with one another is then

$$R_s = \frac{\sqrt{3}}{2} \frac{s}{A} \left(R_{spine} + R_{contact}\right) . \qquad (2\text{-}44)$$

The edge seal thermal resistance network includes conductance along the plane of the glazing and the influence of an insulating window frame (Figure 2-34). Under the assumption of isothermal glazings, the conductance through the edge is given by

$$R_{edge} = \frac{t+d}{kL\,\delta_e} \text{ (K/W)} , \qquad (2\text{-}45)$$

where

d = diameter of glass sphere spacer (m)
t = glass thickness (m)
L = length of the edge (perimeter) = 2(ℓ + w) (m)
ℓ = length of glazing (m)
w = width of glazing (m)
δ_e = width of edge seal (m)
k = thermal conductivity of glass (W/m K) .

The conductance in the plane of the glass sheet into the edge seal is analogous to a heat exchanger fin effect and is treated accordingly.

As seen in Figure 2-34, R_{edge} is in series with the resistance in the plane of the glass, $\frac{1}{2} R_g$, where

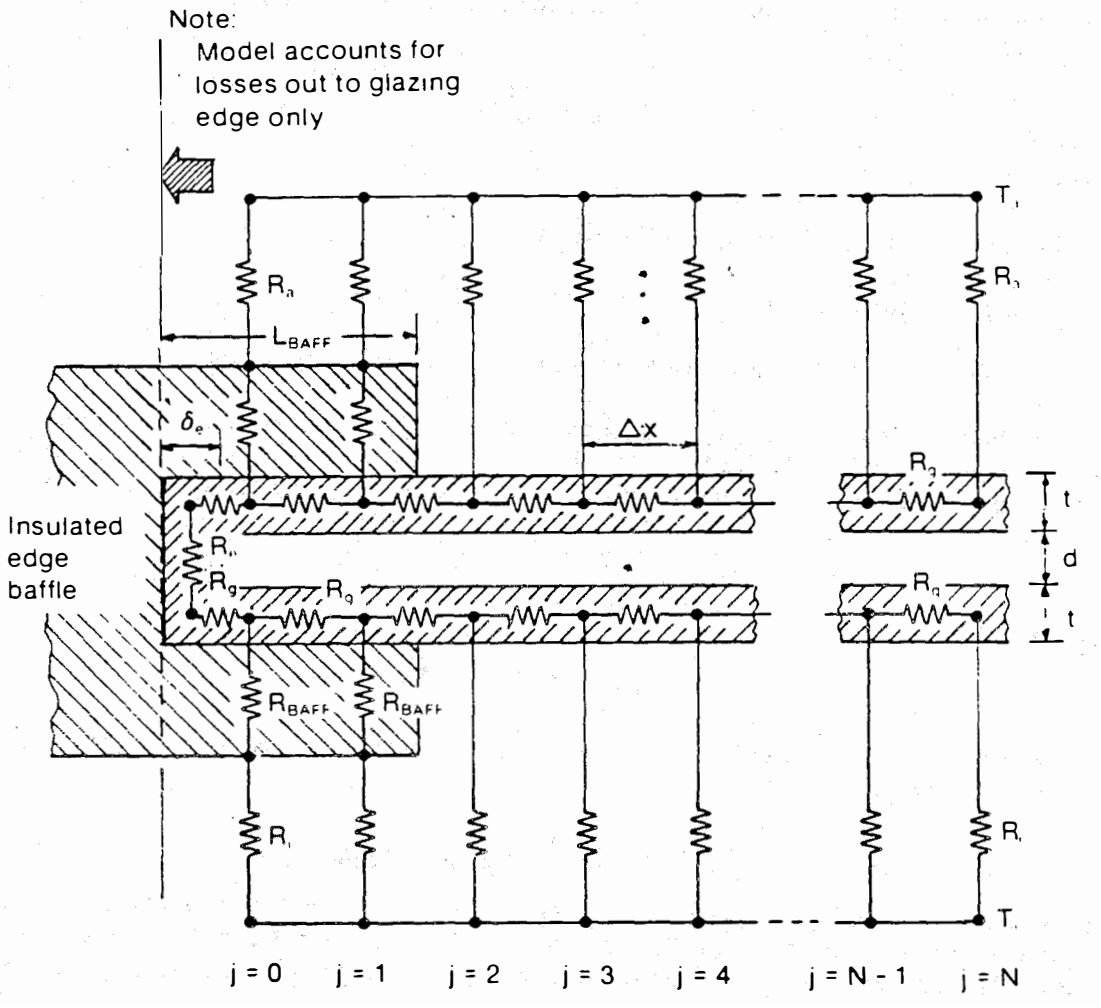

Figure 2-34. Diagram showing the electrical circuit analog used to model heat flow through the insulated perimeter of a vacuum window

$$R_g = \frac{\Delta x}{kLt} \quad (K/W) \tag{2-46}$$

and Δx = nodal spacing ($\approx$0.005 m) .

R_{edge} and R_g are then tied to the interior and ambient conditions by j parallel coupling resistances. The overall edge resistance for j nodes is calculated as

$$R_e = R_{edge} + R_g + R_{\sigma j} + R_{wj} , \tag{2-47}$$

where

$$R_{\sigma j} = \frac{(R_{\sigma,j-1} + R_g)\, R_\sigma}{R_{\sigma,j-1} + R_{\sigma,o}} \tag{2-48}$$

$$R_{\sigma,0} = R_\sigma + R_g \tag{2-49}$$

where

$$R_\sigma = \begin{cases} R_{baff} + R_a & \text{if } j\Delta x \le L_{baff} \\ R_a & \text{if } j\Delta x > L_{baff} \end{cases}$$

and L_{baff} = width of edge baffle (m) .

$$R_a = \frac{R_{r,4-a}\, R_{i,4-a}}{R_{r,4-a} + R_{r,4-a}} \tag{2-50}$$

and similarly for R_{wj} with

$$R_w = \begin{cases} R_{baff} + R_i & \text{if } j\Delta x \le L_{baff} \\ R_i & \text{if } j\Delta x > L_{baff} \end{cases} \tag{2-51}$$

where

$$R_i = \frac{R_{r,1-i}\, R_{c,1-i}}{R_{r,1-i} + R_{c,1-i}} .$$

Convergence is assumed to occur when R_e does not significantly change between j = 1 and j = n. The effective fin width, X_{fin}, is then nΔx. Typically, convergence was found to occur for $X_{fin} \le 0.05$ m (2 in.).

To compute the total resistance, R_t, of the glazing system, the edge seal resistance given by Eq. 2-41 is considered to be in parallel with a resistance, R_z, which accounts for the coupling of the interior and ambient conditions through the glass plates and the heat exchange between the glass plates from the spacer supports and radiative exchange. That is,

$$R_z = R_a + R_{glaze} + R_{rs} + R_{glaze} + R_i \tag{2-52}$$

where $$R_{rs} = \frac{R_{r,2-3} R_s}{R_{r,2-3} + R_s} .$$

The parallel resistances R_e and R_z are then weighted by the glazing area to give

$$R_t = A \left(\frac{R_e R_z}{R_e + R_z} \right) . \quad (2\text{-}53)$$

Surface temperatures can then be calculated as (ASHRAE 1985)

$$T_1 = T_i - \frac{R_i}{R_t} (T_i - T_a) \quad (2\text{-}54)$$

$$T_2 = T_i - \frac{(R_i + R_{glaz})}{R_t} (T_i - T_a) \quad (2\text{-}55)$$

$$T_3 = T_a + \frac{(R_a + R_{glaz})}{R_t} (T_i - T_a) \quad (2\text{-}56)$$

$$T_4 = T_a + \frac{R_a}{R_t} (T_i + T_a) . \quad (2\text{-}57)$$

Following the procedure given by Duffie and Beckman (1980), the updated surface temperatures, T_n, can be used to recompute R_t, until convergence has occurred.

The thermal performance of an evacuated window glazing depends on the successful control of four heat-transfer processes: convection, gas-phase conduction, conduction through the solid window glazing components, and radiative heat transfer across the evacuated space. By choosing a high-quality vacuum, we are able to reduce convection and gas-phase conduction to negligible values, reducing the thermal performance optimization to a problem of dealing with thermal conduction through glass components and thermal radiation between the glass panes.

Figure 2-35 shows summary graphs of predicted vacuum window R-values. In each of these graphs, all design variables are held constant except for one, which is varied from one-half of its base-case value to twice its base-case value. Such graphs show how the overall thermal resistance varies with a particular design parameter.

Taken together as a series (called a "spider" plot), such graphs summarize the effects of the various design parameters on a particular base-case design. For example, in the lower spider plot, for the base case that includes a single low-emissivity coating, the most steeply sloped graph, labeled E, indicates how the overall thermal resistance of the window is predicted to vary as the emissivity of the low-e coating is changed from its base-case value of 0.1. The curve shows that decreasing the emissivity would dramatically increase the thermal resistance of the window (see Section 2.2.1). On

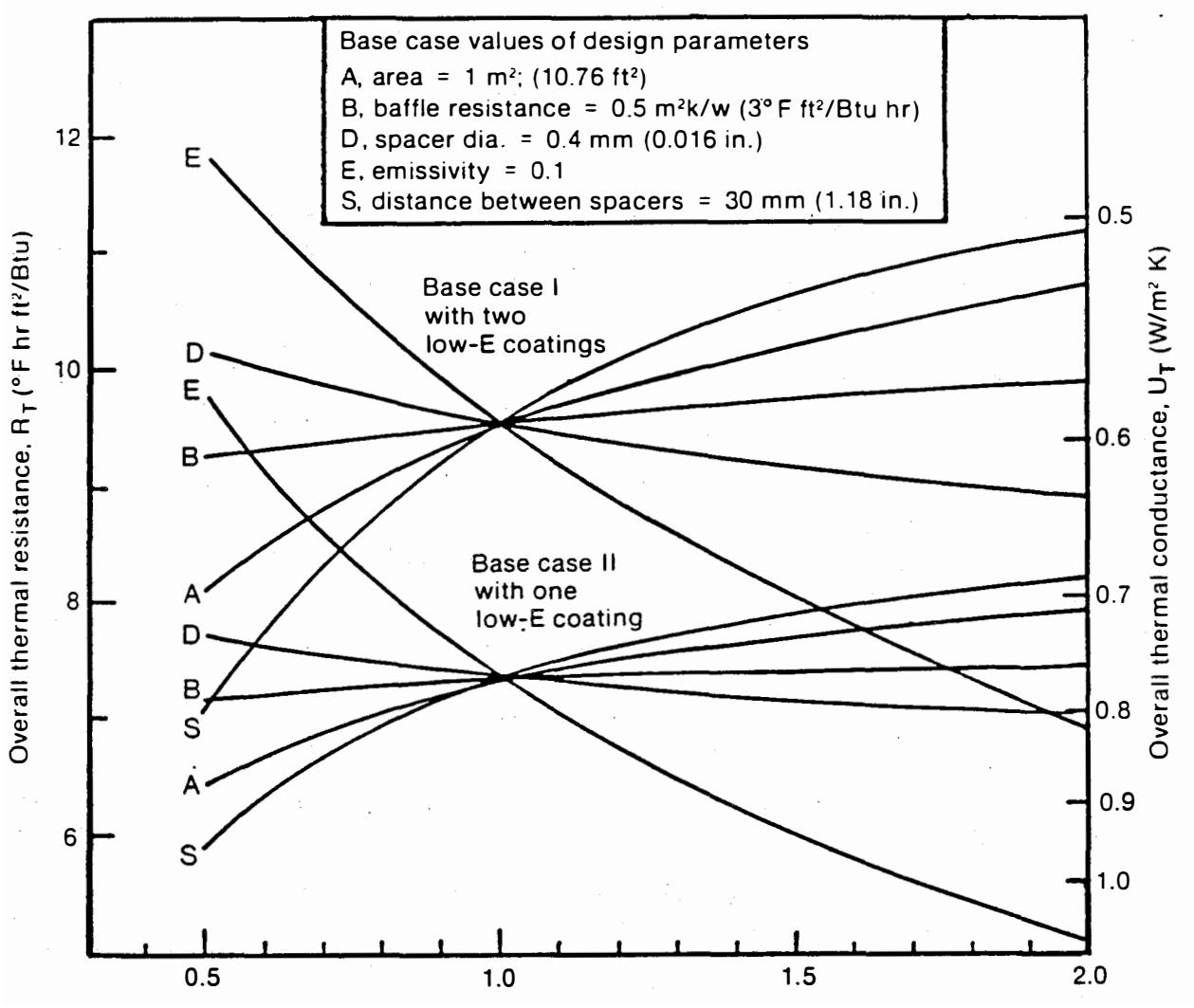

Figure 2-35. **Parametric curves showing the sensitivity of vacuum window performance to design variables.** The top set of curves applies to a vacuum window with two internal low-e coatings. The bottom set applies to a vacuum window with only one low-e coating.

the other hand, curve S shows that decreasing the separation between spherical spacers (and corresponding increase in the number of spacers) dramatically decreases the thermal resistance of the window. The other curves show the less dramatic effects of changing other design parameters such as sphere diameter, D, the thermal resistance of the edge baffle, B, and the total area of the window, A.

The upper spider plot summarizes the predicted dependence of window performance on these same design variables about a base-case design that includes two low-e coatings. The inclusion of the second low-e coating increases the thermal resistance of the window and changes its sensitivity to the other design variables. With two low-e coatings, the vacuum window performance becomes somewhat less sensitive to changes in emissivity but more sensitive to changes in the separation between supports and to the diameter of these supports.

2.1.7 Detailed Window Modeling Results for the Pacific Northwest

The detailed optical and thermal performance algorithms have not been integrated with a whole-building energy performance model. However, some analyses have been done to indicate the nature of results that can be expected from the use of a vacuum window in the BPA service region.

Transmitted solar power and visible daylighting components are shown in Table 2-15 for the indicated hours on the representative winter and summer days, January 21 and July 21, in Portland, Spokane, and Boise. The window configuration is the Case I vacuum window, with design parameters summarized in Figure 2-35.

The detailed algorithm discussed in Section 2.1.5 has been used to characterize the overall performance of the prototype vacuum window in Portland (45.60°N latitude, 122.60°W longitude). Summer and winter performance were represented by detailed hour-by-hour simulations for the typical days, July 21 and January 21. Figure 2-36 shows the predicted values of transmitted solar flux (and the visible, daylight component) for windows facing south, east, west, and north.

These optical modeling results were combined with the thermal performance model and integrated over the complete 24-h periods of July 21 and January 21. Similarly detailed calculations were made for a conventional double-pane, sealed insulating glass window and integrated over the same periods. Table 2-16 compares these two types of window in a south-facing orientation.

Note that the standard, double-pane sealed insulating glass window is predicted to cause a very large net energy loss in the winter, whereas the vacuum window provides a significant net solar energy gain. The daylighting contributions differ by less than 10%. In the summer, the vacuum window is predicted to provide slightly less heat gain than a conventional window.

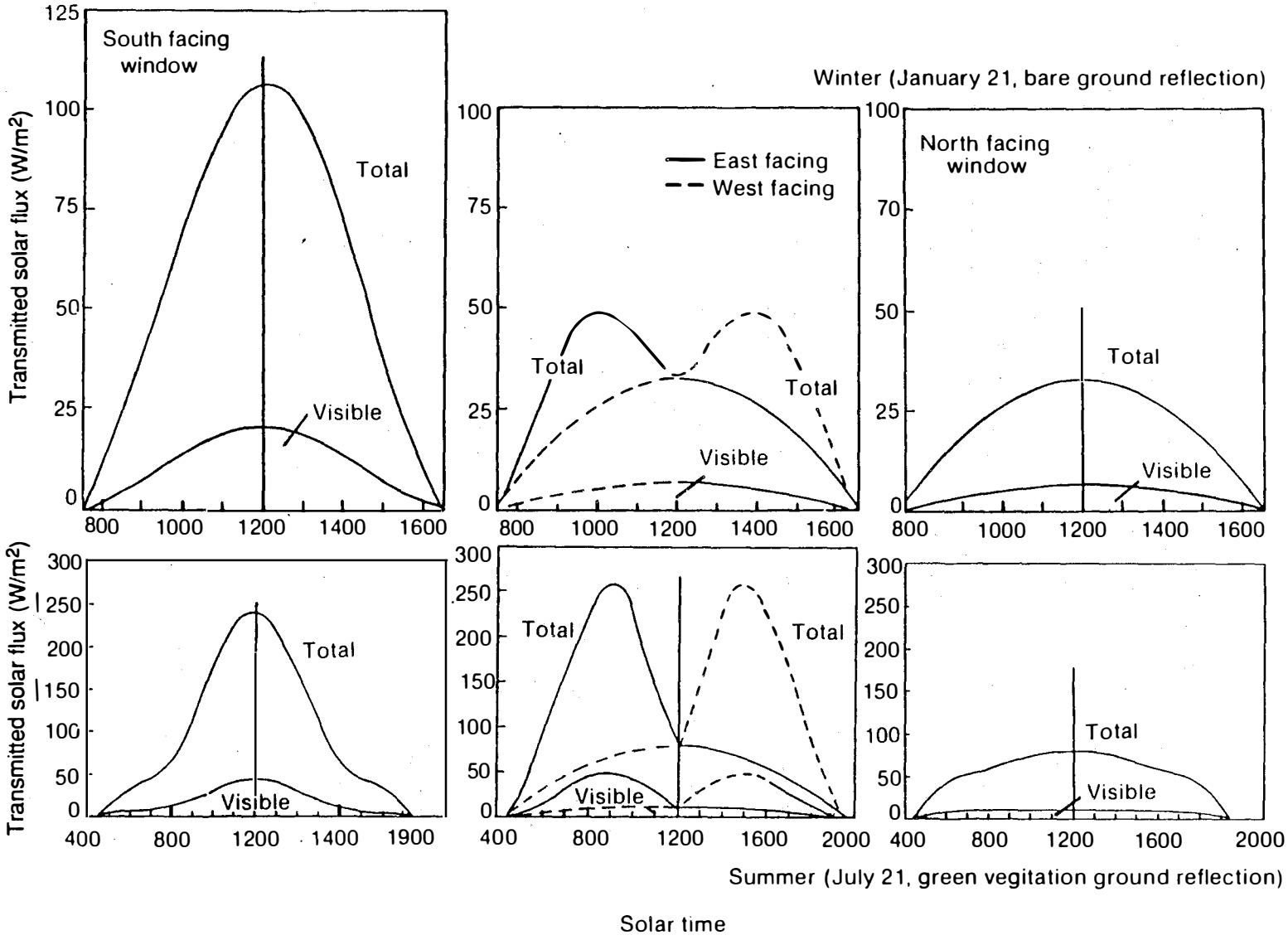

Figure 2-36. Predicted hourly transmittance of a prototype vacuum window in Portland, Oregon

Table 2-15. Transmitted Solar Flux through a Vacuum Window Calculated at Peak Solar Hour

Location	Winter (Jan. 21)				Summer (July 21)			
	K_T	S[a] (1200)[b]	E/W (1000/1400)	N (1200)	K_T	S (1200)	E/W (1000/1400)	N (1200)
Portland	0.295	106[c]	48.9	32.5	0.568	242	258	80.4
Spokane	0.335	112	50.5	34.2	0.659	290	299	88.2
Boise	0.417	164	76.0	46.1	0.726	288	336	94.6

[a]Orientation [b]Time [c]kW/m^2 K_T=clearness index

Table 2-16. Net Daily Energy Flow through South-Facing Windows in Portland, Oregon
(24 hour total)

	Standard Window	Prototype Vacuum Window
Winter (January 21)		
Heat gain (kJ/m^2)	(-2257)	+629
Daylighting (kJ/m^2)	385	362
Summer (July 21)		
Heat gain (kJ/m^2)	+5925	+5467
Daylighting (kJ/m^2)	1062	998

2.2 Laboratory Research

2.2.1 Low-Emittance Coatings

2.2.1.1 Background

The radiative heat transfer across the vacuum gap in a vacuum insulating window can be significant. The power radiated between the parallel glass sheets is

$$p = A\sigma (T_H^4 - T_C^4)/(1/e_C + 1/e_H - 1) \qquad (2\text{-}58)$$

where σ is a universal constant (the Stefan-Boltzmann constant 5.670 x

10^{-8} Wm^{-2} K^{-4}); T_H and T_c are the glass temperatures (in degrees Kelvin); A is the window area (in square meters); e_h and e_c are the emittances of the hot and cold inner surfaces of the glass, and p is the net radiated heat transfer (in watts). If the two glass surfaces are identical, $e = e_h = e_c$, then this equation may be rearranged to define a radiative conductance,

$$C_R = \frac{p}{A\,(T_H - T_c)} = \sigma e\,\left(T_H^2 + T_C^2\right)\left(T_H + T_C\right)/(2-e) \qquad (2\text{-}59)$$

The radiative conductance of a vacuum insulating window when the outdoor temperature is 0°C and the indoor temperature is +25°C (T_H = 298 K, T_c = 273 K) is calculated to be about 3.8 W m^{-2} K^{-1} if the emissivity of uncoated glass (e = 0.84) is used in this equation. This corresponds to a thermal resistance in English units of only about R = 1.5°F ft^2 hr/Btu. Obviously, a lower emittance is required to reduce the radiative conductance in a vacuum insulating window.

Figure 2-35 shows the relation between the overall thermal conductance of a vacuum insulating window and the emittance of its internal surfaces. Even with the effect of radiative conductance diluted by the parallel conductance through the spacers and around the window parameter, the importance of the emittance remains obvious.

2.2.1.2 A New Low-Emittance Coating

The high-temperature vacuum processing required to seal a vacuum insulating window limits the choices for a low-emittance coating. The window must be heated to about 565°C in vacuum during laser welding to prevent thermal shock fracture by the laser beam. The best low-emittance coatings developed for windows will not tolerate this treatment. Some low-emittance coatings such as antimony-doped tin oxide and tin-doped indium oxide will withstand the processing conditions but have emittance greater than 0.1 even when thick coatings are used.

Recently, thin transparent coatings have been developed for use in automotive windshields, where they serve as resistive electrical heaters for defogging and defrosting. Some of these coatings have been designed so that they can be applied to the glass while it is flat and then can withstand the heating and bending of the glass into the curved shape of the windshield. We tested samples of one such coating* and found that its emittance increased and its transmittance decreased drastically upon heating to 565°C in vacuum.

Airco Coating Technology research staff volunteered to fabricate samples of modified coatings on our borosilicate glass substrates for evaluation at SERI. The exact composition of this multilayer sputtered film is proprietary to Airco, but it is known to be of the dielectric/metal/dielectric "sandwich" configuration in which silver is the thin metal layer.

*"Super H" coating developed by Airco Coating Technologies, Concord, California.

2.2.1.3 Characterization of New Low-Emittance Coatings

The coated glass samples were characterized at SERI by optical spectroscopy, infrared reflectometry, and resistivity measurements. The spectral transmittance was measured between 0.26 and 2.6 microns wavelength and integrated to obtain the solar-weighted and visible-weighted (photopic) transmittances. The thermal emittances were calculated from broadband thermal infrared reflectance using the relation

$$\text{emittance} = 1 - \text{thermal infrared reflectance} \qquad (2\text{-}60)$$

applicable to a material which, like glass, is opaque to the thermal infrared radiation. The spectral measurements were made with a Perkin-Elmer Lambda 9 spectrophotometer, and the reflectivity was measured with a Gier-Dunkle Model DB-100 Infrared Reflectrometer. The sheet resistances of coatings were measured with a custom four-point probe apparatus used for measuring thin film semiconductors.

Five different coatings were prepared by Airco on 5-x-5-cm sheets of 3-mm-thick borosilicate (Corning 7740) glass. Each was characterized in the as-received condition and then cut into four 2.5-x-2.5-cm samples. One set of the samples was heat treated in vacuum for a short period and a second set for a longer time. The heat-up and cool-down were slow because of the nature of the SERI vacuum laser welding furnace.

The annealing curves are shown in Figure 2-37. In both cases, the maximum temperature was 565°C and the pressure was maintained at less than 5×10^{-6} torr. The shorter anneal included 1 hour at 565°C and the longer anneal included 12 hours at 565°C. The samples were protected from gross contamination while in the furnace by a canopy of borosilicate glass bridging over and about one millimeter above the coating.

2.2.1.4 Optical and Electrical Properties of Low-Emittance Coatings

Table 2-17 summarizes the measured data for all samples. In general, those coatings that had already been heat treated in air by Airco started out with lower emittances and higher transmittances. Those samples that had not been previously heat treated started out with high emittances and low transmittances. The vacuum heat treatment tended to bring these two different types of samples closer together in optical properties.

Although the emittance of the coating is of paramount importance to the thermal performance of the vacuum insulating window, the solar transmittance is also important to the function of the window. A high visible transmittance is desirable, but it is not as important so long as the appearance of the coating is aesthetically acceptable. A colorless coating with uniform transmittance is considered to be acceptable by the window industry.

A useful figure of merit for coatings to be used in the vacuum insulating window is the ratio of solar transmittance to thermal emittance (Table 2-17). This figure of merit (FOM) has been shown to be correlated with the sheet resistance of the coating for a number of different low-emittance coatings (Benson and Tracy 1985). Figure 2-38 shows a graph of the FOM vs. sheet resistance for three such materials that could be used in the vacuum

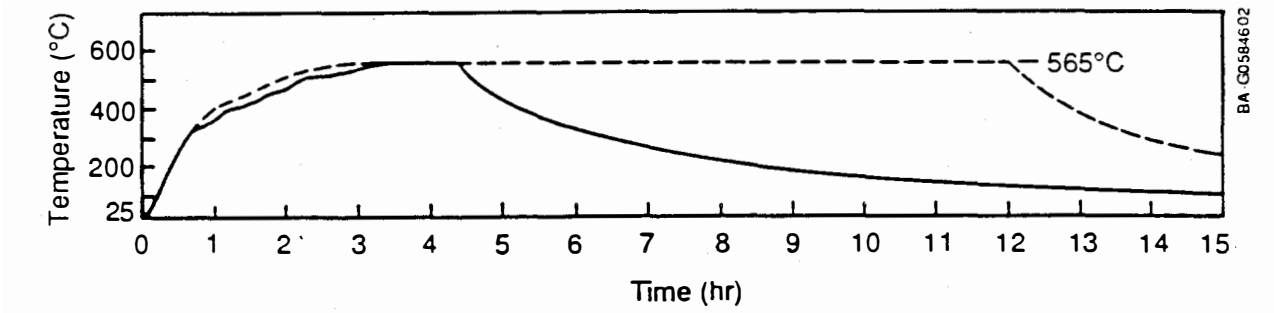

Figure 2-37. Vacuum annealing histories

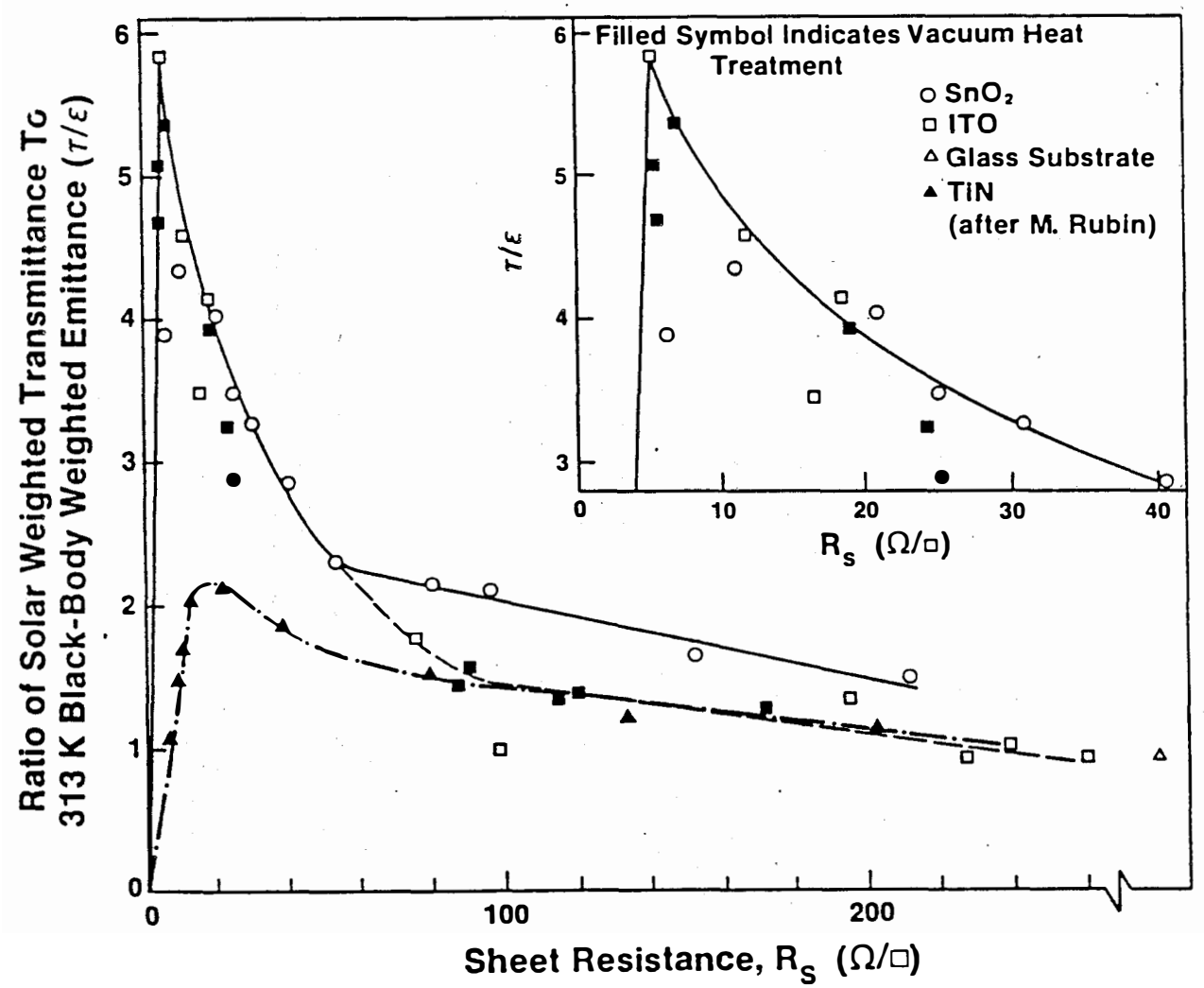

Figure 2-38. Relation between sheet resistance and a figure of merit for low-emittance window coatings

Table 2-17. Low-Emittance Coatings

Sample	e, Emittance			Transmittance τ_s Solar (AM1.5)			Transmittance τ_v, Visible (photopic)			Sheet Resistance (Ω/□)			Figure of Merit (τ_s/e)		
	1*	2	3	1	2	3	1	2	3	1	2	3	1	2	3
1. No. 29P	0.074	0.086	0.100	0.594	0.581	0.579	0.850	0.831	0.830	6.15	7.00	8.10	8.03	6.76	5.79
2. No. 29P	0.189	0.158	0.176	0.310	0.522	0.548	0.447	0.741	0.768	210	17.50	19.50	1.64	3.30	3.11
3. No. 11(P) pre/post	0.069	0.078	0.082	0.624	0.612	0.615	0.821	0.789	0.803	6.24	6.56	6.00	9.04	7.85	7.5
4. No. 11(P) pre/post	0.189	0.116	0.147	0.350	0.520	0.540	0.513	0.628	0.655	214	8.62	9.90	1.85	4.48	3.67
5. No. 11(P) pre/post	0.183	0.128	0.139	0.371	0.515	0.534	0.539	0.624	0.654	208	9.40	9.33	2.03	4.02	3.84
6. No. 29P	0.185	0.135	0.187	0.310	0.527	0.553	0.448	0.752	0.772	214	13.70	30.00	1.68	3.90	2.96
7. No. 29P	0.185	0.155	0.181	0.314	0.526	0.550	0.453	0.746	0.769	234	16.30	23.00	1.70	3.39	3.04
8. No. 10(P) pre/post	0.071	0.078	0.092	0.624	0.605	0.611	0.848	0.809	0.824	5.83	6.20	6.50	8.79	7.76	6.64
9. No. 10(P) pre/post	0.188	0.099	0.121	0.345	0.529	0.561	0.520	0.690	0.730	215	8.60	9.00	1.84	5.34	4.64
10. No. 10(P) pre/post	0.185	0.158	0.171	0.337	0.550	0.569	0.510	0.729	0.748	214	14.10	14.00	1.82	3.48	3.33
11. No. 9(P) pre	0.185	0.170	0.225	0.324	0.563	0.592	0.494	0.762	0.791	210	12.70	19.40	1.75	3.31	2.63
12. No. 9(P) pre,	0.184	0.145	0.209	0.321	0.563	0.596	0.491	0.764	0.796	208	11.70	17.50	1.75	3.88	2.85
13. No. 9(P) pre/post	0.074	0.089	0.086	0.613	0.598	0.606	0.854	0.824	0.842	6.14	8.50	6.45	8.28	6.72	7.05
14. No. 9(P) pre/post	0.186	0.182	0.217	0.324	0.562	0.592	0.494	0.753	0.793	213	15.00	20.6	1.74	3.09	2.73
15. "Super-II"	0.053	0.315	0.483	0.563	0.462	0.464	0.848	0.603	0.584	4.34	81.00	100	10.62	1.47	0.96

*1 = as received
2 = after shorter time vacuum anneal at 565°C (nominal 1 hour)
3 = after longer time vacuum anneal at 565°C (nominal 12 hours)

insulating window. The highest FOM is 5.9 for a very thick coating (450 nm) of sputter-deposited and vacuum-annealed tin-doped indium oxide prepared for SERI on custom order by Applied Films Corporation (Boulder, Colorado). This low-emittance coating had an emittance of 0.12 and a solar transmittance of 0.68. However, its thickness makes it prohibitively expensive to fabricate for use in large windows. The best of the economical alternatives is a fluorine-doped tin oxide (SnO_2) with a FOM of 4.4.

Figure 2-39 shows the relation between FOM and sheet resistance for the Airco experimental low-emittance coatings. The best of these coatings (No. 3 in Table 2-17) has a FOM of 7.85 after vacuum anneal for 1 hour (eventually decreasing only slightly to 7.5 after 12 hours of vacuum anneal). This coating had an emittance of about 0.08 and a solar transmittance of 61% after anneal along with a high visible transmittance of 79% and a uniform, uncolored, aesthetically pleasing appearance. Another coating (No. 8 in Table 2-17) exhibited very similar properties and a FOM of 7.76 after the 1-hour vacuum anneal.

2.2.1.5 Conclusions

New sputter-deposited thin low-emittance coatings produced by Airco Coatings Technology are suitable for use in the vacuum insulating window. These new low-e coatings have high solar and visible transmittances. They are similar to other low-e coatings currently mass produced for architectural and automotive windows and may be expected to be economical.

The new low-e coatings have figures of merit (solar transmittance/emittance ratios) about 33% better than any previously identified usable low-emittance coating, and 78% better than any other previously identified economical option. The emittance of the new coating is lower than the best economical alternative by about 47%.

The use of the new low-emittance coating as a replacement for the best available (fluorine-doped tin oxide) economical alternative would be expected to increase the thermal resistance of the vacuum insulating window by about 20%.

2.2.2 Development of a Vacuum Laser Welding Facility

A facility for fabricating full-sized evacuated window specimens for engineering scale testing has been designed, constructed, and installed at SERI's Field Test Laboratory. The facility consists of three major components: the SERI carbon dioxide laser (400 W maximum CW), a vacuum furnace in which the evacuated window specimen can be edge sealed, and a laser beam steering system that automatically directs the laser beam along its welding path.

The vacuum furnace is needed to heat the glass to a sufficiently high temperature (about 565°C) to prevent thermal shock fracture during the laser welding while maintaining a vacuum ($\sim 3 \times 10^{-6}$ torr) within the window until it is completely sealed. A nonevaporable reactive metal getter strip within the window will be activated at the welding temperature and will trap gases evolved from the internal surfaces of the window during and after the sealing process. When the sealed window is cooled to room temperature, the pressure within it will be further reduced by about a factor of three merely because of the gas

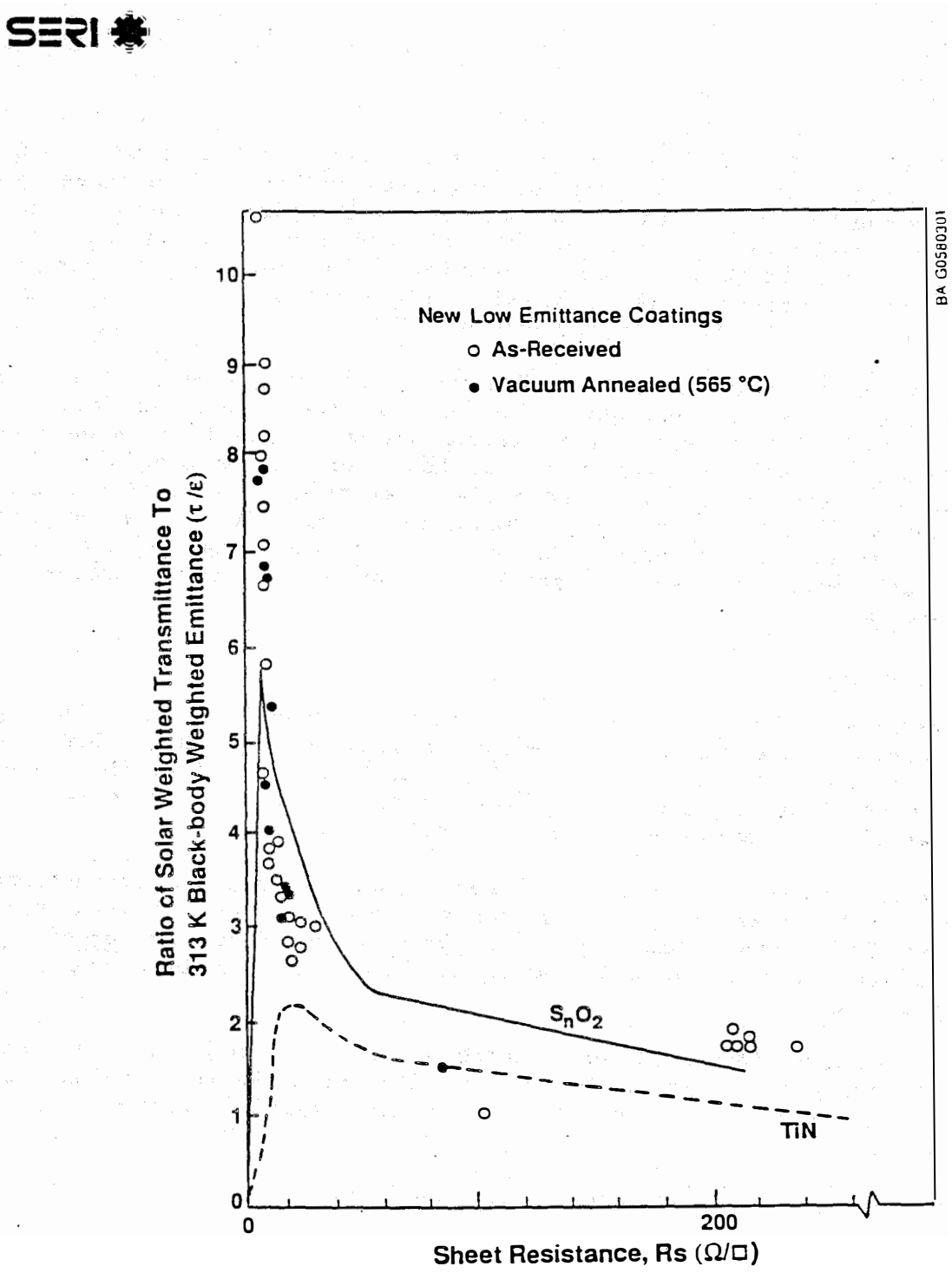

Figure 2-39. Relation between sheet resistance and the figure of merit for AircoCoatings Technology experimental low-emittance coating (No.11(P) in Table 2-17)

contraction with cooling and by as much as a factor of 100 by the continued action of the reactive metal getter.

2.2.2.1 Vacuum Furnace Design

Vacuum furnaces are commonly used in metallurgical applications and in some metal and ceramics fabrication processes. However, such furnaces are designed for much higher temperature use and for rapid processing. Consequently, commercially available vacuum furnaces of the size required to accommodate a 1-m^2 window sample are very expensive. A new, more economical vacuum furnace designed specifically for our purposes was sought through a competitive procurement process. The winning design is described briefly below.

The vacuum furnace is a rectangular parallel-piped stainless-steel box with various doors and ports. The interior surfaces are clean, smooth stainless steel to minimize outgassing and thus minimize the time required to reach operating temperature and pressure, and to assure an acceptably low operating pressure at high temperature. The only insulation used in the furnace is reflective metal, radiative insulation because the vacuum itself is sufficient to reduce gas-phase heat conduction to the furnace walls to a negligible value. A three-layer stack of stainless-steel reflectors surrounding the hot zone effectively blocks the radiative heat transfer.

Metal-sheathed, tubular, electric resistance heaters similar to those found in cooking ovens are distributed to provide radiative heating to the sample holder.

A large pumping capacity, oil diffusion pump, and rotary displacement pump combination is used. A low-vapor-pressure silicone pump oil and a water-cooled baffle limit backstreaming of oil into the furnace. Pneumatic valves are controlled automatically by an electronic controller that uses signals from two ionization and two thermocouple vacuum gauges to sense the status of the pumpdown process.

The opposite sides of the furnace are doors that swing open to provide unobstructed access for positioning the window samples. The laser beam access window and the electro-optical beam steering mechanisms are located in an attached chamber above the furnace hot zone and are thermally isolated from it by radiative heat shields.

All the vacuum seals are either permanent (welded) or use Viton o-rings.

Figure 2-40 shows the general design and dimensions of the vacuum furnace. Figure 2-41 is a photograph of the installed facility including the CO_2 laser on the left and the furnace on the right.

2.2.2.2 Laser Beam Control

A two-axis, computer-controlled, laser beam steering subsystem has been designed and constructed. Novel features of this design improve the energy coupling efficiency between the beam and the glass workpiece.

The 10.6-μm CO_2 laser beam is admitted into the vacuum furnace through a zinc selenide window. A water-cooled copper mirror reflects the beam to the

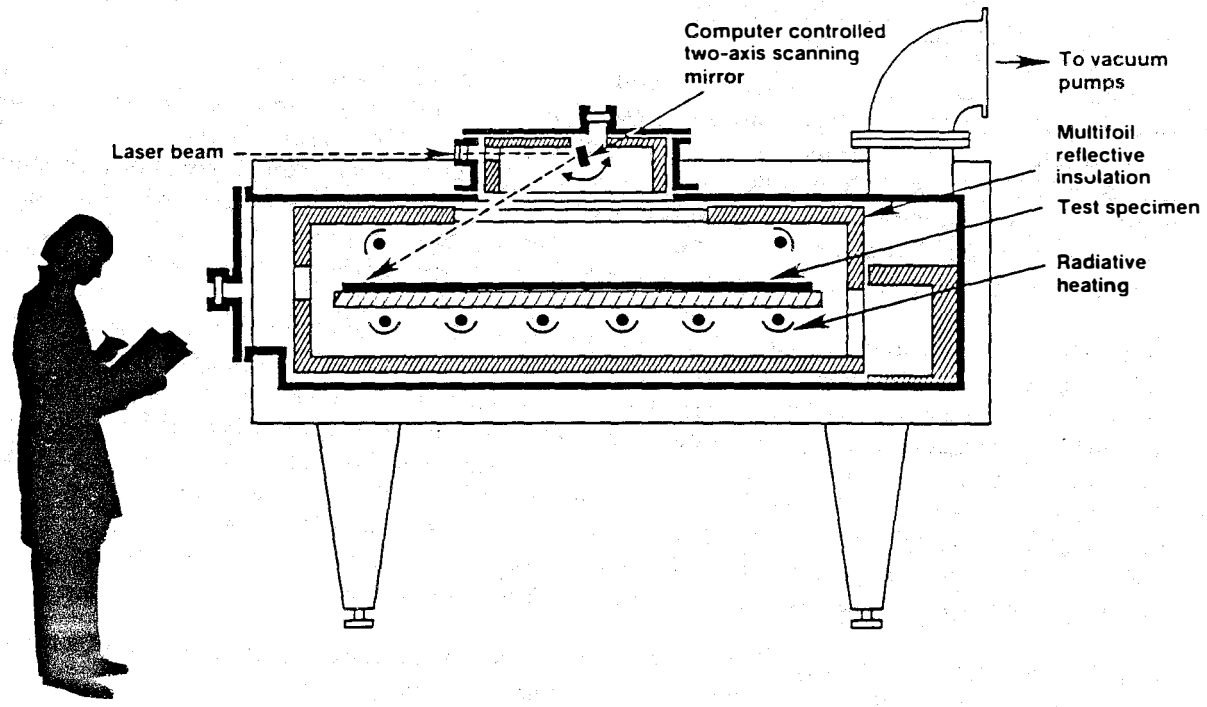

Figure 2-40. Cross-sectional diagram of the vacuum laser welding furnace

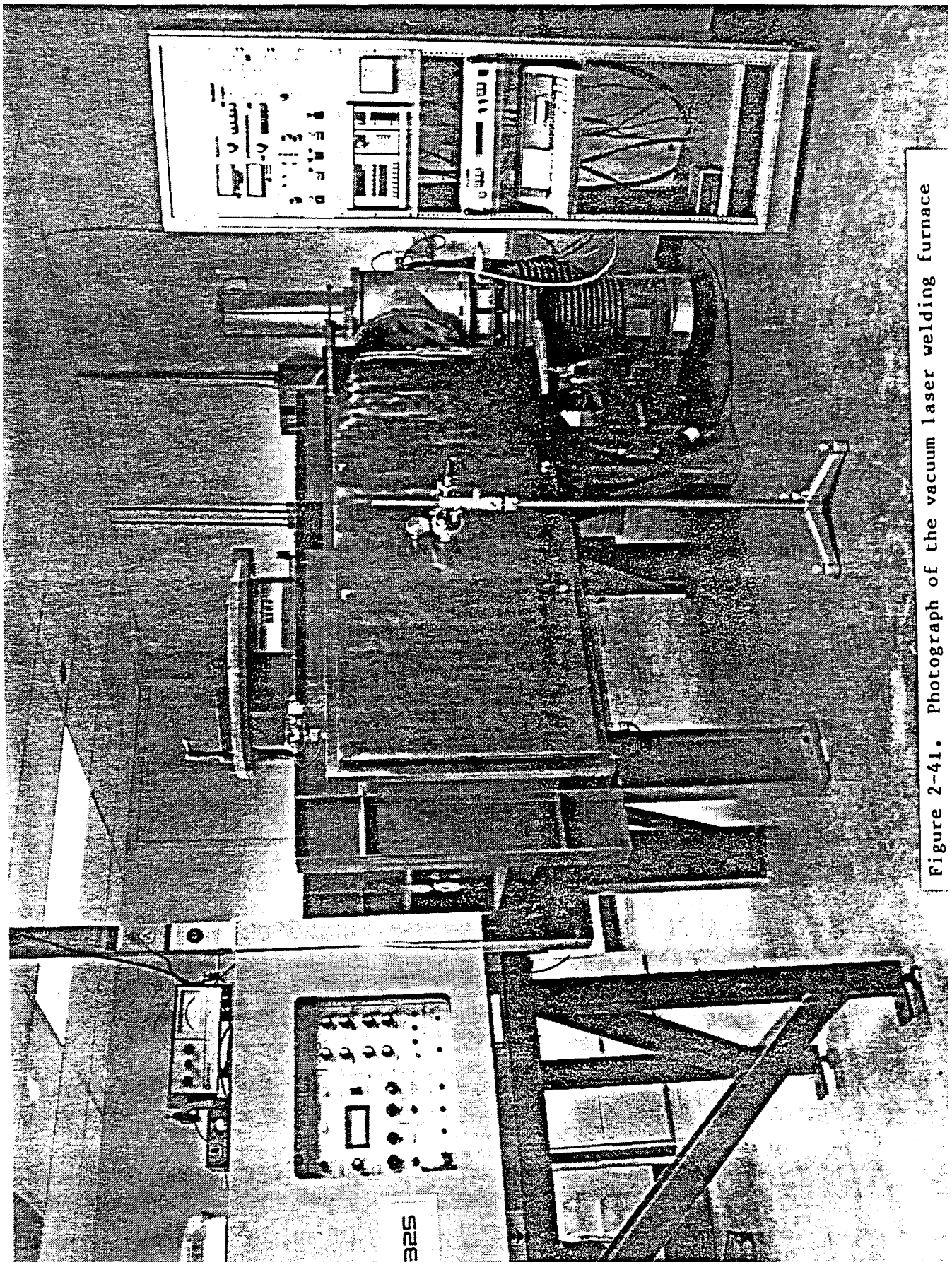

Figure 2-41. Photograph of the vacuum laser welding furnace

workpiece. The mirror is centered about 14 in. above the workpiece and is cradled at the center of rotation of two orthogonally oriented goniometers (Figure 2-42). Each goniometer is driven by a stepper motor under programmer control with a resolution of 0.01° per step. A Hewlett-Packard 85 computer is used to provide control signals for the drivers of the stepper motors.

The laser beam can be directed to any point on the 1-m^2 work surface in the vacuum furnace by proper positioning of the copper mirror. A computer control program allows the mirror to be steadily rotated by the two goniometers to trace out the chosen welding path at a constant linear welding rate.

Figure 2-43 shows a general schematic design of the laser beam steering subsystem.

A helium-neon, visible laser is mounted parallel to the CO_2 laser so that its beam can be inserted into the optical path to facilitate alignment and to test the proper functioning of the beam steering mechanism.

2.2.3 Glass Welding

2.2.3.1 Initial Glass Welding Experiments

Initial glass welding experiments were done over a range of conditions to identify potential problems and to begin to define suitable welding conditions for preprototype vacuum window sample fabrication.

Figure 2-44 shows a set of vacuum laser welds in a borosilicate glass test specimen. The glass specimen consists of two sheets of 3-mm Corning 7740 borosilicate glass stacked together and separated by 0.5-mm-thick glass spacers. The series of weld traces across the sample were accomplished at different laser power levels, different scan speeds, and different glass temperatures.

The weld trace on the far right of Figure 2-44 shows a very rough appearance and a superficial deposit of white powder alongside. The roughness is caused by bubbles formed in the molten glass, and the powder is vaporized glass components that have condensed adjacent to the molten glass along the weld trace. The other weld traces show less evidence of glass vaporization, but some do include occasional bubbles entrapped in the welded glass. In most cases, the upper glass sheet was melted, flowed sufficiently to bridge the 0.5-mm gap, and bonded to the underlying glass sheet.

These results were encouraging but also identified two new technical issues that must be dealt with. First, these results clearly show that the glass configuration required in our preprototype vacuum window samples can be welded in our new vacuum laser welding facility. On the other hand, welding conditions have to be carefully optimized to prevent flaws from forming in welds. The second problem is the glass vapor formation and its condensation onto the laser mirror.

The bubbles seen in some preliminary vacuum welds are dissolved gases evolved from the molten glass in the vacuum furnace. The gases are dissolved into the glass when it is originally formed by the manufacturer. Because glass is a supercooled liquid that has been solidified at atmospheric pressure, it

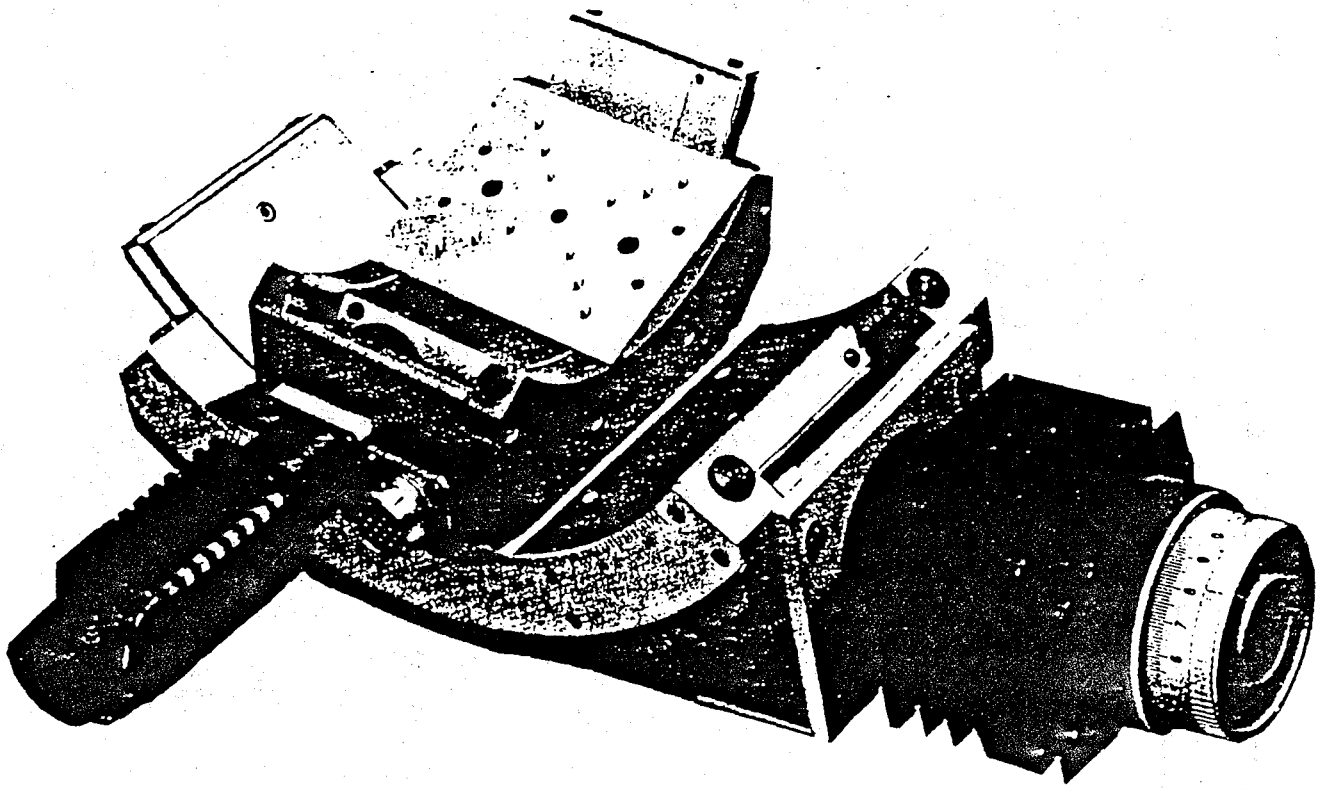

Figure 2-42. Two-axis goniometer cradle with stepper motors for controlling the orientation of the laser beam steering mirror

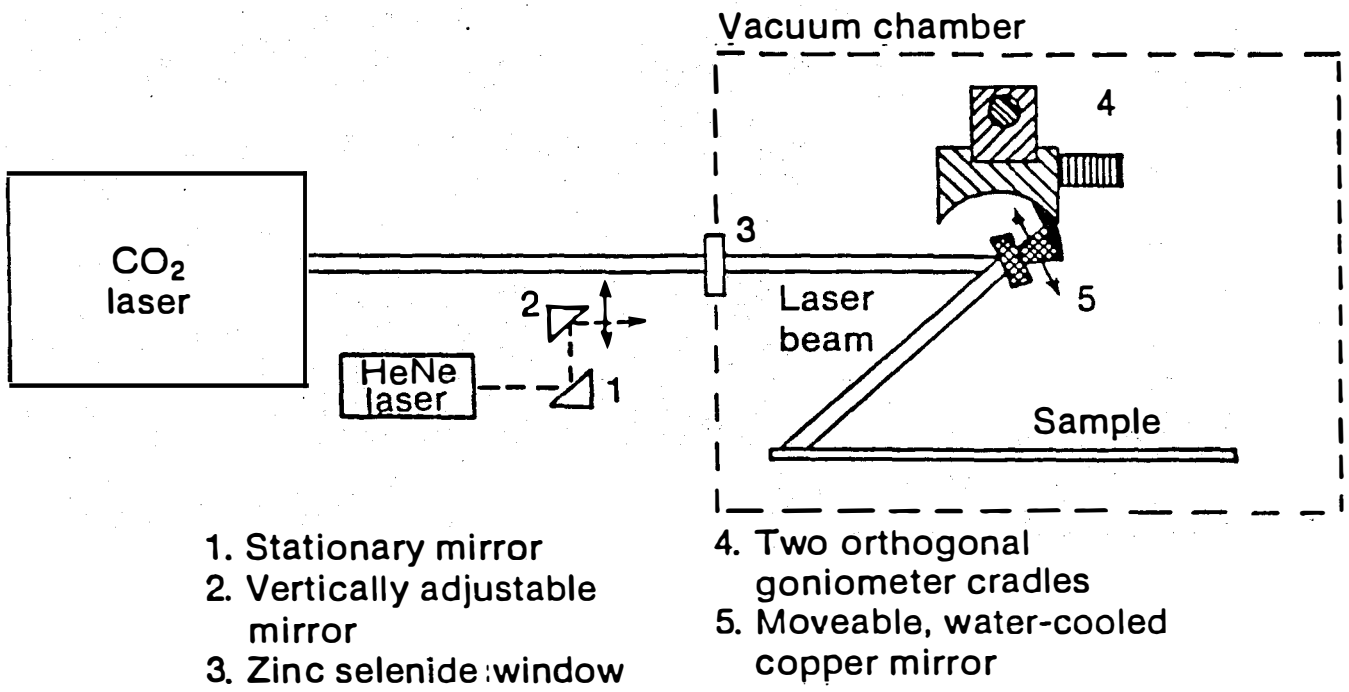

Figure 2-43. Schematic diagram of the basic laser beam optical subsystem

Figure 2-44. Photograph of laser welds in two sheets of Corning 7740 borosilicate glass. Horizontal lines are reflected in the glass surface to delineate the glass surface contours.

contains dissolved gases that are at an equilibrium concentration in a one-atmosphere pressure but are at a nonequilibrium, excess concentration when the glass is in a vacuum environment. Much like the dissolved carbon dioxide in champagne, when the surrounding pressure is reduced there is a tendency for these dissolved gases to come out of solution and form bubbles. This kind of bubble nucleation and growth also occurs under some circumstances when glass is remelted even at atmospheric pressure. A considerable body of research has been reported on bubble nucleation and growth in glasses (Cable 1984) but not in vacuum. However, the basic physical principles involved have been known since 1948 (Fisher 1948), and there is a good theoretical framework for understanding the process in vacuum.

Glass vapor condensation onto the water-cooled copper mirror used to direct the laser beam inside the vacuum furnace is very troublesome. The 10.6-micron wavelength laser beam is ideally suited for glass welding because of its strong absorption within the glass. However, a disadvantage of this strong absorption is the fact that even a very thin layer (~200 nm) of glass vapor condensate on the laser mirror is sufficient to attenuate the laser beam by nearly 50% (depending upon the angle between the beam and the mirror).

The buildup of glass contamination on the laser mirror was rapid enough that controlled welding experiments were frustrated and the complete perimeter welding of test windows was out of the question.

It was necessary to design an alternative contamination-tolerant mirror to direct the laser beam during glass welding.

2.2.3.2 A Novel Contamination-Tolerant Laser Mirror

Several solutions to the glass vapor contamination problem were considered. The mirror could not be shielded from the vapor by a permanent shield because the mirror obviously must have a direct line-of-sight exposure to the molten glass during welding, and any shield would have to be transparent to the laser beam in order to provide that line-of-sight access while blocking the glass vapor. But then the shield would become contaminated and absorb the laser beam.

A moving, transparent shield was considered. It would have to withstand the heat of the furnace, be transparent to the laser beam, and be large enough to accommodate the long welding times that may be required in some experiments and in some sample window fabrications. The space available would not accommodate a large-diameter rigid disk of material (such as silicon) rotating in front of the laser mirror, and such a disk would be very expensive (if available). A moving film shield was considered, but no polymer film could be identified which would be adequately transparent to the laser beam and tolerant of the high temperatures in the furnace.

Finally a moving foil reflector was selected as an alternative to the copper mirror. Experiments were done that showed aluminum foil to be an adequate laser reflector. The foil (in thicknesses of 0.001 to 0.003 in.) was readily available and could be compactly stored on a small supply spool and unrolled continuously to provide fresh reflector surface as the old surface became contaminated.

A basic design was developed at SERI and then a subcontract was let to an engineering design firm to complete the detailed design and fabricate the working device. The engineering firm that had designed and built the SERI vacuum laser welding furnace was chosen for this effort.

The most difficult aspect of the design was the necessity to fit everything into a very limited space so that the moving foil reflector could be rotated about two axes with the same apparatus used to control the small water-cooled copper mirror. The foil supply spool, the foil reflector, the foil take-up spool, and the drive motor all had to be water cooled. They had to fit into a space approximately 10 x 20 x 7 cm in such a way that water cooling lines, electrical wires, and the foil mechanism itself cleared all other parts of the mirror drive mechanism and heat shields as the foil reflector was rotated through all possible positions needed to direct the laser beam around in the furnace.

Figure 2-45 is a photograph of the finished foil reflector apparatus. A small stepper motor (A) drives a take-up spool (B) and draws the 0.001-in. aluminum foil across guide pins to form a flat reflector (C). The foil supply spool (D) is provided with an adjustable, spring-loaded friction brake to keep the foil taut. The entire assembly is attached to a water-cooled baseplate and is cooled by conduction to it. The mechanism is readily disconnected from the baseplate for easy removal from the vacuum furance to replace the foil without having to disconnect the cooling water lines.

The use of the stepper motor and its controller allows us to control the speed of the foil advance by computer if we desire. This facility may help to optimize the operation of the foil reflector. The foil advance may be automatically speeded up when the reflector is in a position where it intercepts a rapid buildup of glass contamination (when the mirror is more nearly parallel to the glass) and slowed or stopped when its orientation minimizes contamination.

The use of commercially available aluminum foil (the same as kitchen wrapping foil) is economical, but does require a compromise in the specularity of the reflected laser beam. The beam is spread out considerably by irregularities in foil surface, which are remnants of its manufacturing process, and by a slight curvature in the foil as it is drawn over its guide pins. However, in our particular application, the more diffuse beam is thought to be beneficial because it will distribute the heat more evenly over the perimeter weld area and reduce the tendency to cause "hot spots" from which large amounts of glass vapor are evolved.

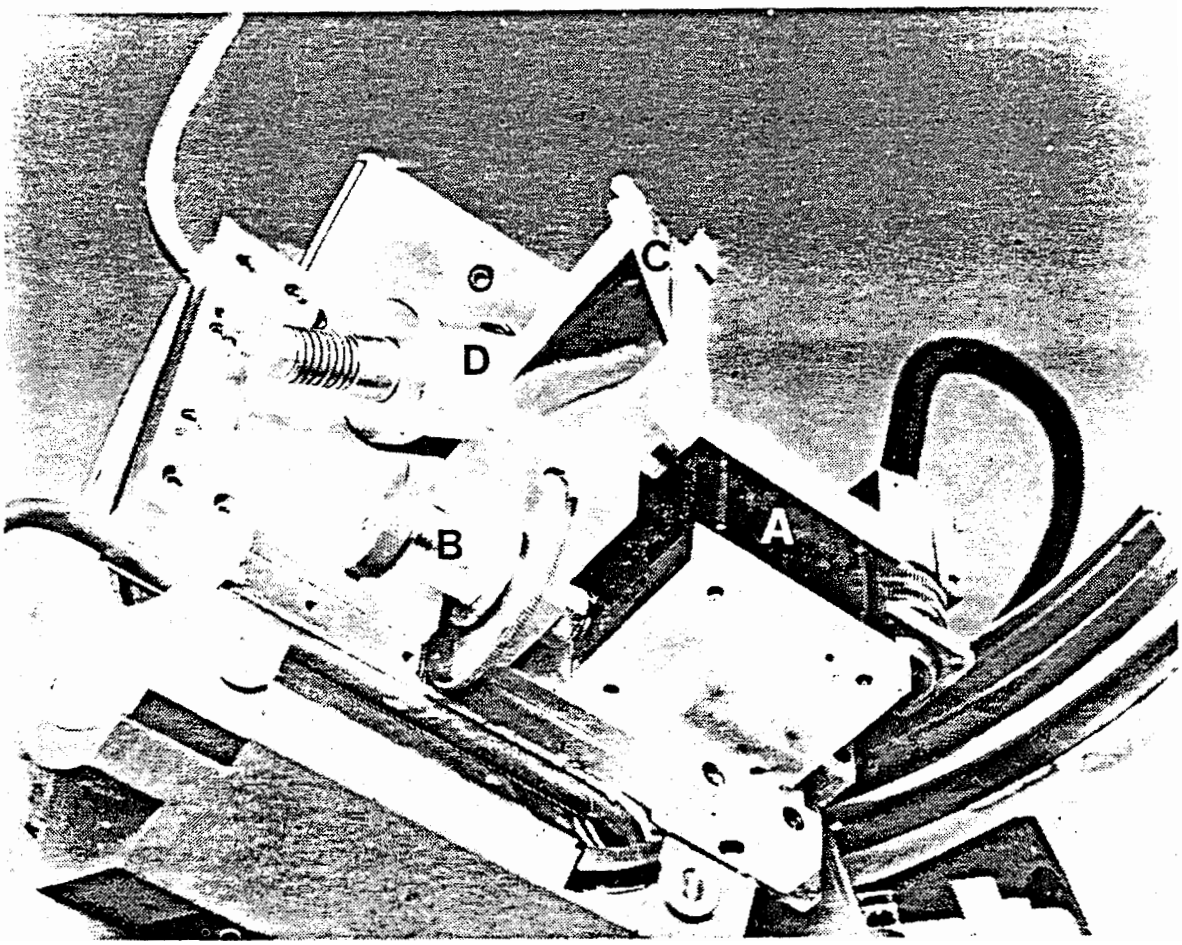

Figure 2-45. Photograph of the moving foil laser beam reflector

3.0 DISCUSSION

The vacuum insulating window has a very high ratio of solar gain to thermal loss* which makes it particularly well suited for use in passive solar heated buildings. The best application for such windows would be in cold climate residential buildings, particularly on the north side where even the diffuse solar radiation admitted by the window would more than offset conductance heat losses and where cold convective drafts from the window would be eliminated. The thin profile of the vacuum window (total glazing thickness about 6.5 mm [0.26 inch]) would also facilitate its use in operable window units.

Whether the vacuum insulating window achieves acceptance by the buildings industry depends upon its cost and its value as perceived by the home owner. The perceived value is determined largely by the aesthetics and comfort provided and is less critically dependent upon the energy savings.

The energy savings potential for highly insulating residential windows is great; but difficult to predict accurately. Conventional methods of computer modeling the solar gains through windows greatly simplify the real complexities of the solar spectrum, the spectral selectivity of the window and they largely ignore the reflectance of the ground near the window which may account for a significant fraction of the solar radiation incident on the window.

As a part of this project, an improved computer modeling program was developed to make use of more recent and complete knowledge of the variable solar spectrum and to account for the actual spectral characteristics of high performance windows and of typical ground covers. This detailed model could not yet be used to predict integrated, annual window performance; but it was used to predict typical daily energy flows through the vacuum window in comparison to a standard double-glazed window in a typical Pacific Northwest climate. These results are probably the most accurate comparisons we can provide at this time.

The vacuum window was shown to provide about the same daylighting level (within 10% of the conventional window) while admitting about 8% less net heat in the summer (July 21) and dramatically converting a wintertime (January 21) heat loss of 2257 kJ/m^2 through the conventional window to a net heat gain of 629 kJ/m^2 through the vacuum window (see Table 2-16).

Other, more conventional methods were used to predict the overall net energy benefits of the vacuum window in comparison with conventional and developmental, insulating windows. The magnitude of errors in conventional modeling approaches was estimated by comparing predictions for a typical low-e window by the two approaches (see Table 2-24). The differences in transmitted light intensities calculated by the new detailed and the conventional, more approximate models were significant. Daylighting intensity predictions differed by 7

*The relative solar gain to thermal loss ratio can be expressed as the ratio of shading coefficient to overall heat-transfer coefficient, SC/U. For the vacuum window, this ratio is expected to be about $8^{\circ}F\ ft^2h/Btu$ compared to 1.8 for a conventional, double-glazed window and 3.2 for a quad-glazed, low-e window.

to 76 percent depending upon window orientation and ground reflectance. The solar-weighted transmittances differed by 1.5 to 11 percent, with the largest difference occurring in the summer. The wintertime predictions which are more important for assessing window benefits, differed by 1.5 to 5.8 percent. The largest wintertime difference occurred in north-facing windows with conventional modeling predictions over estimating solar gains through standard, double-glazed low-e windows, but slightly underestimating solar gains through the vacuum window. From these comparisions, we would expect that our estimates of annual energy savings from vacuum windows are conservative (by 2 to 9%, depending on window type and orientation) when compared to conventional windows.

The conventional approach to building energy performance analysis predicted a net annual energy savings of 636 to 760 MJ/m^2 when the vacuum window replaced a standard double-glazed window in two typical Pacific Northwest climates (Portland and Boise). The savings were 284 to 329 MJ/m^2 when a quad-glazed window with two low-e coatings was replaced by the vacuum windows (see Table 2-2). The savings depended on window orientation and location.

If delivered energy costs were \$10/GJ, the annual value of the vacuum window energy savings would be \$3 to \$7/m^2 when compared to quad-glazed or double-glazed windows respectively. It is worth noting that the historical change from single-glazed to double-glazed windows in the Pacific Northwest provided an annual energy savings of about 800 MJ/m^2, comparable to the ~700 MJ/m^2 provided by substituting vacuum windows for double-glazed windows.

If all existing windows in the Pacific Northwest (about 75 million m^2) were eventually replaced with high performance windows such as the vacuum window, the annual energy savings would be about 84 PJ (0.08 quadrillion Btu).

Any new window must perform reliability, have adequate lifetime, be aesthetically acceptable, and be manufacturable at a marketable cost. There remain several technical issues to be resolved before the vacuum window can meet these requirements.

There is little doubt that the vacuum insulating window will perform thermally as predicted since the physical principles are so well understood and since practical, commercial examples of evaluated glass insulation date back to Sir James Dewar's invention of the vacuum bottle in 1923. However, the other issues of durability, lifetime and manufacturing costs are an interdependent complex which has frustrated several earlier inventors of insulating window designs (see patents cited in Appendix C).

An essential component of the vacuum insulating window glazing is a transparent, low-emittance, internal coating. This low-e coating reduces radiative heat transfer across the vacuum gap by lowering the surface emittance from the high value typical of glass (0.84) to a much lower value. Any such coating must withstand the high temperature (465°C) vacuum welding step in the manufacturing process. Only a few low-e coatings such as conductive oxides of tin and indium will do so; and these oxides must be rather thick (several hundred nanometers) to achieve modestly low emittances on the order of 0.1 to 0.2. These coatings, in the required thicknesses and optical uniformity are relatively expensive.

An improved low-e coating of proprietary design was developed on this project in collaboration with Airco Coating Technologies*. This low-e coating is related to their commercial Super H® transparent conductive coating for self-defrosting automobile windshields and withstands high temperature vacuum processing. This coating provides the significantly lower emittance (0.07) needed to improve the vacuum window glazing performance while having the potential of reducing the fabrication costs as well. The high-speed sputter deposition process used by Airco for such coatings is compatible with an in-line, multi-step manufacturing process for vacuum windows.

Highly insulating window glazings require superior window frames. At present there are no window frames which have sufficiently high thermal resistance to be fully compatible with glazings such as evacuated aerogel, low-conductivity gas filled, multi-glazed or SERI's high-vacuum insulating glazing.

A novel window frame design was analyzed which shows some promise. This design integrates a compact vacuum insulation panel** into the frame for added thermal resistance. Even with this speculative frame design, the overall vacuum window conductance was predicted to be typically 0.66 W/m^2K (R = 8.7°F ft^2hr/Btu) compared to a center-of-glass conductance of only 0.36 W/m^2K (R = 16). Clearly an improved frame design concept will be needed for use with better glazings.

The SERI vacuum insulating window invention involves a vacuum laser welding process for manufacturing the window. Alternative sealing processes suggested by earlier inventors included the use of solder glass or glass-to-metal-to-glass edge seals and subsequent evacuation through a sealable tubulation. Such edge seals, being made up of dissimilar materials, are inherently weaker and more prone to leak than a monolithic, fused glass edge seal. Evacuation through a tube is a slow process which would add to the manufacturing time and costs. Laser sealing the vacuum window inside a vacuum furnace has a potential for significant manufacturing advantages; but no one had ever reported accomplishing this kind of glass seal before. The crux of our feasibility study was testing of this aspect of vacuum window manufacture.

A major effort of the project was the design and construction of a laboratory facility to test the feasibility of laser sealing large area glass windows in vacuum. Earlier experiments at SERI had shown that it could be done smoothly in air. A unique vacuum laser processing facility was completed during this project and laser welding of glass in vacuum was explored.

Two problems were identified; gas bubble formation in the molten glass and glass vapor contamination of the laser optics inside the vacuum furnace. The glass vapor contamination problem prevented a thorough study of the gas bubble problem.

The laser beam reflector in the vacuum furnace was continuously degraded during a welding experiment, accumulating about 200 nm thick layer of glass in

---

*Airco Coating Technologies is a manufacturer of architectural and automotive glass coating equipment.

**Compact vacuum insulation is a SERI invention presently under development.

only a few minutes. This thickness of glass contamination was sufficient to absorb almost half of the laser beam intensity. Consequently, the beam intensity delivered to the glass sample during a welding experiment was continuously changing and controlled experiments were not possible until the contamination problem was solved.

It was possible to show that glass welding could be accomplished in vacuum inspite of the contamination problem. Short weld length experiments at different laser intensities and scanning speeds and furnace temperatures were conducted. Even though the laser intensity at the sample could not be accurately controlled, it was possible to show that good glass seals could be made under some conditions. Under other conditions, gas bubble formed and became trapped in the seal. Such bubbles would be unacceptable flaws leading to loss of mechanical strength and potential leaks in the window. A systemmatic study of the gas bubble nucleation problem and ways to reproducibly circumvent it required a solution to the glass vapor contamination problem.

A novel, moving foil laser mirror was designed and fabricated. The moving foil unwinds from a supply spool, continuously providing fresh reflector surface while the contaminated foil reflector is accumulated on a take-up spool. The device works inside the vacuum furnace under computer control and appears to solve the problem. However, it has not yet been used in systematic studies.

Experiments remain to be done which will define the laser welding conditions which avoid gas bubble formation. It is particularly important to determine how rapidly welding can be done while avoiding these flaws since the speed of welding will largely determine the cost of vacuum window glazing and its potential cost-effectiveness.

4.0 CONCLUSIONS AND RECOMMENDATIONS

This project has succeeded in moving the concept of vacuum insulating windows much closer to reality, but more laboratory work remains to be done before it can be proven to be technically feasible and economically practical.

Two technical issues, gas bubble formation in the glass welds and glass vapor contamination of laser optics, have been identified and require thorough study. Although we have shown that suitable, bubble-free glass welds can be produced, we do not yet know how the speed of the welding process may have to be limited to avoid such flaws. Because the cost of vacuum window production is critically dependent on the speed of fabrication, a serious limitation on welding speed could jeopardize the economic feasibility of the vacuum window concept. The glass vapor contamination problem has probably been solved with our invention and development of a moving foil mirror. However, we have not tested this new mirror in our laser welding facility nor used it yet to study gas bubble formation.

Applications analyses have shown that a highly insulating vacuum window could significantly reduce the heating requirements for residential buildings in the Pacific Northwest. The benefits are particularly impressive for vacuum windows used on the north-facing exposures.

A detailed computer analysis program for predicting the optical performance of high-technology windows was developed as a part of this project. The program explicitly accounts for many aspects of window performance that currently receive only very approximate treatment. Comparisons of results from the detailed and the conventional, less detailed models for window performance suggest needed improvements in the way that high-technology windows such as the vacuum window must be treated in applications analyses. For example, the solar gain benefits of north-facing windows in cold climates, which are already predicted to be substantial, may be underestimated by conventional models.

Our window frame analyses illustrate that a simple one-dimensional model cannot represent the heat flow through frames, because its magnitude is influenced by the resistance through the adjoining glazing and spacer. Thermal improvements in the frame result in a greater percentage increase in overall window thermal resistance when advanced spacers and advanced glazings are used.

The results have been promising, and the authors recommend continuing the research and development of the SERI vacuum window concept. Specifically, the authors recommend the following activities:

- Systematically study the formation and growth of gas bubbles in glass during laser welding.

  This activity is necessary in order to develop a sufficient understanding of this potentially serious fabrication problem. We must be able to determine the limitations (if any) this problem imposes on the maximum fabrication speed, because any such limitation will strongly affect the potential economic feasibility of vacuum window manufacture.

- Fabricate small, initial vacuum window test specimens (12 in. × 12 in.).

  These small test specimens will be used to develop the full fabrication procedure and to test the vacuum seal integrity of the laser welding process. Samples will include a nonevaporable reactive metal getter. A getter manufacturer has agreed to test our vacuum window samples for vacuum integrity as part of his evaluation of the effectiveness of his getters in this application. These small test specimens are not well suited to thermal performance or mechanical strength/durability testing. Thermal losses around the perimeter are too great, and the small linear dimensions do not allow thermal expansion stresses to reach the high levels that will occur in full-sized windows.

- Fabricate full-sized vacuum window test specimens (approximately 36 in. × 36 in.).

  These full-sized test specimens will be suitable for realistic engineering performance tests of thermal resistance, mechanical strength, acoustic transmittance, and vacuum integrity. Several private companies (glass and window manufacturers) have expressed willingness to assist in testing full-sized specimens in their window testing laboratories.

- Conduct a manufacturing cost analysis.

  If the remaining technical barriers are overcome, then a preliminary analysis of probable manufacturing costs should be made to assess the economic feasibility of the vacuum insulating window.

- Transfer the technology to private industry.

  If the steps outlined above are carried out with favorable results, the vacuum window concept will have been proven technically and economically feasible. The further steps required to develop a commercial vacuum window product are quite difficult and expensive and are more properly the responsibility of private industry. DOE has waived its rights to the SERI vacuum window patent in favor of Midwest Research Institute Ventures (MRIV), a for-profit subsidiary of the SERI prime contractor, Midwest Research Institute of Kansas City, Missouri. MRIV has begun to solicit from private industry interest in the licensing or purchase of the vacuum window patent rights as the first step in the technology transfer.

5.0 REFERENCES

ASHRAE, 1977, "Fenestrations," ASHRAE Handbook: 1977 Fundamentals, Atlanta: American Society of Heating, Refrigerating and Air-Conditioning Engineers, Inc.

ASHRAE, 1985a, "Fenestrations," ASHRAE Handbook: 1985 Fundamentals, Atlanta: American Society of Heating, Refrigerating and Air-Conditioning Engineers, Inc.

ASHRAE, 1985b, ASHRAE Handbook: 1985 Fundamentals, p. 27.18, Atlanta: American Society for Heating, Refrigeration and Air-Conditioning Engineers.

ASHRAE, 1989, "Fenestrations," ASHRAE Handbook: 1989 Fundamentals, Atlanta: American Society of Heating, Refrigerating, and Air-Conditioning Engineers, Inc.

Abramowitz, M., and I. A. Stegun, 1964, Handbook of Mathematical Functions, National Bureau of Standards Applied Mathematics Series 55, p. 81.

Anon., 1981, I.E.S. Lighting Handbook, Reference Volume, Illuminating Engineering Society of North America, New York, NY, Figs. 3-7, pp. 3-5.

Anon., 1985, "High Insulation Technology Window," Document No. 50518/1, Geilinger AG, Winterthur, Switzerland.

Anon., 1989, "DOE-2.1C, Complete User Documentation", PB85211449, NTIS, Springfield, VA 22161.

Arasteh, D., et al., 1986, User and Reference Guide for WINDOW2: A Computer Program for Calculating U-values and Shading Coefficients of Windows, Windows and Daylighting Group, Berkeley: Lawrence Berkeley Laboratory, University of California.

Arasteh, D., J. Hartmann, and M. Rubin, 1987, "Experimental Verification of a Model of Heat Transfer through Windows," ASHRAE Transactions, Vol. 93, Part 1, Atlanta: American Society for Heating, Refrigerating, and Air-Conditioning Engineers, Inc., pp. 1425-1431.

Arasteh, D. K., M. S. Reilly, and M. D. Rubin, 1989, "A Versatile Procedure for Calculating Heat Transfer Through Windows," ASHRAE Transactions, Vol. 95, Pt. 2. Atlanta: American Society for Heating, Refrigerating, and Air-Conditioning Engineers, Inc.

BPA, November 1988, "Economic Forecasts for the Pacific Northwest," Northwest Power Planning Council and Bonneville Power Administration.

Balcomb, J. D., et al., 1984, Passive Solar Heating Analysis, Atlanta: American Society of Heating, Refrigerating and Air-Conditioning Engineers.

Benson, D. K., et al., 1987a, "Vacuum Window Glazings for Energy Efficient Buildings - FY 1986 Annual Progress Report," SERI/PR-3159 (draft), Golden, CO: Solar Energy Research Institute.

Benson, D. K., and C. E. Tracy, 1986, "Vacuum Window Glazings for Energy Efficient Buildings," SERI/PR-255-2901 (draft), Golden, CO: Solar Energy Research Institute.

Benson, D. K., and C. E. Tracy, 1987b, "Laser Sealed Vacuum Insulation Window," U.S. Patent No. 4,683,154.

Benson, D. K., and C. E. Tracy, 1985, "Evacuated Window Glazings for Energy Efficiency Buildings," Proceedings of the 29th Annual SPIE Conference, San Diego, 19-24 Aug.

Benson, D. K., and T. Potter, 1989, "Compact Vacuum Insulation," International Patent Cooperation Treaty (PCT) Number WO89/09860, World Intellectual Property Organization.

Biggers, Brett, July 1989, Personal Communication, Washington, D.C., National Association for Home Builders.

Bird, R. E., R. L. Hulstrom, and L. J. Lewis, 1983, "Terrestrial Solar Spectral Data Sets," Solar Energy, 30, p. 563.

Bird, R. E., and C. Riordan, 1986, "Simple Solar Spectral Model for Direct and Diffuse Irradiance on Horizontal and Tilted Planes at the Earth's Surface for Cloudless Atmospheres," Journal of Climate and Applied Meteorology, Vol. 25, No. 1, pp. 87-97.

Cable, M., 1984, "Principles of Glass Melting," in Glass: Science and Technology, pp. 1-40, D. R. Uhlmann and N. J. Kreidel, eds., New York: Academic Press.

Carpenter, S., 1987, "The Effect of Frame Design on Window Heat Loss, Phase 1: Final Report," Waterloo, Ontario: Enermodal Engineering Limited.

Chen, C. K., and C. L. Tien, 1973, "Conductance of Packed Spheres in Vacuum," Transactions of the ASME, p. 302, August.

Christensen, C. B., Personal Communications, 1988.

Clark, Robert, 1987, Personal Communications, Alpen, Inc., Boulder, CO.

Collares-Pereira, M., and A. Rabl, 1979, "The Average Distribution of Solar Radiation--Correlations Between Diffuse and Hemispherical and Between Daily and Hourly Insulation Values," Solar Energy, 22, p. 155.

Collins, R. E., and S. J. Robinson, 1990, "Evacuated Glazing," to be published in Solar Energy.

Duffie, J. A., and W. A. Beckman, 1980, Solar Engineering of Thermal Processes, New York: John Wiley and Sons, pp. 122 and 202.

Enermodal, 1988, "FRAME: A Finite-Difference Computer Program to Evaluate Thermal Performance of Window Frame Systems, Version 1.2," Waterloo, Ontario: Enermodal Engineering Limited.

Fisher, J. C., 1948, "The Fracture of Liquids," J. Applied Physics, 19, pp. 1062-1067.

Gilmore, E., 1986, "Superwindows," Popular Science, pp. 76-78, March.

Harrison, S. J., and Barakat, S. A., 1983, "A Method for Comparing the Thermal Performance of Windows", ASHRAE Transactions, Vol. 89, Part 1A, Atlanta: American Society of Heating, Refrigerating and Air-Conditioning Engineers.

Hay, J. E., and J. A. Davies, 1978, Proceedings of the First Canadian Solar Radiation Data Workshop, J. E. Hay and T. K. Wan, eds., Toronto, Canada.

Johnson, K. L., 1982, "One Hundred Years of Hertz Contact," Proceedings of Instrumentation and Mechanical Engineers, Vol. 196, p. 363.

Jonsson, Bertil, 1985, Heat Transfer through Windows: During the Hours of Darkness with the Effect of Infiltration Ignored, Stockholm: Swedish Council for Building Research.

Knapp, C. L., T. L. Stoffel, and S. P. Whitaker, 1980, Insulation Data Manual, SERI/SP-755-789, Golden, CO: Solar Energy Research Institute.

LBL, Oct. 1988, "Window 3.1: A PC Program for Analyzing Window Thermal Performance," Berkeley: Lawrence Berkeley Laboratory, University of California.

Lampert, C. M., 1981, Solar Energy Materials, 6, p. 1.

Lauer, B. E., 1953, Heat Transfer Calculations, Tulsa: The Petroleum Publishing Co., p. 2.

Lillesand, T. M., and R. W. Kieffer, 1979, Remote Sensing and Image Interpretation, New York: John Wiley, p. 18.

McGowan, Alex, June 1989, Personal Communication, Waterloo, Ontario: Enermodal Engineering.

Means Systems Cost, 9th Edition, 1984, Kingston, MA: Robert Snow Means Company.

Neeper, D. A., 1985, "Impacts of Research on New and Existing Buildings," Proceedings of the Solar Buildings Conference, March 18-20, 1985, Washington, D.C., pp. 132-137.

Owens Corning, Product Literature, 1988.

Parekh, Anikl, and Timothy Mayo, 1989, "Thermal Analysis and Energy Savings with High-Performance Windows," Ottawa, Ontario: Energy, Mines, & Resources Canada.

Palmiter, L., M., M. Toney and I. Brown, 1988, "Preliminary Evaluation of Two Short-Term Building Test Methods" (a microcomputer version of SERIRES is also available commercially as SUNCODE-PC™) from ECOTOPE, Inc., Seattle, WA 98112.

Powell, A. M., Jr., 1986, "A Simple Solar Spectral Model for Studying the Effects of Cloud Cover and Surface Albedo on the Incoming Radiation," Ph.D. Thesis, Ann Arbor: University of Michigan.

Quantum Optics, Inc., August 1988, "Aerogel: A Transparent Insulator," Quantum Optics Inc.

Reilly, Susan, September 1989, Personal Communication, Berkeley: Lawrence Berkeley Laboratory, University of California.

Robinson, Paul, and John Littler, 1988, "Methodology of Window Thermal Performance Assessment Techniques in the U.S. and the U. K.," Research in Building Group, Polytechnic of Central London, London: Crown.

Rubin, M., 1985, Solar Energy Materials, 12, p. 275.

Rubin, M., and Selkowitz, S., 1981, "Thermal Performance of Windows Having High Solar Transmittance," Proceedings of the Sixth National Passive Solar Energy Conference, Boulder CO: American Solar Energy Society.

Rubin, M., and C. M. Lampert, 1983, "Transparent Silica Aerogels for Window Insulation," Solar Energy Materials, 7, pp. 393-400.

Rubin, M., 1982, "Calculating Heat Transfer through Windows," Energy Research, Vol. 6, pp. 341-349.

Selkowitz, S., 1985, Discussion at the NFC/DOE Low-E Roundtable Conference, Las Vegas, NV, Aug. 28-29.

Siegel, R., and J. R. Howell, 1972, Thermal Radiation Heat Transfer, New York: McGraw-Hill.

Soule, D. E., 1988, "Spectral Model For Instantaneous Advanced Window Performance", Proc. 13th National Passive Solar Conf., Cambridge, MA, pp. 377-382.

Soule, D. E., 1989, "Daily Advanced Window Performance from a Spectral Model", Proc. 14th National Passive Solar Conf., Denver, CO, pp. 316-321.

Stephenson, D. G., 1965, Solar Energy, 9, pp. 2, 81-86.

Sullivan, R., D. Arasteh, G. Sweitzer, R. Johnson, and S. Selkowitz, April 1988, "The Influence of Glazing Selection on Commercial Building Energy Performance in Hot and Humid Climates," Berkeley: Lawrence Berkeley Laboratory, University of California.

U.S. Census Bureau, 1987, "Characteristics of New Housing,' Maryland: U.S. Census Bureau.

Wray, W. O., 1983, "Passive Solar Design Manual for Naval Installations," LA-UR-83-2236, Los Alamos, NM: Los Alamos National Laboratory.

APPENDIX A. MODELING OF WINDOW FRAME EFFECTS

A.1 Methods to Predict Thermal Performance of Windows

Laboratory and field testing are too expensive and time consuming for initial window design and optimization or for comparing window performance. An analytic model eliminates these problems and allows unbiased comparisons for determining the effects of minor design changes or for comparing alternative designs.

A standard measure of the thermal resistance of a window assembly assumes no solar radiation, moisture, or infiltration to influence the window's thermal performance (ASHRAE 1989). Heat transfer results from the combined effects of conduction, convection, and infrared radiation and is assumed to be proportional to the inside-to-outside difference in air temperature.

A.2 One-Dimensional Model of Window Performance

A simple analytic procedure was developed to calculate heat flow through windows in order to standardize the reporting of window heat-transfer indices (ASHRAE 1989). It assumes parallel heat-flow paths through three component parts of the window: the center of glass, the edge of glass, and the frame as shown in Figure A-1. The resistance through each component is area-weighted to determine the overall window R-value as shown in Eq. A-1.

$$R_o = \frac{1}{\frac{A_{eg}}{A_o} * \frac{1}{R_{eg}} + \frac{A_{eg}}{A_o} * \frac{1}{R_{eg}} + \frac{A_f}{A_o} * \frac{1}{R_f}} \qquad \text{(A-1)}$$

or

$$U_o = \frac{A_{eg}}{A_o} * U_{eg} + \frac{A_{eg}}{A_o} * U_{eg} + \frac{A_f}{A_o} * U_f$$

where

o = Overall window assembly

f = Window frame

cg = Center-of-glass

eg = Edge-of-glass

A = Area

R = Thermal resistance

U = Thermal conductance (1/R)

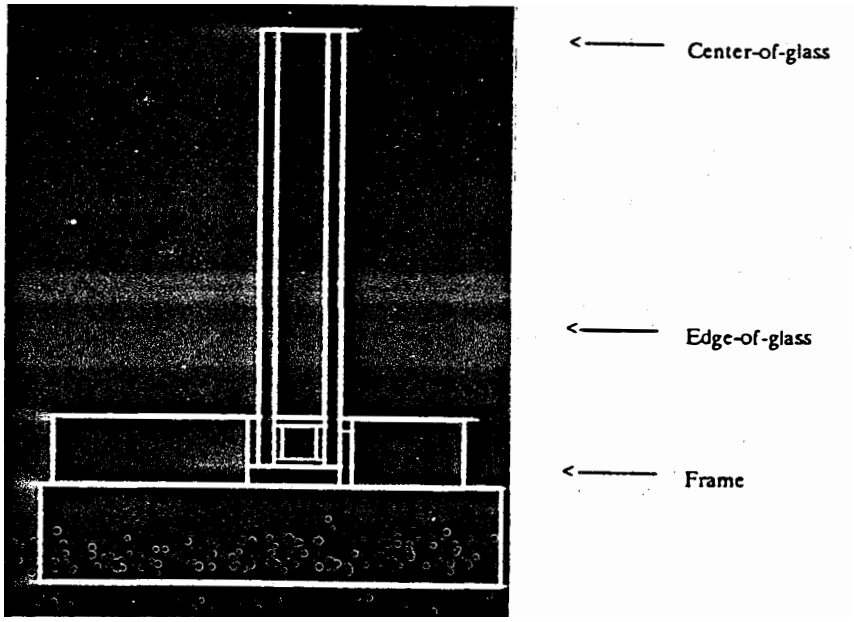

Figure A-1. Component heat-transfer model

Standard heat-transfer computations are used to determine the center-of-glass R-value (R-values and/or U-values are given in ASHRAE 1989 and in manufacturers' catalogs). Simplified correlations between center-of-glass R-values and various spacer types are used to estimate the edge-of-glass R-value. Frame R-values are approximated for a few generic frame types. The computer program Window 3.1 (LBL 1988), which is based on these assumptions, can be used to obtain the same result. Good correlations between this theoretical model and laboratory measurements have been reported (Arasteh, Hartmann, and Rubin 1987).

The graph in Figure A-2 illustrates the relative effects of coupling glazings and frames of different thermal resistances. The graph was created using the same assumption that overall window R-values can be approximated by parallel, area-weighted, heat-flow paths through window components. To represent the model in this simplified graphic form, we reduced the number of variables by combining the edge-of-glass and frame components into one variable as shown in Eqs. A-2 and A-3. The R-value of the window assembly is plotted as a function of both glazing R-values (center-of-glass) and frame R-values (average resistance of frame and edge-of-glass combined), assuming that 25% of the window assembly area is occupied by the frame (frame area excluding edge-of-glass area). (This graph is slightly modified from the graph presented in Benson and Tracy [1986].) An alternative representation of this model could have combined the edge-of-glass and center-of-glass components. We combined the edge-of-glass and frame components, leaving the center-of-glass an independent variable because the resistance of the center-of-glass can be easily found.

$$R_{fe} = \frac{1}{\frac{A_f}{A_o} * \frac{1}{R_f} + \frac{A_{eg}}{A_o} * \frac{1}{R_{eg}}} \qquad \text{(A-2)}$$

where

R_fe = Combined parallel resistance of frame and edge-of-glass

$$R_o = \frac{1}{\frac{A_{fe}}{A_o} * \frac{1}{R_{fe}} + \frac{A_{eg}}{A_o} * \frac{1}{R_{eg}}} \qquad \text{(A-3)}$$

The main problem with this computational method is in estimating the component R-values for the frame and edge-of-glass. Thermal performance information on frames is very limited, although it is the focus of current research (Arasteh, Reilly, and Rubin 1989), and it is complicated by the various configurations, thicknesses, and material combinations used in frame construction. Approximate edge-of-glass R-values are available for aluminum spacers used with various types of glazings, but very limited information is available for ther types of spacers. This method, therefore, is inappropriate to evaluate window thermal performance with new g azing, spacer, and frame types w'th unknown component R-values.

Another problem inherent in this model is the simplification of parallel heat flow through the three components. Recent studies confirm that there is a thermal interaction between the frame and the edge-of-glass, particularly when thermally conductive frames are used (Reilly 1989). To overcome these problems we used a two-dimensional model.

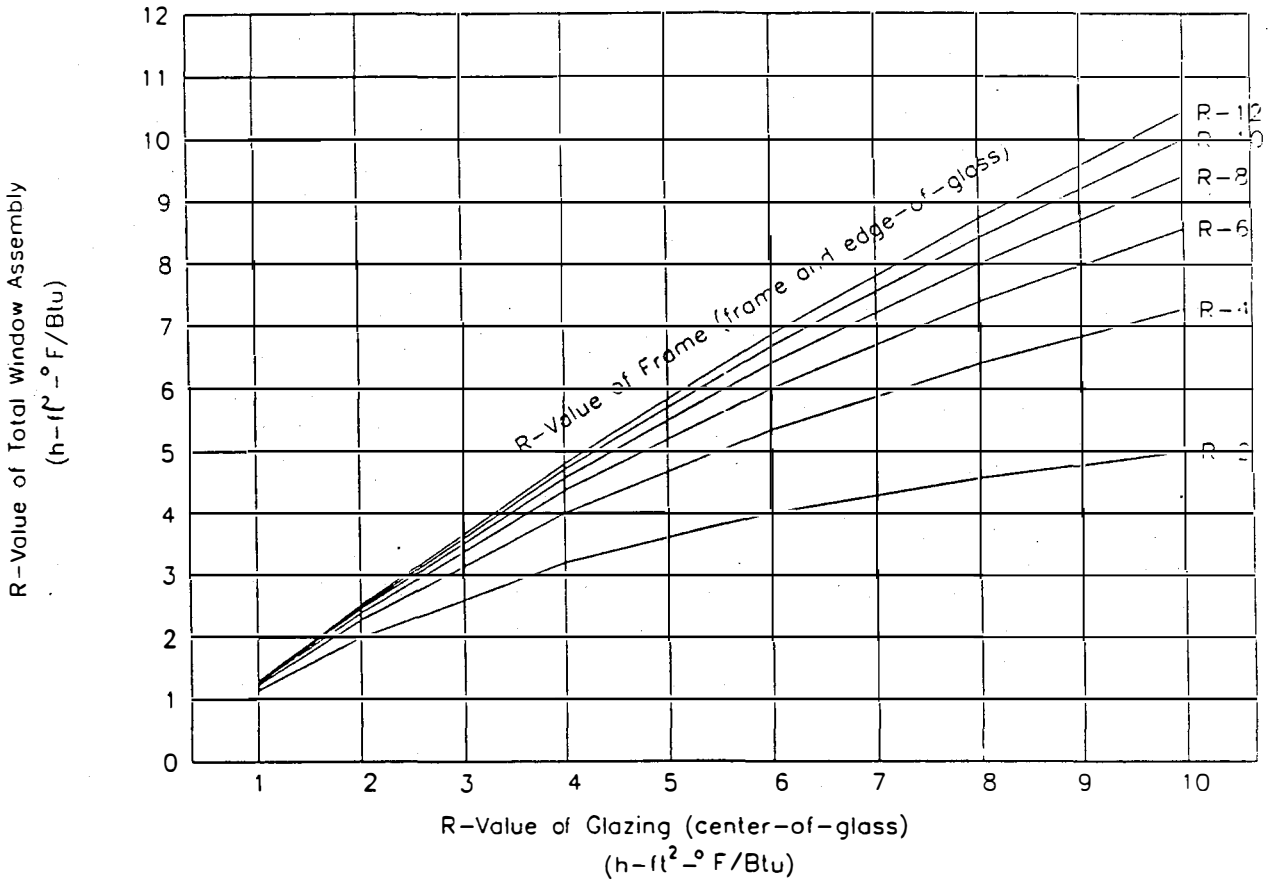

Figure A-2. Window assembly R-value vs. R-value of glazing (center-of-glass) and frame (frame and edge-of-glass) components

A.3 Two-Dimensional Model of Window Performance

The FRAME computer program is designed to model custom configurations of window frames and glazings, to determine the heat flow through the window cross section, and to predict the R-value of the entire window assembly (Enermodal 1988). Based on the Swedish computer program, BJ2ST (Jonsson 1985), FRAME is a two-dimensional, steady-state, finite-difference procedure. FRAME allows for two-dimensional heat transfer, which has been shown to occur in the edge-of-glass region, particularly along the spacer that separates the panes of glass. The BJ2ST program was found to be accurate within 10% in predicting the overall R-value of a window assembly (Jonsson 1985). Initial validations of the FRAME program show comparable accuracy (Carpenter 1987).

The user supplies the cross-section geometry of a frame and glazing edge in the form of rectangles as shown in Figure A-1. Each rectangular component is assigned a thermal conductivity. The user specifies the boundary conditions, which include the indoor and outdoor temperatures (usually the design temperatures), the air film resistances on each exposed glazing surface, and the temperatures of the adjoining wall and the adjoining center-of-glass (which are commonly assumed to be adiabatic surfaces with infinite resistance and temperatures that do not vary at the boundary). The user then delineates the finite-difference grid of temperature nodes to specify the accuracy in determining the heat-flow path through each portion of the frame.

FRAME calculates the heat transfer through the cross section and produces graphic output of isotherms or heat-flow plots, as shown in Figure A-3. FRAME assumes that the cross section is representative of each of the four sides of the window frame and that the overall window thermal performance can be calculated from this representation.

The cross section excludes the center-of-glass region (because one-dimensional heat transfer takes place here and the two-dimensional capability of FRAME is not necessary). FRAME assumes one-dimensional heat transfer through the center-of-glass, in a parallel heat-flow path with the two-dimensional frame/edge-of-glass section. This resembles the modified one-dimensional theoretical model, except that the combined edge-of-glass and frame resistance is determined by FRAME (see Eq. A-3). The FRAME output is given in terms of W/m. The following equation, Eq. A-4, is used to calculate the overall R-value of the window assembly.

$$R_o = \frac{(Qt \,/\, (T_i - T_o)) \;+\; (\,1/R_cg * A_cg\,)}{A_tw} \qquad \text{(A-4)}$$

where

R_o = Overall window R-value

T_i = Indoor temperature

T_o = Outdoor temperature

R_cg = Thermal resistance of center-of-glass

A_cg Area of the center-of-glass

A_tw = Area of the total window

$Q_t = q_1 * L$

where

Q_t = Total heat flow through frame and edge-of-glass

q_1 = Heat flow through cross section

L = Average perimeter distance around frame/edge-of-glass

FRAME has two advantages over the ASHRAE/WINDOW methods: (1) It allows for interaction between the frame and the edge-of-glass regions, and (2) it can model unusual frame or window configurations and types for which component R-values are otherwise unknown.

A.4 Methodology

We used the FRAME program to evaluate the effects of various glazings, frames, and spacers on the overall thermal performance of windows. We modeled two different glazing types: double-pane glazing and vacuum glazing.

With these glazings we modeled four different types of frames. We obtained detailed drawings and specifications on an insulation-filled frame and modeled it as accurately as possible. We used this same configuration to model a wood frame, so that direct comparisons between frames could be made. In the third and fourth cases, we thermally improved both frames by adding insulation to their exterior-facing surfaces.

We modeled three types of spacers. We modeled double-pane glazing with a conventional aluminum channel spacer. We modeled the vacuum glazing with two different forms of spacers. One was just the fused edge of the glazing, which formed a constant gap thickness throughout the unit as shown. Another type assumed that the glazing was expanded at the edge in an attempt to improve its resistance to heat transfer.

The thermal performances of the double-pane glazing with each frame type served as reference cases.

A.5 The Window Model

The FRAME methodology assumes one-dimensional heat flow through the center-of-glass, so it is unnecessary to model this portion of the glazing in the two-dimensional segment of the FRAME program. The center-of-glass contribution is included in the final overall window performance calculation, as discussed in Section A.4, after the edge-of-glass/frame heat flow is determined.

The standard ASHRAE center-of-glass R-value of 2.04 h-ft^2-^{o}F/Btu (0.36 m^2-^{o}C/W) was used in this calculation for the double-pane glazing. For the vacuum glazing we used the center-of-glass R-value of 16 h-ft^2-^{o}F/Btu (2.8 m^2-^{o}C/W), based on predictions of a vacuum glazing computer model.

We used the two-dimensional segment of the FRAME program to model the edge-of-glass and frame portions of the window (excluding the center-of-glass portion). The edge-of-glass has been defined as the portion of the visible glazing that extends approximately 2.5 in. (64 mm) toward the center-of-glass; beyond this point, at the center-of-glass, the heat flow becomes one-dimensional (ASHRAE 1989). We modeled this band as 3 in. (76 mm) because the point of one-dimensional flow in vacuum glazing is unknown.

The double-pane glazing was modeled with a conventional aluminum spacer and assembly as shown in Figure A-3. The aluminum spacer is a rectangular channel having a hollow air-filled core. The desiccant granules that commonly fill this core were not modeled. The spacer is held in place with glazing tape and butyl rubber. A rebate (an air space to allow for glass expansion) separates the spacer/glass edge and the frame. A vinyl bead with an air space forms the weather-stripping along the interior glass pane (not shown in this figure).

The vacuum glazing was more difficult to model. A reasonably accurate and verifiable model of the vacuum glazing edge was necessary. Because of the two-dimensional restriction using the FRAME program and the way that FRAME models gaps (specified gases with an effective thermal conductivity to represent the combined radiation and convection effects), the vacuum glazing could not be modeled in a precise and detailed construction (refer to Figure 1-1). A very simplified, yet conceptually valid, model of the vacuum glazing was therefore developed. Because it is apparent that the glass envelope will act as a fin to transfer heat from the warm to the cold side, this important feature was modeled as accurately as possible. The unit was modeled as two panes of glass separated by the gap and linked at the perimeter with a glass "spacer." The gap within the glass envelope was modeled as a homogenous material with an effective thermal conductivity that combines the radiation heat transfer through the vacuum with the solid conduction through the spherical spacers. This effective thermal conductivity was derived from a more detailed heat-transfer model (Section 2.1.6). Figure A-4 shows the vacuum glazing model with its welded glass spacer.

A modified version of the vacuum glazing spacer was created by elongating the spacer as shown in Figure A-5. This elongates the heat-transfer path in an effort to maximize the resistance to heat flow through the spacer.

The selected frame is a residential-type operable casement model. For simplicity, we assumed a uniform configuration for the sill, head, and right and left jambs. We used the typical size of a residential window as specified by ASHRAE: 3 ft x 4 ft (0.9 m x 1.2 m).

We obtained detailed drawings and specifications on a fiberglass-insulated frame and modeled it as accurately as possible, as shown in Figure A-6. The specifications (thickness and thermal conductivity) of each component are proprietary; however, the individual components at the frame/glazing interface are listed in Table A-1. We then modeled this frame configuration as a wood frame by assigning a thermal conductivity of wood to each frame component.

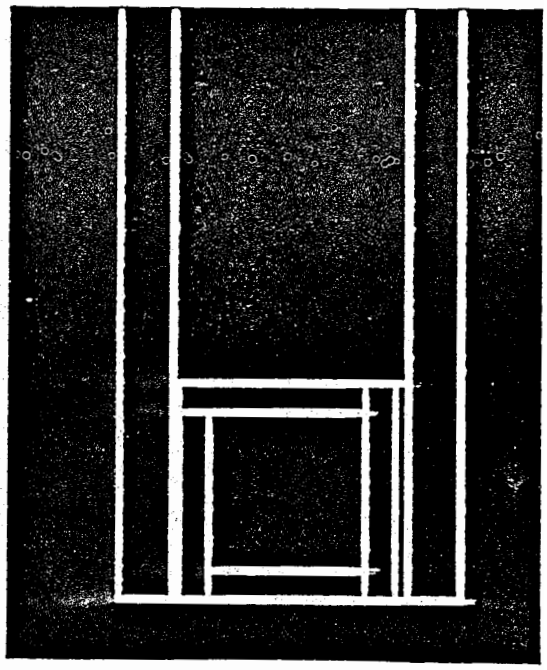

Figure A-3. Close-up of double-pane glazing model with aluminum channel spacer

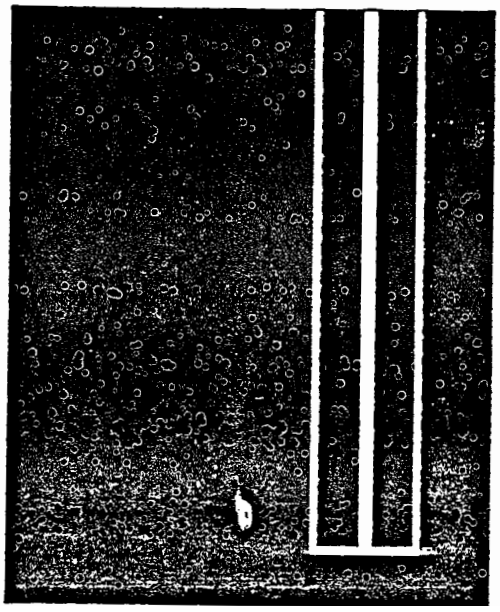

Figure A-4. Close-up of vacuum glazing model with welded glass spacer

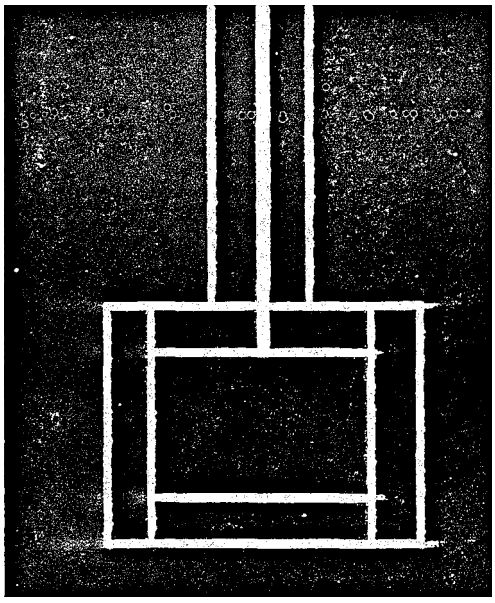

Figure A-5. Close-up of vacuum glazing model with modified welded glass spacer

Table A-1. Fiberglass-Insulation-Filled Frame Details

Frame/Glazing Interface Components (as shown in Figure A-6 from left to right)
Frame bite (fiberglass insulation inside calcium carbonate skin)
Glass
Butyl caulk (to bind glass to spacer)
Aluminum spacer channel with internal air cavity
Butyl caulk (to bind spacer to glass)
Glass
Glass tape adhesive
Weatherstripping (vinyl bead with air space between vinyl and glass)

In the third and fourth cases, we modeled a compact insulation attached to the exterior of either frame, leaving a gap between the exterior insulation and the glazing so that the otherwise increased bite would not interfere with the results (see Figure A-7). A frame with an exterior jacket of compact vacuum insulation (CVI) is proposed. CVI is an insulation under development by SERI that is a spinoff technology of SERI's vacuum glazing. It is very similar in concept and design except that instead of glass panes, two sheets of metal are welded together to enclose a high-quality vacuum. In its developed form it is expected to be approximately 0.1 in. thick and have a thermal resistance of about R-10 hr-ft^2-^{o}F/Btu (1.75 m^2 ^{o}C/W).

We assumed a set of winter design conditions for the outside and inside air temperatures (outdoors: 0^{o}F, -18^{o}C; indoors: 70^{o}F, 21^{o}C [ASHRAE 1989]). Heat flow from the window frame into the surrounding insulated walls was assumed negligible, so this boundary was regarded as adiabatic.

The truncated glazing (at the center-of-glass/edge-of-glass boundary) was treated as adiabatic, following the rationale that one-dimensional heat flow occurs beyond this edge. The surface between the frame and the adjoining wall was also assumed to be adiabatic. In order to achieve these conditions, the boundaries were specified as having infinite resistance.

A change in the bite size was modeled for the vacuum-glazing/wood-frame window. Windows with a larger bite will have a smaller percentage glazing for a window with the same overall dimensions. In order to compare the windows on an equal glazing size and an equal percentage glazing size, a new base case was designated following guidelines in Carpenter (1987). An additional strip of insulated wall was added to the perimeter such that the total center-of-glass and edge-of-glass areas remains the same. One-dimensional parallel heat flow through this strip was assumed.

A.6 References

ASHRAE, 1989, "Fenestrations," ASHRAE Handbook: 1989 Fundamentals, Atlanta: American Society of Heating, Refrigerating, and Air-Conditioning Engineers, Inc.

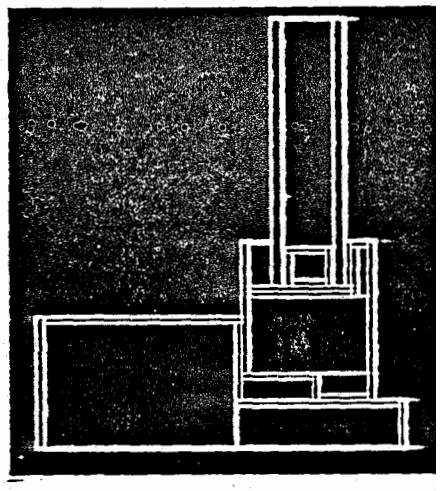

Figure A-6. Double-pane glazing in wood frame or fiberglass-insulated frame

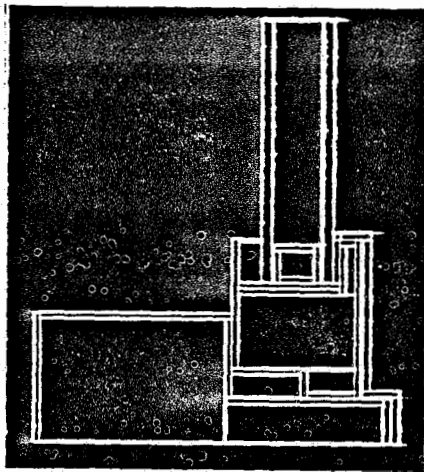

Figure A-7. Double-pane glazing in wood frame or fiberglass-insulated frame with CVI cladding

Arasteh, D., J. Hartmann, and M. Rubin, 1987, "Experimental Verification of a Model of Heat Transfer through Windows," ASHRAE Transactions, Vol. 93, Part 1, Atlanta: American Society for Heating, Refrigerating, and Air-Conditioning Engineers, Inc., pp. 1425-1431.

Arasteh, D. K., M. S. Reilly, and M. D. Rubin, 1989, "A Versatile Procedure for Calculating Heat Transfer Through Windows," ASHRAE Transactions, Vol. 95, Pt. 2, Atlanta: American Society for Heating, Refrigerating, and Air-Conditioning Engineers, Inc.

Benson, D. K., and C. E. Tracy, 1986, "Vacuum Window Glazings for Energy Efficient Buildings," SERI/PR-255-2901 (draft), Golden, CO: Solar Energy Research Institute.

Carpenter, S., 1987, "The Effect of Frame Design on Window Heat Loss, Phase 1: Final Report," Waterloo, Ontario: Enermodal Engineering Limited.

Enermodal, 1988, "FRAME: A Finite-Difference Computer Program to Evaluate Thermal Performance of Window Frame Systems, Version 1.2," Waterloo, Ontario: Enermodal Engineering Limited.

Jonsson, Bertil, 1985, Heat Transfer through Windows: During the Hours of Darkness with the Effect of Infiltration Ignored, Stockholm: Swedish Council for Building Research.

LBL, Oct. 1988, "Window 3.1: A PC Program for Analyzing Window Thermal Performance," Berkeley: Lawrence Berkeley Laboratory, University of California.

Reilly, Susan, September 1989, Personal Communication, Berkeley: Lawrence Berkeley Laboratory, University of California.

APPENDIX B

LISTING OF THERMAL ANALYSIS PROGRAM

```
10 REM ************************************************************************
20 REM                                VGMOD.BAS
30 REM      THIS PROGRAM COMPUTES THE THERMAL PERFORMANCE OF AN ADVANCED
40 REM                             VACUUM WINDOW
50 REM ************************************************************************
60 ON ERROR GOTO 3000
70 REM                                BASE CASE PARAMETERS
80 REM
90 REM ********* WINDOW GEOMETRY ***************
100 L=1                           'LENGTH OF GLAZING EDGE IN METERS
110 W=1                           'WIDTH OF GLAZING IN METERS
120 A=L*W                         'AREA OF GLAZING IN SQUARE METERS
130 D=.0004                       'DIAMETER OF SPHERICAL SPACERS IN METERS
140 R=D/2                         'RADIUS OF SPHERES IN METERS
150 LG=.003                       'THICKNESS OF GLASS IN METERS
160 LE=.003                       'WIDTH OF EDGE WELD IN METERS
170 S=.03                         'GRID SPACING OF SPHERES IN METERS
180 LBAFF=.0127                   'EDGE BAFFLE WIDTH IN METERS
190 REM
200 REM ********* GLASS PROPERTIES ***************
210 REM      (CORNING 7740 "PYREX" GLASS)
220 K=1.05                        'THERMAL CONDUCTIVITY OF GLASS IN W/MK
230 E=6.37E+10                    'YOUNG'S MODULES IN N/M^2
240 NU=.21                        'POISSON'S RATIO
250 EPS1=.84                      'EMITTANCE OF SURFACE 1
260 EPS2=.07                      'EMITTANCE OF SURFACE 2
270 EPS3=.07                      'EMITTANCE OF SURFACE 3
280 EPS4=.84                      'EMITTANCE OF SURFACE 4
290 REM
300 REM ********* FRAME PROPERTIES ***************
310 BAFF=5                        'BAFFLE RESISTANCE IN FT^2 F HR/BTU
320 REM
330 REM ********* CONDITIONS ***********************
340 REM (ASHRAE STANDARD WINTER)
350 TA=-17.78                     'OUTSIDE TEMPERATURE IN CELSIUS (oF)
360 TI=21.11                      'INSIDE TEMPERATURE IN CELSIUS (70F)
370 V=6.7                         'WIND SPEED IN M/S (15 M/HR)
380 P=101325!                     'ATMOSPHERIC PRESSURE IN N/M^2
390 REM
400 REM ********** MODEL PARAMETERS **************
410 XFIN=.005            'FIN EFFECT CALCULATION NODE SPACING IN METERS
420 SIGMA=5.67032E-08             'STEFAN BOLTZMAN CONSTANT IN W/M^2 K^4
430 PI=3.14159265#                'DEFINE PI
440 CTOK=273.15                   'DEGREES C TO DEGREES KELVIN CONVERSION
450 TA=CTOK-17.78                 'OUTSIDE TEMPERATURE IN K
460 TI=CTOK+21.11                 'INSIDE TEMPERATURE IN K
470 RTOR=.176094      'CONVERSION FACTOR FROM FT^2 F HR/BTU  TO M^2 K/W
480 DT=10                         'INITIAL TEMPERATURE DIFFERENCE IN K
490 T4=TI-DT                      'INSIDE TEMPERATURE IN K
500 T3=T4                         'INITIAL TEMPERATURE OF SURFACE 3
510 T2=TA+DT                      'INITIAL TEMPERATURE OF SURFACE 2
520 T1=T2                         'INITIAL TEMPERATURE OF SURFACE 1
530 DT=TI-TA           'REDEFINE DT TO BE TOTAL TEMPERATURE DIFFERENCE
540 EPSLON=.00005                 'CONVERGENCE CRITERION FOR TEMPERATURE
```

```
550 EPSLONR=.005              'CONVERGENCE CRITERION FOR EDGE RESISTANCE
560 JJ=15                         'EDGE RESISTANCE ITERATION CONTROL FLAG
610 RBAFF=BAFF*RTOR
620 N=2*A/((S^2)* (SQR(3)))     'HEXAGONAL ARRAY OF SPHERES
630 RC=((3/8)*(SQR(3))*(P/E)*(1-NU^2)*(S^2)*D)^(1/3)  'CONTACT RADIUS
640 REM
650 REM       ITERATE UNTIL CONVERGENCE ON OVERALL THERMAL RESISTANCE
660 REM
670 RO=0
680 GOSUB 960                     'OBTAIN RO
690 GOSUB 2350                    'OBTAIN RI
700 GOSUB 1130                    'OBTAIN RT
710 REM
720 REM
730 REM            CHECK FOR CONVERGENCE
740 REM
750 IF ABS(RT-RO)/RT<EPSLON THEN GOTO 855
760 RO=RT
770 REM
780 REM             RECOMPUTE TEMPERATURES
790 REM
800 T4=TI-RI*DT/RT
810 T3=TI-(RI+RGLAZ)*DT/RT
820 T2=TA+(RO+RGLAZ)*DT/RT
830 T1=TA+RO*DT/RT
835 GOTO 680
840 REM ************************************************************
850 REM
855 GOSUB 2430                    'PRINT HEADINGS
860 GOSUB 2500                    'PRINT OUTPUT
870 PRINT "HAVE FINISHED":END
880 REM
890 REM ************************************************************
900 REM
910 REM     SUBROUTINE TO COMPUTE THERMAL RESISTANCE BETWEEN OUTER
920 REM     GLAZING AND AMBIENT,RO
930 REM
940 REM ************************************************************
950 REM
960 HC1A=6.5181446#*(V^.75)     'CONVECTIVE CONDUCTANCE
970 REM
980 TSKY=TA                       'SKY TEMPERATURE
990 XSKY=EPS1*SIGMA*(TA+TSKY)*(T1*T1+TSKY*TSKY)*(T1-TSKY)
1000 HR1A=XSKY/(T1-TA)            'RADIATIVE CONDUCTANCE
1010 RO=1/(A*(HC1A+HR1A))         'OUTER SURFACE RESISTANCE IN K/W
1020 REM
1030 RETURN
1040 REM
1050 REM ************ ***************************************************
1060 REM
1070 REM   SUBROUTINE TO COMPUTE THERMAL RESISTANCE BETWEEN INNER AND
1080 REM   OUTER GLAZINGS (HEXAGONAL ARRAY OF SPACERS)
1090 REM
1100 REM ************************************************************
1110 REM    OBTAIN RT
```

```
1120 REM
1130 IF ITER>1 THEN GOTO 1160  'ONLY HAVE TO COMPUTE SPHERE & EDGE ONCE
1140 GOSUB 1760                'OBTAIN RS, SPHERE RESISTANCE
1150 GOSUB 2110                'OBTAIN RE, EDGE RESISTANCE
1160 GOSUB 2220         'OBTAIN RR23, RADIATIVE RESISTANCE BETWEEN GLAZS
1170 REM
1180 REM
1190 REM   OBTAIN EDGE RESISTANCE USING ELECTRICAL ANALOG
1200 REM
1210 LEDGE=2*(L+W)
1220 RE=(D+LG)/(LE*LEDGE*K)
1230 RG=XFIN/(LG*LEDGE*K)
1240 ROUT1=A*(RO+RBAFF)/(XFIN*LEDGE)
1250 ROUT2=A*RO/(XFIN*LEDGE)
1260 RIN1=A*(RI+RBAFF)/(XFIN*LEDGE)
1270 RIN2=A*RI/(XFIN*LEDGE)
1280 J=JJ
1290 J=J-1
1300 R3IN=RIN2
1310 R3OUT=ROUT2
1320 REM
1330 FOR I=1 TO J
1340 R1IN=RG+R3IN:R1OUT=RG+R3OUT
1350 FIN=(J-I)*XFIN
1360 IF FIN>LBAFF THEN GOTO 1440
1370 REM
1380 REM            FIN<=LBAFF SO USE BAFFLED NODE
1390 REM
1400 R2IN=RIN1:R2OUT=ROUT1:GOTO 1460
1410 REM
1420 REM            FIN>LBAFF SO USE UNBAFFLED NODE
1430 REM
1440 R2IN=RIN2:R2OUT=ROUT2
1450 REM
1460 R3IN=R1IN*R2IN/(R1IN+R2IN)
1470 R3OUT=R1OUT*R2OUT/(R1OUT+R2OUT)
1480 REM
1490 NEXT I
1500 ROUTJ=R3OUT
1510 RINJ=R3IN
1520 RTOTJ=ROUTJ+RINJ
1530 IF J=JJ-1 THEN GOTO 1550
1535 PRINT "ABS(RTOTJ-RLAST)/RLAST=",ABS(RTOTJ-RLAST)/RLAST
1540 IF (ABS(RTOTJ-RLAST)/RLAST)<EPSLONR THEN GOTO 1580
1550 RLAST=RTOTJ
1560 GOTO 1290
1570 REM *** EDGE RESISTANCE CALC HAS CONVERGED
1580 RTOTJ=RLAST+RE+RG          'TOTAL RESISTANCE THRU EDGE
1590 REM
1600 REM                        'OBTAIN TOTAL AREA AVERAGED RESISTANCE
1610 REM
1620 RGLAZ=LG/(A*K)             'RESISTANCE THROUGH THICKNESS OF GLASS
1630 RRS=RS*RR23/(RS+RR23)      'PARALLEL RESISTANCE OF RS AND RR23
1640 RZ=RO+RGLAZ+RRS+RGLAZ+RI    'TOTAL RESISTANCE
1650 REM
```

```
1660 RT=RZ*RTOTJ/(RZ+RTOTJ)     'PARALLEL RESISTANCE OF RZ AND RTOTJ
1670 RETURN
1680 REM
1690 REM
1700 REM ************************************************************
1710 REM
1720 REM  SUBROUTINE TO COMPUTE THERMAL RESISTANCE DUE TO N SPHERES,
1730 REM  RCONTACT
1740 REM ************************************************************
1750 REM
1760 GOSUB 1890                 'OBTAIN RCONTACT, THE CONTACT RESISTANCE
1770 GOSUB 2000                 'OBTAIN REPINE. THE SPINE RESISTANCE
1790 RS=(RCONTACT+RSPINE)/N     'RESISTANCE OF N SPHERES IN K/W
1800 REM
1810 REM
1820 RETURN
1830 REM
1840 REM ************************************************************
1850 REM
1860 REM    SUBROUTINE TO COMPUTE THE CONTACT RESISTANCE OF ONE SPHERE
1870 REM
1880 REM ************************************************************
1890 REM
1900 RCONTACT=.53/(K*RC)
1910 REM
1920 RETURN
1930 REM
1940 REM ************************************************************
1950 REM
1960 REM   SUBROUTINE TO COMPUTE SPINE RESISTANCE OF ONE SPHERE, RSPINE
1970 REM
1980 REM ************************************************************
1990 REM
2000 ARG=SQR(1-RC/R)
2010 RSPINE=(1/K*PI*R)*(1+ARG/(1+.28*ARG^2))
2020 REM
2030 RETURN
2040 REM
2050 REM ************************************************************
2060 REM
2070 REM   SUBRCUTINE COMPUTE THE RESISTANCE OF PERIMETER EDGE SEAL, RE
2080 REM
2090 REM ************************************************************
2100 REM
2110 RE=D/(2*K*LE*(W+L))
2120 REM
2130 RETURN
2140 REM
2150 REM ************************************************************
2160 REM
2170 REM    SUBROUTINE TO COMPUTE THE RADIATION RESISTANCE BETWEEN THE
2180 REM    TWO GLAZINGS, RR23
2190 REM
2200 REM ************************************************************
2210 REM
```

```
2220 X23=SIGMA*A*(T2+T3)*(T2*T2+T3*T3)
2230 Y=1/EPS2+1/EPS3-1
2240 RR23=Y/X23
2250 REM
2260 RETURN
2270 REM
2280 REM ************************************************************************
2290 REM
2300 REM   SUBROUTINE TO COMPUTE THERMAL RESISTANCE BETWEEN INNER
2310 REM   GLAZING AND INTERIOR, RI
2320 REM ************************************************************************
2340 REM
2350 HC4I=1.77598*((TI-T4)^.25)                    'CONVECTIVE CONDUCTANCE
2360 REM
2370 HR4I=EPS4*SIGMA*(T4+TI)*(T4*T4+TI*TI)         'RADIATIVE CONDUCTANCE
2380 REM
2390 RI=1/(A*(HC4I+HR4I))                  'INNER SURFACE RESISTANCE IN K/W
2400 REM
2410 RETURN
2420 REM ************************************************************************
2430 REM   SUBROUTINE TO PRINT HEADINGS
2440 REM ************************************************************************
2441 PRINT
2442 PRINT
2450 PRINT "         RT         UT          "
2455 LPRINT "          RT         UT          "
2460 PRINT " (FT^2 F HR/BTU) (W/M^2 K)        "
2465 LPRINT " (FT^2 F HR/BTU) (W/M^2 K)        "
2470 PRINT
2480 RETURN
2490 REM ************************************************************************
2500 REM    SUBROUTINE TO PRINT OUTPUT
2510 REM ************************************************************************
2520 PRINT "      ";:PRINT USING "##.##";RT*A/RTOR;
2525 LPRINT "      ";:LPRINT USING "##.##";RT*A/RTOR;
2530 PRINT "      ";:PRINT USING "##.##";1/(RT*A)
2535 LPRINT "      ";:LPRINT USING "##.##";1/(RT*A)
2540 PRINT
2550 RETURN
2560 REM ************************************************************************
3000 A=ERR:B=ERL
3010 PRINT A,B
3020 RESUME NEXT
```

APPENDIX C

United States Patent [19]

Benson et al.

[11] Patent Number: 4,683,154

[45] Date of Patent: Jul. 28, 1987

[54] LASER SEALED VACUUM INSULATION WINDOW

[75] Inventors: David K. Benson; C. Edwin Tracy, both of Golden, Colo.

[73] Assignee: The United States of America as represented by the United States Department of Energy, Washington, D.C.

[21] Appl. No.: 767,218

[22] Filed: Aug. 19, 1985

[51] Int. Cl.[4] E06B 3/24; E06B 7/12; B32B 17/00

[52] U.S. Cl. 428/34; 52/171; 52/741; 52/788; 156/107; 156/109

[58] Field of Search 428/34; 52/171, 172, 52/741, 788; 156/107, 109

[56] References Cited

U.S. PATENT DOCUMENTS

3,960,538	6/1976	Oates	65/43
3,990,201	11/1976	Falbel	52/171
4,039,718	8/1977	Kallenborn	428/398
4,198,254	4/1980	LaRoche et al.	156/107
4,204,015	5/1980	Wardlaw et al.	428/34
4,339,482	7/1982	Glaser et al.	428/13

FOREIGN PATENT DOCUMENTS

1138992 1/1969 United Kingdom .

Primary Examiner—John E. Kittle
Assistant Examiner—Patrick J. Ryan
Attorney, Agent, or Firm—Kenneth L. Richardson; John M. Albrecht; Judson R. Hightower

[57] ABSTRACT

A laser sealed evacuated window panel is comprised of two glass panes held spaced apart in relation to each other by a plurality of spherical glass beads and glass welded around the edges to provide an evacuated space between the glass panes that is completely glass sealed from the exterior. The glass welded edge seal is obtained by welding the edges of the glass panes together with a laser beam while the glass panes and bead spacers are positioned in a vacuum furnace and heated to the annealing point of the glass to avoid stress fracture in the area of the glass weld. The laser welding in the furnace can be directed around the perimeter of the glass panel by a combination of rotating the glass panel and linearly translating or aiming the laser with a relay mirror.

19 Claims, 8 Drawing Figures

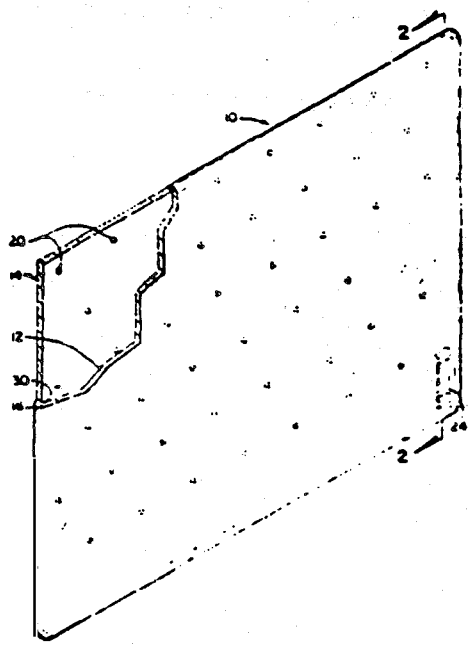

U.S. Patent Jul. 28, 1987 Sheet 1 of 6 4,683,154

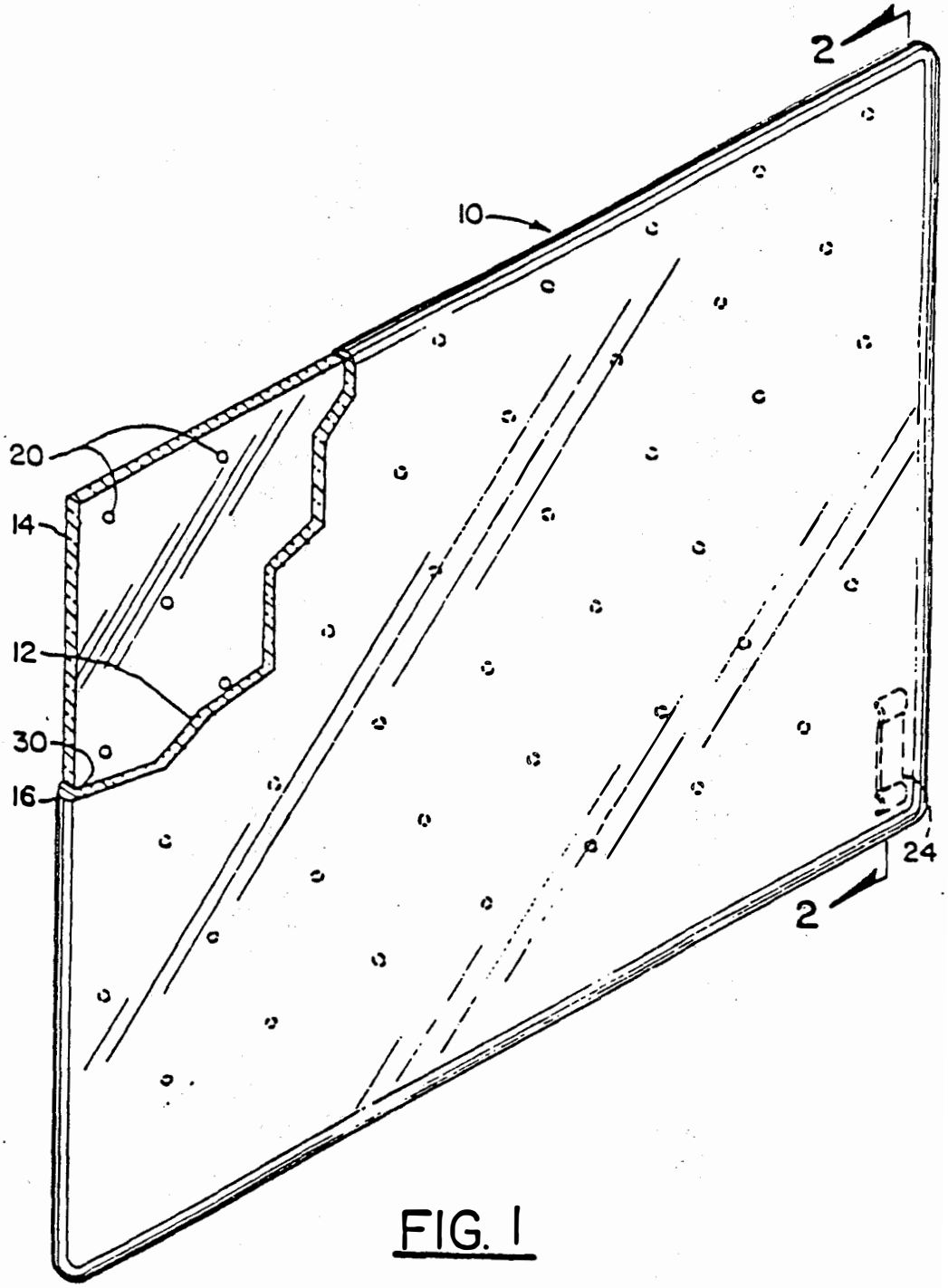

FIG. 1

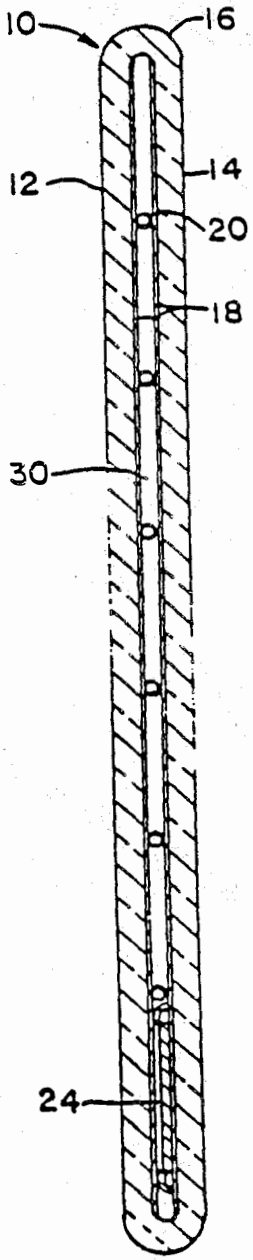

FIG. 2

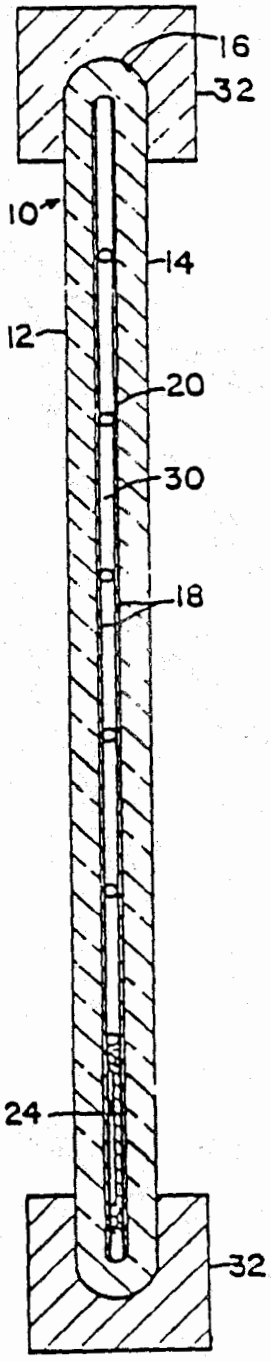

FIG. 3

U.S. Patent Jul. 28, 1987 Sheet 3 of 6 4,683,154

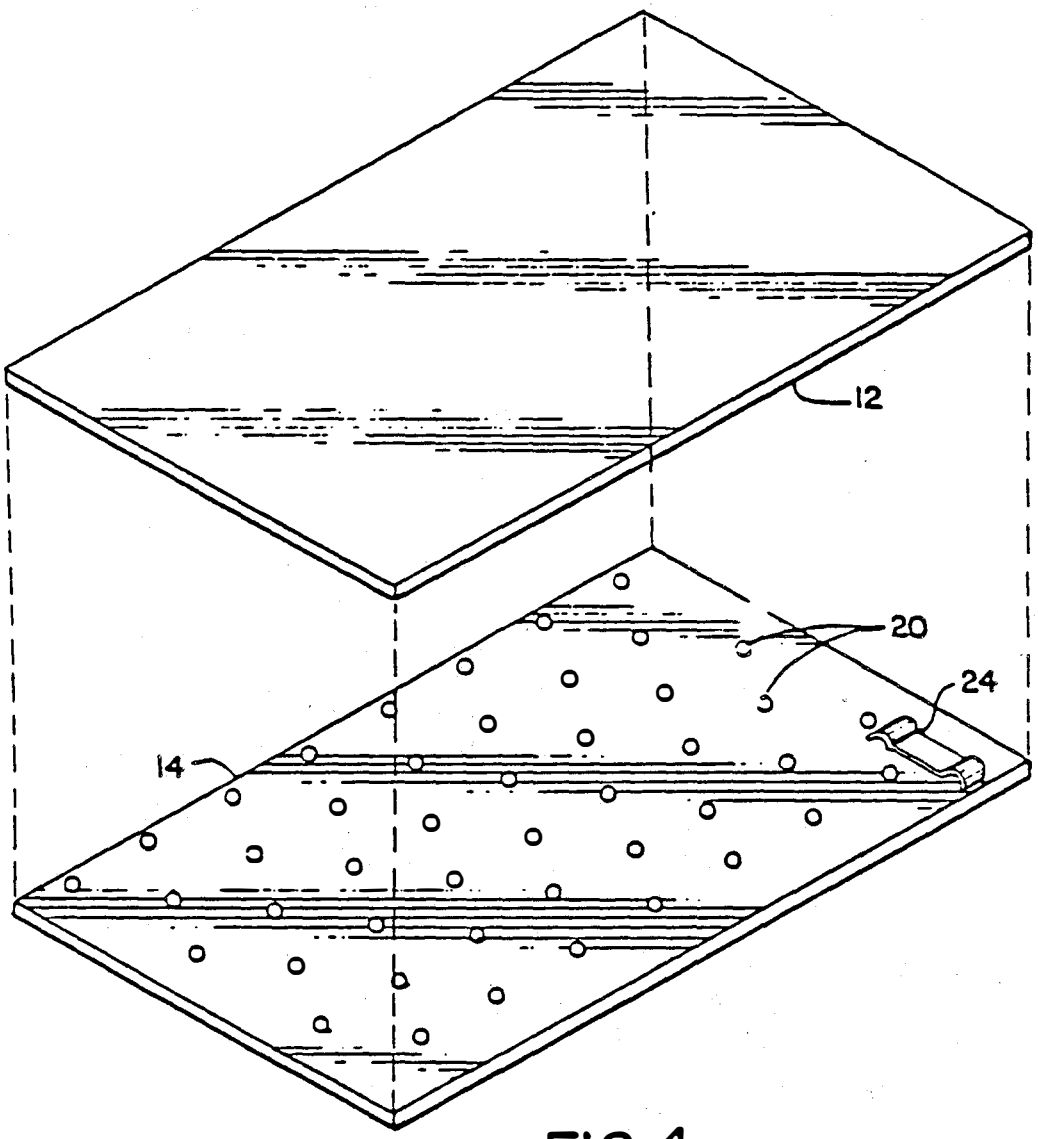

FIG.4

U.S. Patent Jul. 28, 1987 Sheet 4 of 6 4,683,154

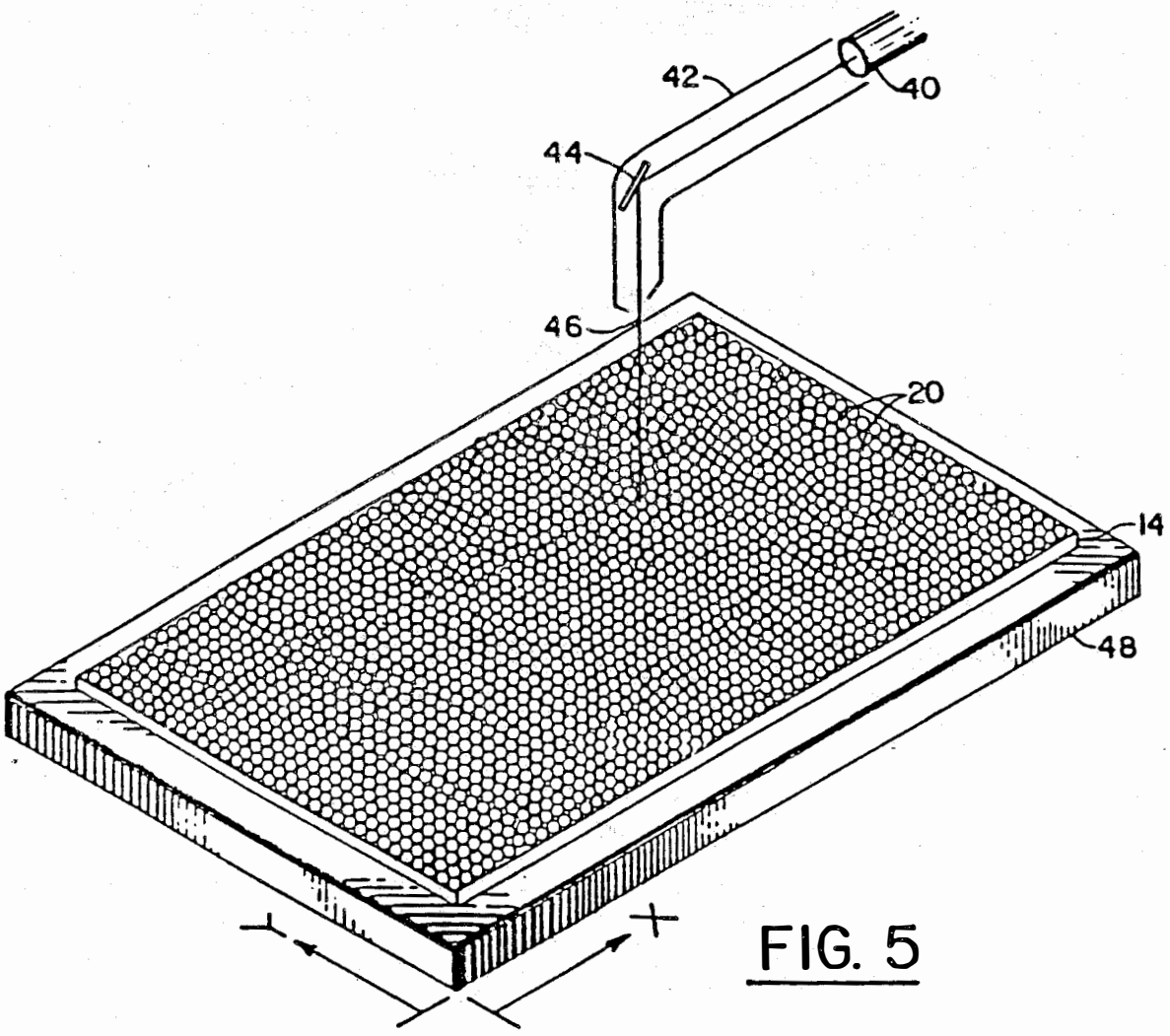

FIG. 5

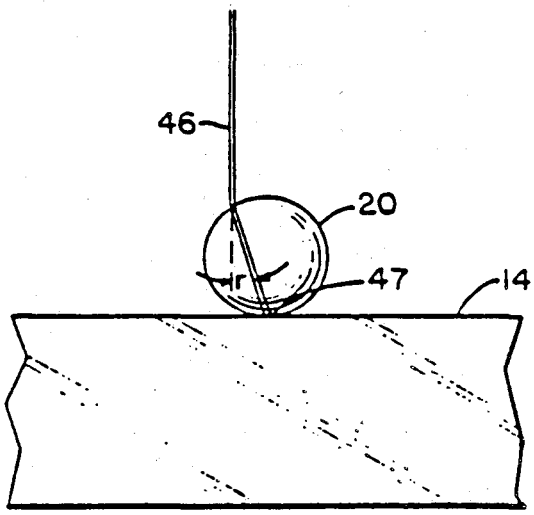

FIG. 6

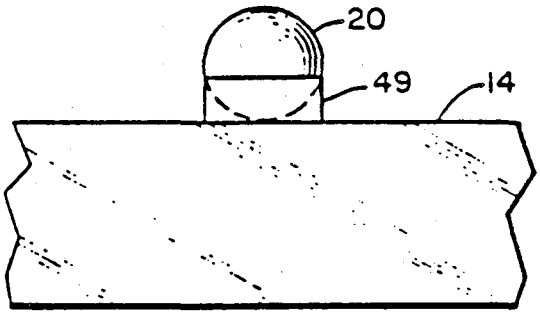

FIG. 7

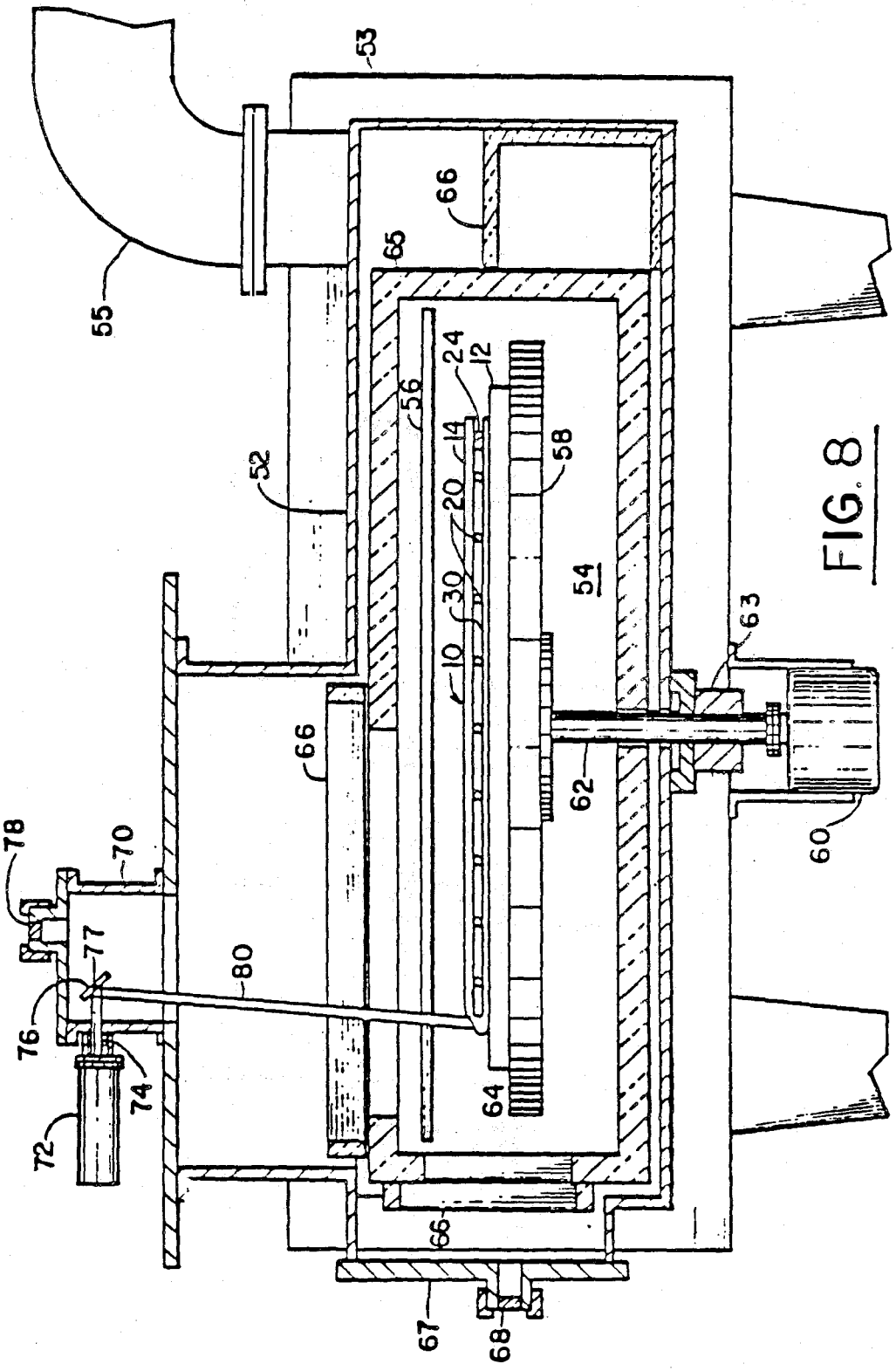
53
55
66
65
24
12
56
14
58
52
20
30
54
10
63
66
62
60
78
70
77
80
76
74
72
64
66
67
68

FIG. 8

LASER SEALED VACUUM INSULATION WINDOW

CONTRACTUAL ORIGIN OF THE INVENTION

The U.S. Government has rights in this invention under Contract No. DE-AC02-83CH10093 between the U.S. Department of Energy and the Solar Energy Research Institute, a Division of Midwest Research Institute.

BACKGROUND OF THE INVENTION

1. Field of the Invention

This invention is generally related to thermal insulated windows and more specifically to a vacuum-sealed glass thermal pane window and a method of sealing same using laser energy.

2. Description of the Prior Art

Panes of glass are in common use in situations wherein it is desired to allow visible light into a structure while preventing heat from escaping. Such situations include windows in buildings and solar collector panels. In solar heating applications, both in active solar heating systems where solar collector panels are used to capture solar energy and in passive solar heated buildings where solar energy is admitted through large window areas, the heat gain over a period of time is a very important consideration that needs improvement. The heat gain is the difference between the heat energy collected in the structure from the sun's radiation less the heat lost from the structure. The ideal window or glass panel, therefore, would be one that is completely transparent to solar radiation and a perfect heat insulator. Such an ideal is, or course, unattainable, but improvements toward that ideal could significantly increase the efficiency of active and passive solar heating systems.

It is well known and generally accepted that multiple, parallel, spaced-apart panes of glass provide more resistance to heat transfer than single panes of glass. An example of such a thermal pane window is shown in U.S. Pat. No. 4,295,305, issued to L. Shelver. Such thermal pane windows, as illustrated in the Shelver patent with two parallel, spaced apart panes of glass with an edge seal comprised of plastic, mastic, silicone, caulk, or the like, are generally effective to provide an R value of about 2.5 to 2.6. (R value is a standard unit indicative of resistance to heat transfer through a substance in terms of °F-ft²hr/BTU.)

The air space between the panes inhibits direct conductance of the heat through the window; however, it does not inhibit heat loss by radiation. Further, it is known that the heat energy causes convection currents of air in the space between the panes. Such convection currents are very effective heat transfer vehicles for transferring heat from one pane to the other, thus negating much of the thermal resistance for which the air space between the glass panes is intended.

It is also known that evacuating the air and gases from the space between the glass panes minimizes or nearly eliminates the convection current therein. The U.S. Pat. No. 4,312,457, issued to R. Allaire, and the U.S. Pat. No. 4,393,105, issued to W. Kreisman, illustrate prior art attempts to provide evacuated window panes or structures to increase thermal resistance, i.e., to increase the R value.

Several problems are encountered in the prior art evacuated thermal pane windows. First, the vacuum between the glass panes causes the glass panes to bow or deflect toward each other. Such deflection can cause stress areas or even cracks in the glass. If they deflect enough to touch each other, short circuit heat transfer through direct conduction can occur, thus reducing thermal resistance significantly. The U.S. Pat. No. 3,990,201, issued to Falbel, shows the use of insulation spacers between panes of glass to solve this problem. However, such spacers are difficult to place in mass production, and they do transfer some heat because of their large contact surface areas with the glass panes, particularly when the spacing between the glass is small. Larger spacing between the panes of glass results in undesirable bulkiness. Further, one of the most significant disadvantages of the Falbel approach is that such spacers are visible in transparent glass panels and are unsightly and distracting when used as windows in a building.

Another problem in prior art evacuated thermal pane windows is the difficulty of maintaining the vacuum over long periods of time. In general, the normal atmospheric pressure of about 1000 torr must be reduced to about 10^{-4} torr before any insulating benefits occur. To be beneficial in a practical insulating sense the pressure should be reduced even further to about 10^{-6} Torr. Sealing such a vacuum over an extended period of time is extremely difficult. Even effective short term seals that give off gases themselves or are even minutely gas permeable cannot maintain this kind of vacuum for very long. Therefore, known prior art seals of plastic, mastic, silicone, Styrofoam insulation, caulk, and the like are practically ineffective for this purpose. To be economical, the vacuum should be maintainable even up to 20–30 years or more. Plastics, silicone pastes, and caulks are permeable to air, and Styrofoam insulation materials give off gases themselves. Exposure to the sun speeds up this process.

Even the electrostatically bonded metal spacer frames taught by U.S. Pat. No. 4,393,105, issued to W. Kreisman, are not effective over longer periods of time. Such metal-to glass seals are subject to chemical attack and degradation, and are also susceptible to fatigue from stress cycles, deformation, and the like.

The prior art has, however, quite successfully solved the problem of reradiation of heat through the glass. For example, it is known that a coating of tin-doped indium oxide (ITO) semiconductor material sputtered onto a glass substrate is selectively transparent to light in the solar spectrum but highly reflective to heat or infrared radiation from heated bodies. Such a tin-doped indium oxide layer deposited on a glass window pane will allow solar radiation, including solar infrared in the range of 2.2 microns wavelength, to pass through the glass into a building or into a solar collector panel while reflecting reradiated heat or infrared in the range of 7 to 10 microns. Thus, the captured heat energy is retained in the building or solar collector and not lost to the atmosphere.

SUMMARY OF THE INVENTION

Accordingly, a general object of the present invention is to provide a more thermal transfer resistant transparent panel for such uses as windows in passive solar heated buildings, solar panels, and the like.

A more specific object of this invention is to provide an evacuated thermal pane glass panel in which an ex-

treme vacuum can be maintained for prolonged periods of time, such as 20 to 30 years or more.

It is also a specific object of this invention to provide an evacuated thermal pane glass structure with effective transparent supports in the space between the glass panels that do not short circuit or transfer any significant amount of heat from one glass pane to the other.

A further specific object of this invention is to provide a method of sealing an evacuated space between adjacent panes of glass in a manner that will hold a vacuum approximately of 10^{-4} Torr over a prolonged period of 20 to 30 years or more.

Additional objects, advantages, and novel features of the invention are set forth in part in the description that follows, and in part will become apparent to those skilled in the art upon examination of the following specification or may be learned by the practice of the invention. The objects and advantages of the invention may be realized and attained by means of the instrumentalities, combinations, and method particularly pointed out in the appended claims.

To achieve the foregoing and other objects and in accordance with the purposes of the present invention, as embodied and broadly described herein, the article and apparatus of this invention may comprise two adjacent glass panes spaced closely together with a plurality of spherical glass beads positioned between the panes to maintain the spacing therebetween and sealed with a glass seal around the edges. A selectively transparent coating on the interior surface of at least one of the glass panels is provided to reflect heat infrared radiation while allowing solar radiation to pass through. Further, the method of this invention includes depositing a selectively transparent layer on one of two glass panes, attaching a plurality of spherical glass bead spacers to the surface of one or two glass panes, positioning one of the glass panes on the other with the spacers between the two glass panes, positioning this assembly in a vacuum furnace, heating the assembly in a vacuum to the annealing temperature of the glass, and welding the edges of the glass panes together by directing a laser beam of sufficient energy thereon to heat the edges of the glass panes to the melting point. A reactive metal getter can also be positioned in the evacuated space to eliminate trace gases accumulated therein.

BRIEF DESCRIPTION OF THE DRAWINGS

The accompanying drawings, which are incorporated in and form a part of the specifications illustrate the preferred embodiments of the present invention, and together with the description explain the principles of the invention. In the drawings:

FIG. 1 is a perspective view of the evacuated thermal pane glass panel of the present invention with a portion of a corner broken away to reveal the structure thereof;

FIG. 2 is a cross-sectional view of the evacuated thermal pane glass panel of the present invention taken along lines 2—2 of FIG. 1;

FIG. 3 is a cross-sectional view similar to FIG. 2, but with the addition of an insulating baffle around the edges of the glass panel;

FIG. 4 is a perspective view of one of the glass panes with a plurality of glass beads affixed thereto before to assembly with the second glass panel;

FIG. 5 is a perspective view illustrating a preferred method of affixing the glass beads to the glass pane;

FIG. 6 is an enlarged elevation view illustrating the spot welding of a glass bead on the glass pane substrate;

FIG. 7 is an enlarged elevation view illustrating an alternate method affixing the glass bead to the glass pane substrate with a sodium silicate solution; and

FIG. 8 is a cross-sectional view of a vacuum furnace arrangement suitably equipped for laser sealing of the edges of the evacuated thermal pane glass panel of the present invention.

DETAILED DESCRIPTION OF THE PREFERRED EMBODIMENTS

The laser-sealed vacuum insulating window 10 of the present invention is best shown in FIG. 1, with secondary reference to FIG. 2. The window panel 10 according to the present invention is comprised of two panes of glass 12, 14 positioned adjacent to each other in parallel, closely spaced-apart relation to each other. The edges are sealed together, as indicated at 16, to completely enclose and seal an evacuated space 30 between the glass panes 12, 14. A plurality of spherical glass bead spacers are positioned in spaced apart relation to each other throughout the evacuated space 30 between the glass panes 12, 14 to maintain the distance between the glass panes 12, 14, in spite of the intense vacuum sealed therein. A metal alloy getter 24 is also positioned in the evacuated space 30 for purposes that will be described more fully below.

Referring primarily now to FIG. 2, the spherical glass spacers 20 positioned between the panels 12, 14 maintain the distance and parallel relationship between the glass panels 12, 14. In the absence of the spacers, the extreme vacuum, preferably in the range of 10^{-4} Torr would collapse or deform the glass panels 12, 14 into contact with each other, thereby short circuiting thermal transfer of energy directly therethrough by conduction and defeating the insulating purpose of the evacuated space. A selectively transparent coating 18, which is transparent to solar radiation and light in the visible spectrum but is reflective to infrared heat radiation, is deposited on the interior surface of one or both of the glass panels 12, 14.

The glass beads 20 are preferably spherical and approximately 0.5 mm in diameter. The size and spherical shape of such glass beads 20 are significant in this application for several reasons. The spherical shape provides very small area, almost point, contacts between the beads 20 and the glass panes 12, 14. The smaller the sphere diameter, the smaller the contact area. A smaller contact area results in less area for heat conduction, thus more thermal resistance of the glass panel 10. Further, smaller beads 20 have less cross-sectional area and provide less of a conduction path through the bulk of the beads 20 themselves than larger beads. Therefore, thermal resistance of the glass panel 10 increases significantly as the size of the beads 20 is reduced, particularly in the range smaller than 1.0 mm diameter. We have found that a glass panel 10 with beads 20 in the range of about 0.5 mm provides very good thermal resistance. It is possible to use even smaller beads 20 in the range of about 0.3 mm diameter, if the glass panels 12, 14 are very flat. For 0.5 mm diameter beads, spacing between beads 20 in the range of 2.5 to 3.5 cm is satisfactory to maintain the spacing between the glass panels 12, 14.

Another advantage of the glass beads 20 for use as spacers between the glass panes 12, 14 is that they are transparent like the glass. Thus, they are barely visible and do not detract from the appearance of the glass panel 10 or do not block a view therethrough when the glass is used as a window.

According to the present invention, the sealed vacuum insulating window panel 10, which has a highly evacuated space 30 between the two glass panels 12, 14 and an all glass seal 16 around the edges of the individual panels 12, 14 is highly effective as a transparent insulating panel or window. Solar radiation can pass freely therethrough into the interior of a building structure or solar collector panel, however, the heat absorbed inside the building or in a solar collector panel is very effectively prohibitied from transfer back through the glass panel 10. The selective coating 18, preferably of a layer of tin-doped indium oxide sputtered onto the surface of the glass, effectively reflects infrared heat radiation back into the building structure or solar panel. Further, the separation of the glass panels 12, 14 by the space 30 prevents conduction of heat from one side of the window 10 to the other. Still further, the extreme vacuum of approximately 10^{-4} Torr in the space 30 between the panes 12, 14 effectively eliminates any convection currents in the space 30 which would otherwise transfer heat from one pane to the other. The result is a transparent window panel 10 that is exceptionally resistant to heat transfer therethrough. Theoretical calculations on window panels 10 constructed according to the present invention have indicated that they are expected to have an R value of approximately of 10 to 12, as opposed to conventional thermal pane windows that have an R value of only about 2.5.

FIG. 3 shows a preferred mounting structure for the evacuated glass panel 10 for the present invention. The edges 16 of the glass panel 10 are preferably embedded in an insulated baffle 32 to minimize thermal conductance losses through the edge seal 16 of the glass panel 10. The edge seals 16 are the only places where a significant cross-section of glass could provide a direct path for heat transfer by conduction from one side of the glass panel 10 to the other. Therefore, in order to prevent such a thermal short circuit, it is important to shield the end seal 16 from exposure to heat to prevent heat transfer therethrough. We have found that thermal resistance of a 1 m^2 glass panel is decreased by as much as 30% when the edge seals 16 are not shielded by the insulation baffle 32.

The sealed vacuum insulating window panel 10 of the present invention is preferably constructed by using a laser to weld or seal the edges of the glass panels 12, 14 together. Before sealing the edges together, however, it is necessary to first deposit the selective transparent coating on the interior surface of at least one of the glass panes 12, 14. As mentioned above, it is preferred that a selective coating of a transparent layer of tin-doped indium oxide semiconductor material is deposited on the surface of the glass pane by a vacuum deposition or sputtering process. Then, the uniformly sized glass beads are attached to the interior surface of one of the glass panels 14, as shown in FIG. 4.

Uniformly sized spherical glass beads are inexpensive and readily available. They can be produced by persons skilled in the art, usually by spraying molten glass into a cool free-falling atmosphere. During the free fall, the droplets of molten glass solidify into almost perfect spheres. The spherical beads can be screened for sizing to obtain uniform sizes for particular glass panel applications. It is preferred that the spherical glass beads used in this invention be approximately 0.5 mm in diameter.

The glass beads 20 can be affixed to the glass pane substrate 14 in a number of ways. One such method illustrated in FIG. 5 is to "flood" or completely cover the entire surface of the glass pane substrate 14 with uniformly sized glass beads 20. Then, a laser beam 46 can be used to spot weld the individual glass beads 20 in the desired locations on the glass pane substrate 14. A convenient method of accomplishing this task is to position the glass panel substrate 14 on a translation platform 48 that can be moved in predetermined precise X and Y directions under a stationary laser head. When the translation platform 48 is in the desired position, a laser beam 46 is produced by a laser head 40 and directed through a shroud 42 and relay mirror 44 to the surface of the glass pane substrate 14 as shown in FIG. 5.

If the laser beam 46 is aimed at the glass substrate 14 in a vertical orientation, as shown in FIG. 6, then it does not matter whether the laser beam 46 is perfectly aligned with any particular glass sphere 20. As shown in FIG. 6, it is the nature of a spherical body 20 to refract a beam 46 to the contact point 47 between the spherical bead 20 and the glass substrate 14 where the spot welding takes place, regardless of which point on the surface of the spherical bead 20 the beam 46 is incident. Therefore, with the surface of the glass substrate 14 folded with beads 20, as shown in FIG. 5, any place the laser beam 46 is aimed at the substrate 14 in a vertical orientation thereto, a glass bead 20 will be spot welded to the glass substrate 14 at that selected location. When the laser beam 46 has been aimed at all of the selected locations where one desires to affix a glass bead 20 to the glass substrate 14, the remainder of the glass beads can merely be dumped or poured off the surface of the substrate 14, leaving a selected number of glass beads 20 affixed to the surface of the glass pane 14 at selected positions as shown in FIG. 4. Spot welding the beads 20 to the glass panel 14 in this manner has the advantage of keeping the contact area between the beads 20 and the glass pane 14. The spot welds are also transparent, so they do not detract from the appearance of the window 10.

FIG. 7 illustrates another method of attaching the glass beads 20 to the substrate 14. In this method, the glass beads 20 are dipped in a sodium silicate solution and positioned at the desired locations on the glass substrate 14. The sodium silicate solution will harden and adhere the glass bead 20 to the surface of the glass substrate 14. An advantage of this method is that the sodium silicate does not produce any gases, is transparent, and provides a durable adhesion or bonding of the glass bead 20 to the glass substrate 14. A disadvantage is that the hardened sodium silicate 49 provides a larger surface area on at least one glass pane 14 to which it is affixed for thermal transfer by conduction.

After the glass beads 20 are affixed at the desired locations to the glass pane 14, as shown in FIG. 4, the other glass pane 12 is positioned on the glass beads 20. Then, the metal getter 24 is positioned between the glass panels and, as best illustrated in FIG. 8, the assembly of glass panes 12, 14 and beads 20 is preferably positioned in a vacuum furnace 50 where the assembly can be heated to the annealing temperature of the glass while the edges 16 are sealed by a laser beam 76.

A suitable vacuum furnace assembly 50 is illustrated in cross-section in FIG. 8. It includes a vacuum chamber 54 enclosed by a vacuum shell 52. Reinforcing housing 53 provides additional structural support for the vacuum shell 52. A rotatable turntable platform 58 is positioned in the chamber 54 to support the glass win-

dow panel 10 during laser welding. The turntable 58 is supported by a rotatable shaft 62 journaled in a water-cooled bearing 63. A stepper motor 60 connected to the shaft 62 rotates the turntable 58 in precisely measured increments of angular rotation in response to the stepper motor control apparatus (not shown).

The glass panel assembly 10 on the turntable is heated by a plurality of radiant heating elements, such as the radiant heating element 56 in FIG. 8 positioned over the turntable 58. Primary reflective insulation layers 65 protect the vacuum shell from the radiant heat in the chamber, and secondary reflective insulation layers 66 further shield structural and functional components of the furnace from the heat radiation. A view glass assembly 68 in removable end plate 67 allows an operator to view the interior of the chamber 54.

A laser optics housing unit 70 is mounted above the turntable platform 58 and has a laser head 72 mounted thereon. A relay mirror 76 is mounted on a pivotal axis 77 in laser optics housing 70 in alignment with a gallium arsenide laser window 74. The relay mirror 76 can direct laser beam 80 generated in the laser head 70 to a desired location on the turntable platform 58.

In use, the glass panel assembly 10 comprised of the glass panes 12, 14, glass bead spacers 20, and metal getter 24 is positioned in the vacuum furnace 50 on a thermofax board insulator 64 on the platform 58. The furnace 50 is closed and sealed, and the chamber 54 is evacuated through port 55 to about 10^{-6} Torr pressure. Then the radiant heaters 56 heat the glass panel assembly 10 to its annealing temperature or slighly above. For borosilicate glass, which is the preferred glass suggested for this invention, the annealing temperature is approximately 565° C.; therefore, it is preferred that the glass assembly is heated to approximately 580° C., at which temperature the glass can deform slightly under stress without fracturing. While maintaining the glass assembly at or slightly above the annealing temperature, the laser beam 81 is directed at the edges of the glass panes 12, 14 to melt and weld them together to form a glass seal. The laser beam 76 must have sufficient energy to raise the temperature of the glass at the edges enough to melt it. The melting temperature for borosilicate glass is approximately 1200° C. to 1300° C. With the laser beam 80 melting the glass at the edges of the panes 12, 14, the turntable platform 58 is rotated by stepper motor 60 in the appropriate increments. Simultaneously, the relay mirror 76 is rotated at appropriate increments and speeds to slowly move the laser beam 76 around the entire edge of the glass panels 12, 14 until they are completely welded and sealed by a glass seal. By appropriately controlling the relay mirror 76 and the turntable 58 simultaneously, preferably by computer program, any pattern or configuration of glass panel 10 can have its edges laser welded to seal an evacuated space 30 therein as described above. This process can be watched through the view windows 68, 78. Of course, other vacuum furnace structures and laser control techniques can also be used to accomplish the laser welding of the glass edges of panel 10.

Once the entire edge of the glass panel assembly 10 is welded in a vacuum tight glass seal as described above, it is cooled. While the glass panel 10 is cooling from the 580° C. oven temperature, it will give off minute amounts of water vapor, carbon dioxide, and other miscellaneous gases such as nitrogen, oxygen, hydrocarbons, and the like. These gases are emitted into the space 30 between the panes 12, 14, as well as to the exterior. However, the reactive metal getter 24, positioned between the glass panes 12, 14, is activated at the high oven temperature during the sealing process. This metal getter 24, comprised preferably of an alloy of zirconium, vanadium and iron, will chemically react or combine with the minute amounts of gases produced during the cooling process to form solid compounds on the surface of the metal getter, thus virtually eliminating such gases from the space 30. With these gases eliminated, the 10^{-6} Torr vacuum is maintained in the space 30 and the likelihood of heat loss caused by to convection currents therein is virtually eliminated.

The amount of metal getter 24 to position in a particular evacuated glass panel 10 according to the present invention can be predetermined according to the size of the window panel 10 being produced. For example, an evacuated window panel, 10 of approximately one square meter requires a metal getter that is approximately 10 cm long by 0.08 cm wide by 0.35 cm thick, when the metal getter is an alloy of zirconium, vanadium and iron, as preferred in this invention. Other kinds of metal alloy getters can also be used for the same purpose.

While the above described laser welding edge seal is preferred, an alternative method of providing a glass edge seal is to use a glass solder technique. A solder glass is a powdered glass having a low melting temperature that can be used to bond glasses with higher softening or melting points together. In such an alternative embodiment, the powdered solder glass would have to be placed between the edges of the adjacent glass panes 12, 14. Then, the laser directed at the edges would not have to raise the temperature of the glass panes 12, 14 to their melting points but would merely have to be of sufficient energy to melt the powdered glass solder at lower melting points.

The foregoing description illustrates only the principles of the invention. Further, since numerous modifications and changes will readily occur to those skilled in the art, it is not desired to limit the invention to the exact construction and processes shown and described above. Accordingly, all suitable modifications and equivalents may be resorted to falling within the scope of the invention as defined by the claims that follow.

The embodiments of the invention in which an exclusive property or privilege is claimed are defined as follows:

1. A thermal resistant panel comprising two panes of glass positioned closely spaced apart in substantially parallel relation to each other, a plurality of spherical glass bead spacers positioned between said two panes of glass to maintain the spacing while minimizing the thermal conduction between said panes, and a continuous glass joint around the periphery of said panel sealing the edges of said two panes together.

2. The thermal resistant panel of claim 1, wherein the space between said glass panes is evacuated.

3. The thermal resistant panel of claim 2, wherein the space between said glass panes is evacuated to a pressure in the range of 10^{-5} to 10^{-6} Torr.

4. The thermal resistant panel of claim 2, including getter means positioned in said evacuated space between said glass panes.

5. The thermal resistant panel of claim 3, wherein said getter means is an activated metal alloy comprising zirconium, vanadium, and iron.

6. The thermal resistant panel of claim 1, wherein said glass beads are in the range of about 0.3 mm to 1.0 mm in diameter.

7. The thermal resistant panel of claim 1, wherein said glass beads are affixed to one of said panels.

8. The thermal resistant panel of claim 1, including transparent selective coating means on the surface of one of said glass panes for allowing solar radiation and light in the visible spectrum to pass therethrough while reflecting infrared heat radiation that is not in the visible spectrum.

9. The thermal resistant panel of claim 1, wherein said panel includes an insulated baffle around the periphery of said panel enclosing said glass joint in said insulated baffle.

10. A thermal resistant panel conprising two panes of glass positioned closely spaced apart in relation to each other, at least one surface of one of said panes of glass having deposited thereon a layer of material that is transparent to solar radiation and light in the visible spectrum and reflective to infrared heat radiation that is not in the visible spectrum, a plurality of spherical glass bead spacers attached to one of said panes of glass and positioned in the space between said two panes of glass to maintain the spacing while minimizing the thermal conduction between said panes of glass, a continuous welded glass joint around the periphery of said panel sealing the edges of said two panes of glass together, and a vacuum in the space between said panes of glass.

11. A process of producing a thermal resistant panel comprising the steps of positioning two glass panes closely spaced apart in relation to each other, positioning a plurality of spherical glass bead spacers between said panes to maintain the spacing while minimizing the thermal conduction between said panes, evacuating the atmosphere around said panes, and joining the edges of said glass panes together to form a completely glass seal around the periphery of the panel.

12. The process of claim 11, including the step of glass soldering the edges of said glass panes together.

13. The process of claim 11, including the step of affixing a plurality of glass bead spacers to one of said glass panes by flooding the surface of said pane with a plurality of beads and then spot laser welding selected numbers thereof to said surface before welding the edges of said glass panes together.

14. The process of claim 12, including the step of affixing a plurality of glass bead spacers to one of said glass panes before welding the edges of said glass panes together.

15. The process of claim 12, including the step of welding the edges of said glass panes together by directing a laser beam at such edges of sufficient power to raise the temperature of the glass at the edges of the panes to the melting point.

16. The process of claim 15, including the step of heating said glass panes to at least the annealing temperature of the glass and maintaining such temperature during the laser welding of the edges together.

17. The process of claim 16, including the step of positioning metal getter means in the space between the glass panes prior to heating and welding the edges.

18. The process of claim 12, including the step of depositing a material on a surface of one of said glass panes that is transparent to solar radiation and visible light and reflective to infrared heat radiation that is not in the visible spectrum.

19. The process of claim 18, including the step of sputter depositing a layer of tin-doped indium oxide semiconductor material on a surface of one of said glass panes.

* * * * *

Document Control Page	1. SERI Report No. SERI/TP-212-3684	2. NTIS Accession No. DE90000344	3. Recipient's Accession No.

4. Title and Subtitle
Vacuum Window Glazings for Energy-Efficient Buildings: Summary Report

5. Publication Date
May 1990

6.

7. Author(s) D.K. Benson, L.K. Smith, C.E. Tracy, T. Potter, C. Christensen, D.E. Soule

8. Performing Organization Rept. No.

9. Performing Organization Name and Address
Solar Energy Research Institute
1617 Cole Boulevard
Golden, Colorado 80401-3393

10. Project/Task/Work Unit No.

11. Contract (C) or Grant (G) No.
(C)
(G)

12. Sponsoring Organization Name and Address

13. Type of Report & Period Covered
Technical Report

14.

15. Supplementary Notes

16. Abstract (Limit: 200 words)
The technical feasibility of a patented, laser-welded, evacuated insulating window was studied. The window has two edge-sealed sheets of glass separated by 0.5-mm glass spheres spaced 30 mm apart in a regular array. A highly insulating frame is required and several designs were analyzed. The vacuum window's combination of high solar transmittance and low thermal conductance makes it superior to many other windows in cold climates. In the U.S. Pacific Northwest, the vacuum window could save about 6 MJ of heating energy annually per square meter of window in comparison to conventional, double-glazed windows. A large, vacuum laser-welding facility was designed and installed to conduct glass welding experiments and to fabricate full-sized vacuum windows. Experiments confirmed the feasibility of laser-sealing glass in vacuum but identified two difficulties. Under some circumstances, bubbles of dissolved gases form during welding and weaken the seal. Glass also vaporizes and contaminates the laser beam steering mirror. A novel moving metal foil mirror was developed to circumvent the contamination problem, but it has not yet been used to complete welding experiments and fabricate full-sized vacuum windows.

17. Document Analysis
a. Descriptors Vacuum window glazings ; energy-efficient buildings ; insulation ; laser-welding

b. Identifiers/Open-Ended Terms

c. UC Categories 232

18. Availability Statement
National Technical Information Service
U.S. Department of Commerce
5285 Port Royal Road
Springfield, VA 22161

19. No. of Pages
144

20. Price
A07